EFFECT OF SIZES AND SHAPES OF ZINC OXIDE ON PROPERTIES OF POLYPROPYLENE WITH AND WITHOUT COMPATIBILIZER

By
Thitipong Sanitchai

A Thesis Submitted in Partial Fulfillment of the Requirements for the Degree
MASTER OF ENGINEERING
Department of Chemical Engineering
Graduate School
SILPAKORN UNIVERSITY
2010

EFFECT OF SIZES AND SHAPES OF ZINC OXIDE ON PROPERTIES OF POLYPROPYLENE WITH AND WITHOUT COMPATIBILIZER

By
Thitipong Sanitchai

A Thesis Submitted in Partial Fulfillment of the Requirements for the Degree
MASTER OF ENGINEERING
Department of Chemical Engineering
Graduate School
SILPAKORN UNIVERSITY
2010

การศึกษาผลของขนาดและรูปร่างของซิงค์ออกไซด์ที่มีต่อสมบัติของพอลิพอพิลีนที่มีและไม่มีสารช่วยผสม

โดย
นายฐิติพงษ์ สนิทไชย

วิทยานิพนธ์นี้เป็นส่วนหนึ่งของการศึกษาตามหลักสูตรปริญญาวิศวกรรมศาสตรมหาบัณฑิต
สาขาวิชาวิศวกรรมเคมี
ภาควิชาวิศวกรรมเคมี
บัณฑิตวิทยาลัย มหาวิทยาลัยศิลปากร
ปีการศึกษา 2553

The Graduate School, Silpakorn University has approved and accredited the Thesis title of "Effect of sizes and shapes of zinc oxide on properties of polypropylene with and without compatibilizer" submitted by Mr.Thitipong Sanitchai as a partial fulfillment of the requirements for the degree of Master of Engineering in Chemical Engineering

…….....
(Assistant Professor Panjai Tantatsanawong, Ph.D.)

Dean of Graduate School

...../...../.....

The Thesis Advisor

Assistant Professor Sirirat Wacharawichanant, D.Eng.

The Thesis Examination Committee

..... Chairman
(Assistant Professor Worapon Kiatkittipong, D.Eng.)
...../...../.....

..... Member
(Associate Professor ML. Supakanok Thongyai, Ph.D.)
...../...../.....

.....Member
(Supakij Suttiruengwong, Dr.Ing.)
...../...../.....

.....Member
(Assistant Professor Sirirat Wacharawichanant, D.Eng.)
...../...../.....

50404201 : MAJOR : CHEMICAL ENGINEERING
KEY WORDS : POLYPROPYLENE/ ZINC OXIDE/ COMPOSITES/ COMPATIBILIZER
THITIPONG SANITCHAI : EFFECT OF SIZES AND SHAPES OF ZINC OXIDE ON PROPERTIES OF POLYPROPYLENE WITH AND WITHOUT COMPATIBILIZER. THESIS ADVISORS : ASST.PROF.SIRIRAT WACHARAWICHANANT, D.Eng., 153 pp.

This research studied the morphology, mechanical, thermal and electrical properties of polypropylene (PP) filled with different sizes and shapes of zinc oxide (ZnO) composites without and with compatibilizer. Two shapes of ZnO were rod and sphere. Three sizes of sphere shape with an average particle size of 71, 100 and 250 nm were used. ZnO rod and sphere 100 nm were synthesized by simple chemical route from the reaction between zinc chloride ($ZnCl_2$) and ammonium hydroxide (NH_4OH). The composites of PP and ZnO were mixed by a twin screw extruder and molded by compression method. The morphology of PP/ZnO composites was observed by scanning electron microscope (SEM). It was found that the dispersion of ZnO particles in the PP matrix of all composites after adding polypropylene-graft-maleic anhydride (PP-g-MA) was better than the composites without PP-g-MA. The results found that the suitable of compatibilizer was PP-g-MA (0.55 %MA content) at 3 wt%. The mechanical properties of the PP/ZnO 71, 100, 250 nm and rod composites after adding PP-g-MA improved but thermal and electrical properties did not significantly change. For comparison between ZnO 71 and 250 nm, it was found that the mechanical properties after adding PP-g-MA of the PP/ZnO 71 nm composites was slightly higher than the composites filled with ZnO 250 nm while the PP/ZnO 71 nm composites before adding PP-g-MA was lower than the composites filled with ZnO 250 nm. In case of rod and sphere shapes, it was found that the PP/ZnO rod composites before adding PP-g-MA show the higher mechanical properties than PP/ZnO 71 nm composites but the composites of PP/ZnO 71 nm composites after adding PP-g-MA show the higher improvement in mechanical properties than the composites filled with ZnO rod.

Department of Chemical Engineering Graduate School, Silpakorn University Academic Year 2010
Student's signature .....
Thesis Advisor's signature .....

50404201 : สาขาวิชาวิศวกรรมเคมี
คำสำคัญ : พอลิพอพิลีน/ซิงค์ออกไซด์/คอมโพสิต/สารช่วยผสม

ฐิติพงษ์ สนิทไชย : การศึกษาผลของขนาดและรูปร่างของซิงค์ออกไซด์ที่มีต่อสมบัติของพอลิพอพิลีนที่มีและไม่มีสารช่วยผสม. อาจารย์ที่ปรึกษาวิทยานิพนธ์ : ผศ.ดร.ศิริรัตน์ วัชรวิชานันท์. 153 หน้า.

งานวิจัยนี้ศึกษารูปแบบโครงสร้างสัณฐาน สมบัติทางกล สมบัติทางความร้อน และสมบัติทางไฟฟ้าของพอลิพอพิลีนที่เติมด้วยซิงค์ออกไซด์ที่มีขนาดและรูปร่างที่แตกต่างกันโดยใช้และไม่ใช้สารช่วยผสม รูปร่างของซิงค์ออกไซด์ที่ใช้ในงานวิจัยประกอบไปด้วยรูปร่างที่มีลักษณะเป็นแท่ง และทรงกลม สำหรับรูปร่างที่เป็นทรงกลมจะใช้ซิงค์ออกไซด์ที่มีขนาดอนุภาคต่างกัน 3 ขนาด คือ 71 100 และ 250 นาโนเมตรตามลำดับ โดยได้ทำการสังเคราะห์ซิงค์ออกไซด์ที่มีรูปร่างแบบแท่ง และแบบทรงกลมที่มีขนาดอนุภาค 100 นาโนเมตรขึ้นมา ด้วยการทำปฏิกิริยาระหว่างซิงค์คลอไรด์และแอมโมเนียมไฮดรอกไซด์ การเตรียมพอลิเมอร์คอมโพสิตระหว่างพอลิพอพิลีนและซิงค์ออกไซด์ทำโดยใช้เครื่องผสมเกลียวหนอนคู่ และขึ้นรูปด้วยวิธีอัดขึ้นรูป รูปแบบโครงสร้างสัณฐานของคอมโพสิตศึกษาโดยกล้องจุลทรรศน์อิเล็กตรอนแบบส่องกราด จากการทดลองพบว่าหลังจากเติมสารช่วยผสมลงไปในพอลิพอพิลีนทำให้เกิดการกระจายตัวของอนุภาคซิงค์ออกไซด์ดีขึ้น ผลการทดลองพบว่าสารช่วยผสมที่เหมาะสมคือพอลิพอพิลีนกราฟมาเลอิคแอนไฮไดร์ (ปริมาณมาเลอิคแอนไฮไดร์ 0.55 เปอร์เซ็นต์โดยน้ำหนัก) ปริมาณ 3 เปอร์เซ็นต์โดยน้ำหนัก สมบัติเชิงกลของวัสดุคอมโพลิตปรับปรุงไปในทางที่ดีขึ้นหลังจากที่เติมสารช่วยผสม ส่วนสมบัติทางความร้อนและสมบัติทางไฟฟ้าไม่พบการเปลี่ยนแปลงที่ชัดเจนมากนัก ผลจากการศึกษาขนาดของอนุภาคซิงค์ออกไซด์ระหว่างขนาด 71 และ 250 นาโนเมตรพบว่าซิงค์ออกไซด์ขนาดอนุภาค 71 นาโนเมตรทำให้สมบัติเชิงกลดีกว่าขนาดอนุภาค 250 นาโนเมตรหลังจากเติมสารช่วยผสม ในขณะที่ก่อนเติมสารช่วยผสมขนาดอนุภาค 250 นาโนเมตรให้สมบัติเชิงกลที่ดีกว่า ในส่วนของรูปร่างของซิงค์ออกไซด์แบบแท่งและแบบทรงกลมพบว่า ก่อนเติมสารช่วยผสมซิงค์ออกไซด์ที่มีรูปร่างแบบแท่งทำให้คอมโพสิตมีสมบัติเชิงกลดีกว่ารูปร่างแบบทรงกลม แต่หลังจากเติมสารช่วยผสมแล้วซิงค์ออกไซด์รูปร่างแบบทรงกลมจะทำให้สมบัติเชิงกลของคอมโพสิตดีขึ้นมากกว่ารูปร่างแบบแท่ง

ภาควิชาวิศวกรรมเคมี บัณฑิตวิทยาลัย มหาวิทยาลัยศิลปากร ปีการศึกษา 2553

ลายมือชื่อนักศึกษา.....

ลายมือชื่ออาจารย์ที่ปรึกษาวิทยานิพนธ์ .....

ACKNOWLEDGEMENTS

The author wishes to express his sincere gratitude and appreciation to his advisor, Assistant Professor Dr. Sirirat Wacharawichanant for their valuable suggestions, stimulating, useful discussions throughout this research and devotion to revise this thesis otherwise it cannot be completed in a short time. In addition, the author would also be grateful to Assistant Professor Dr. Worapon Kiatkittipong, as the chairman, Associate Professor Dr. ML. Supakanok Thongyai, and Dr. Supakij Suttiruengwong as the members of the thesis committee.

Most of all, the author would like to express his highest gratitude to his parents who always pay attention to through these years for suggestions and their wills. The most success of graduation is devoted to my parents.

Finally, Many thanks for kind suggestions and useful help to Mr. Noppol Wiriyanukul, Mr. Parinya Intaracharoen, the members of Department of Chemical Engineering, Faculty of Engineering and Industrial Technology, Silpakorn University for their assistances. The author would like to thank the Center of Excellence on Catalysis and Catalytic Reaction Engineering, Department of Chemical Engineering, Faculty of Engineering, Chulalongkorn University for dielectric constant and TGA test of samples.

TABLE OF CONTENTS

List of Figures

CHAPTER 1

INTRODUCTION

At present, plastics are material that is used for many applications in our life. They are everywhere from your pillows and mattresses to cars, hi-tech computers and surgery. Our life has participated with plastics when we get up until go to bed again. Because its lightweight, does not rust or rot, helps lower transportation costs and conserves natural resources is the reason for which plastic has gained this much popularity (www.thinkquest.org). Composite materials made from two or more constituent materials with significantly different physical or chemical properties, which remain separate and distinct at the macroscopic or microscopic scale within the finished structure. Polymer composites have become attractive because of their wide applications and low cost. The properties of polymer filled with particle made its properties better than a commercial polymer. In general, the mechanical and thermal properties of composite materials depend strongly on size, shape and distribution on filler particles in the matrix polymer and good adhesion at the interface surface (Bose *et al.*, 2004).

PP is a thermoplastic polymer used in wide application such as packaging, textile, stationery, plastic parts and reusable containers of various types, laboratory equipment, loudspeakers, automotive components, etc. It is one of the most extensively used polyolefins (Hongxia *et al.*, 2006) due to its good process ability, relatively high mechanical properties, great recycle ability and low cost. However, owing to its low modulus, high notch sensitivity and poor impact resistance (Yang *et al.*, 2006) make uses of PP still limited. There are many researches to improve mechanical properties and thermal properties of PP with using filler such as calcium carbonate ($CaCO_3$) (Chi-Ming *et al.*, 2002), silica (Chun *et al.*, 2002 and Suryadiansyah *et al.*, 2008), cellulose (Ljungberg *et al.*, 2006), bio-flour (Hee-Soo *et al.*, 2007), etc. It challenges to filled particles into PP matrix because the hydrophobic

character of PP made the dispersion of hydrophilic fillers difficult (Ljungberg *et al.*, 2006).

Zinc oxide (ZnO) is one of the multifunctional inorganic has drawn increasing attention in recent years due to its prominent physical and chemical properties, such as chemical stability, low dielectric constant, high luminousis transmittance, high catalysis activity, effective antibacterial and bactericide, intensive ultraviolet and infrared absorption (Erjun *et al.*, 2006). It is an environmentally benign material and is used not only for traditional inorganic UV-absorbing materials and cosmetics, but also for optoelectronic materials such as solar cell and light emitting diode (Sato *et al.*, 2008). Moreover, the advance of ZnO particles could improve the mechanical and optical properties of the polymer matrix (Erjun *et al.*, 2006). The optoelectronic properties of ZnO nanoparticles depend on particle sizes, which can be controlled by reaction conditions during their preparation and by attachment of organic compounds onto the surfaces. ZnO has many nanostructures among all one-dimensional. ZnO nanocrystals with various shapes included one-dimensional (rod, tube, wire and nail), two-dimensional (sheet, hexagon, tower and comb) and multi-dimensional (flower), have been successfully demonstrated (Zhang *et al.*, 2007). There are many researched to synthesis ZnO and easy to control the particle sizes and shapes such as flame spray pyrolysis (Joon *et al*, 2006), chemical route (Singh *et al.*, 2008), solvothermal reaction (Tonto *et al.*, 2006 and Wei *et al.*, 2008), etc. However, ZnO particle has high surface energy which may result in the agglomeration of particles when ZnO particles are dispersed in organic solvent and matrices. Thereafter, it is necessary to prepare ZnO/polymer composites to prevent the formation of agglomerated nanoparticles (Erjun *et al.*, 2006). In recent years, it has been suggested that introduction of organic compounds into the ZnO nanoparticle surfaces stabilizes the ZnO nanoparticle sizes without aggregation between ZnO nanoparticles. The ZnO nanoparticles have been disclosed to show significant UV-shielding property (Sato *et al.*, 2008). So, the synthesis and properties of ZnO are very attractive to use ZnO as filler in this research.

The development of an interphase layer makes the good dispersion of filler particles in the polymer matrix. Change in interfacial interactions between particles and polymer matrix can modify the debonding mechanism, failure behavior and thus, the overall performance of composites. The most used technique to change the particle-particle and polymer-particle interactions is the coverage of filler surface with a low molecular weight organic compound such as zinc stearate (Zuiderduin *et al.*, 2003). Treatment of nanoparticles or modified polymer chains had a complex method. But in many researches have used a maleated form of polypropylene (PP-g-MA) as compatibilizer for polypropylene (PP)/clay nanocomposites without treatment of PP (Fan *et al.*, 2007; Gcwabaza *et al.*, 2008; Dong *et al.*, 2008; Yang *et al.*, 2008 and Rozanski *et al.*, 2008). PP-g-MA has been widely used to improve the interfacial surface between filler and polymer matrix that can be enhanced the mechanical, thermal, and chemical properties (Wulin *et al*, 2005) due to the polar groups could interact with functional groups on the inorganic filler while the PP backbone of PP-g-MA was able to anchor to the polymer matrix via physical entanglements and van der Waals interactions (Suryadiansyah *et al.*, 2008).

In this work, we focused on the study of composites of PP with various sizes and shapes of ZnO. The effect of addition two types of dispersing agent (PP-g-MA and zinc stearate) was also investigated, in particular, miscibility between PP matrix and ZnO. The effects of ZnO with various sizes and shapes without and with PP-g-MA on mechanical, thermal, electrical and morphological properties of PP/ZnO composites were studied. The effect of maleic anhydride (MA) content on mechanical, thermal, electrical properties and morphology were prepared by an internal mixer were also investigated. PP/ZnO composites with varying concentration of ZnO were prepared by melt mixing technique in a twin screw extruder. The dispersion of ZnO in PP matrix was observed by scanning electron microscope (SEM). The thermal properties were observed by thermo gravimetric analyzer (TGA) and differential scanning calorimeter (DSC). The mechanical properties of PP/ZnO composites were investigated by tensile and impact testing. An electrical property was also investigated by LCR meter equipment.

CHAPTER 2

THEORY

1. Polypropylene (PP)

PP is a thermoplastic material that is produced by polymerizing propylene molecules, which are the monomer units, into very long polymer molecule or chains.

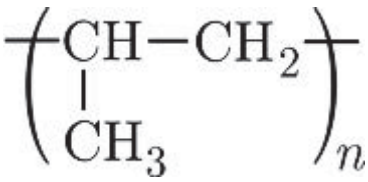

Figure 1 The repeating unit of PP (www.taggedwiki.zubiaga.org)

As is typical with most thermoplastic materials, the main properties of PP in the melt state are derived from the average length of the polymer chains and the breadth of the distribution of the polymer chain lengths in a given product. In the solid state, the main properties of the PP material reflect the type and amount of crystalline and amorphous regions formed from the polymer chains. PP has excellent and desirable physical, mechanical, and thermal properties when used in room-temperature applications. It is relatively stiff and has a high melting point, low density, and relatively good resistance to impact. These properties can be varied in a relatively simple manner by altering the chain regularity (tacticity) content and distribution, the average chain lengths, the incorporation of a comonomer such as ethylene into the polymer chains, and the incorporation of an impact modifier into the resin formulation (Kissel, 2003).

PP is used in a wide variety of application such as packaging, automotive components, textiles, laboratory equipment and etc. Due to its good processability,

relatively high mechanical properties, great recycle ability and low cost (Hongxia *et al.*, 2006) so these properties make PP is very interesting material.

PP is one of the most widely used polyolefin polymers; it has no polar groups in the chain (O'Donnell *et al.*, 1995; Modesti *et al.*, 2005; Ljungberg *et al.*, 2006 and Hee-Soo *et al.*, 2007) and then it direct intercalation or exfoliation in the silicate galleries is very difficult (Modesti *et al.*, 2005). There are many research to improve the polarity of PP that make the good dispersion of filler in PP matrix by using PP-g-MA (Modesti *et al.*, 2005; Fan *et al.*, 2007; Hee-Soo *et al.*, 2007; Gcwabaza *et al.*, 2008; Dong *et al.*, 2008; Yang *et al.*, 2008 and Rozanski *et al.*, 2008).

Advantages/Disadvantages

Some properties that are usually considered inherent advantages of PP are (Hanna, 1990)

- Low specific gravity (density)
- Excellent chemical resistance
- High melting point (relative to volume plastics)
- Good stiffness/toughness balance
- Adaptability to many converting methods
- Great range of special-purpose grades
- Excellent dielectric properties
- Low cost (especially, per unit volume).

Properties usually considered disadvantages of PP are

- Flammability
- Low-temperature brittleness
- Moderate stiffness
- Difficult printing, painting and gluing
- Low UV resistance
- Reduced extruder output (relative to soft/amorphous resins)
- Haziness
- Low melt strength.

2. Zinc Oxide (ZnO)

The zinc compound most frequently used is ZnO. It can be produced according to a number of different processes such as French process and American process (Porter, 1991). There are many research to study the preparation of different size and shape of ZnO such as gas condensation, hydrolysis in polyol medium, polymeric precursor method, aerosol spray pyrolysis, hydrothermal method, sol-gel process, chemical route and a solid-state microwave decomposition method (Dang *et al.*, 2003), but chemical route has attracted much attention due to the flexibility of controlling the shape and size of the structures by tuning the different growth conditions (Sharma *et al.*, 2009). ZnO has some interesting characteristics, such as wide band gap (3.20 eV), large exciton binding energy (60meV), friendliness to the environment and cheapness. One-dimensional ZnO nanostructures have been proved to be valuable candidates for many applications, such as solar cells, field emission displays, sensors and other devices (Meng *et al.*, 2008). ZnO has uses as filler for many nanocomposite such as polyamide 11 (PA11) (Meng *et al.*, 2008), low density polyethylene (LDPE) (Dang *et al.*, 2003), polyethylene glycol (PEG), polymethyl methacrylate (PMMA) (Hong et al., 2009), polyoxymethylene (POM) (Wacharawichanant et al., 2008) and etc.

3. Polypropylene-graft-maleic anhydride (PP-g-MA)

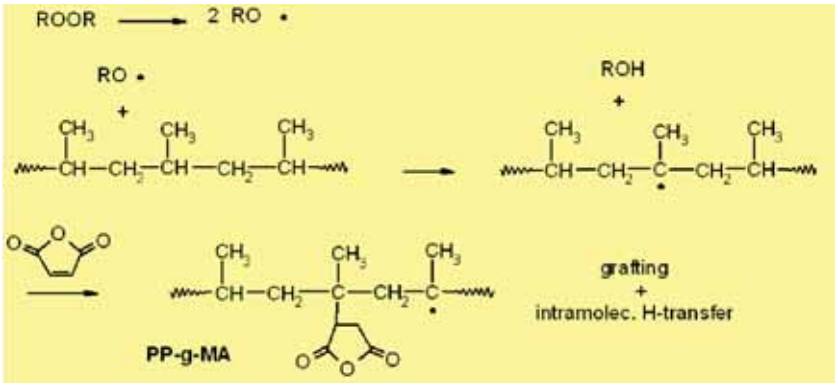

Figure 2 Grafting of Maleic Anhydride (MA) onto PP (http://otech7.tuwien.ac.at)

By reactive extrusion low-cost commercially available polymers such as polyethylene (PE), PP or polystyrene (PS) can be converted into materials with tailor-made properties of increased value. They are upgraded by chemical reactions during processing. Extruders act simultaneously as conventional polymer processing machinery and as pressure vessels for chemical synthesis in highly viscous media. Unlike organic chemistry, where the final product very often is obtained by multi-step synthesis, reactive extrusion requires high-yield one-step synthesis with very short reaction times. Only volatile unreacted monomers [e.g. maleic anhydride (MA)] and by-products can be removed in the venting section. Additional purification and separation processes are uneconomical. The modification of conventional reactor polypropylene, usually having a relatively high molecular weight (MW) and broad molecular weight distribution (MWD), in an extruder through the action of peroxides is a well-established method nowadays. In this so-called controlled rheology PP, random chain scission reactions reduce MW and narrow MWD, thus reducing viscosity and elasticity. This type of PP shows improved processing characteristics for specialized applications (e.g. lower melt processing temperatures and higher speeds in melt spinning of very thin fibers). Controlled degradation at elevated temperatures leads to low-molecular waxes. By reactive extrusion with monomers such as maleic anhydride polar functional groups are covalently bonded to the PP matrix (http://otech7.tuwien.ac.at).

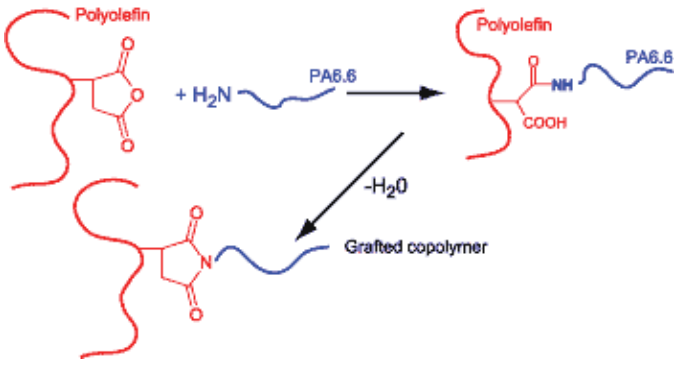

Figure 3 Reaction between a maleated polymer and -NH_2 end groups of polyamides (PA) in order to compatibilize PA/polyolefin blends (www.specialchem4 polymers.com)

Maleated resins are also used to (www.specialchem4polymers.com):

- Increase adhesion of plastics to metal.
- Improve cohesion between a polymer and fillers (ex ATH, wood, mica).
- Improve adhesion between polymer and glass fiber in thermoplastics and composites.
- Impact modification.

3. Twin screw and twin rotor processing equipment

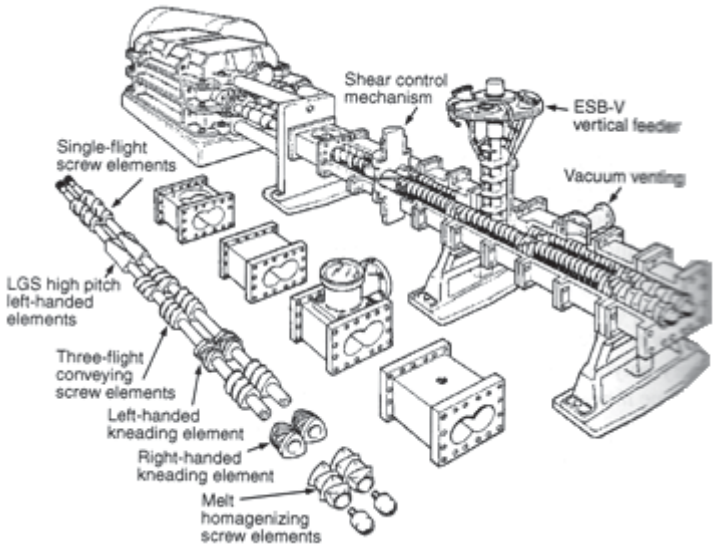

Figure 4 Schematic representation of the modular screw-element sequences and barrel sections of an intermeshing, co-rotating TSE (Tadmor, 2006)

Most twin screw-based machines are in fact extruders, and perform the same elementary polymer processing steps as single screw extruders (SSEs). However, because of the unique time-varying screw-to-screw interactions that take place in

them, which are absent in single screw-based machines, additional physical mechanisms emerge that primarily and particularly affect the elementary steps of melting and mixing. Due to these additional mechanisms, the twin-screw machines offer important advantages over single screw machines, enabling them to carry out the melting and mixing steps more efficiently and uniformly. Specifically, melting can take place in a manner involving the entire mass of the compressed particulates, which results in very rapid and uniform melting over a very short (1-2 L/D) axial length, and hence narrow residence time distribution (RTD) in the molten state. Consequently, a large amount of mechanical energy is needed in this axial rotor section to provide for the enthalpy of heating and melting. Equally important, mixing in many twin screw extruders (TSEs) benefits from the existence of three-dimensional, time-varying, extensional melt "folding" chaotic flows, generated by screw-to-screw interactions. The result is very fine and rapid dispersive mixing that, in the case of immiscible blends, is independent of the component viscosity ratio and rapid and uniform distributive mixing, requiring less twin shaft mechanical energy input, since extensional flow kinematics are very efficient for distributive mixing (Tadmor, 2006).

Typically, the TSE is custom designed to fit the process and product requirements by utilizing a wide array of interchangeable screw elements and screw element sequences "skewered" onto polygonal shafts. This capability, together with the wide use of segmented barrel sections, enables twin screw-based machines to specify or fit the location of any of the elementary steps, as well as the downstream introduction of additional component feed streams, or removal of volatiles at the needed locations. The versatility of screw and barrel design in twin screw-based machines is shown schematically in the exploded view of a common variant of such equipment, the intermeshing, co-rotating TSE. Customized and flexible screw-element and barrel segment designs, and fast and efficient melting and mixing (both dispersive and distributive) in most TSEs make such equipment very well suited and almost exclusively used for the following polymer processing operations (Tadmor, 2006):

- Very high rate postpolymerization reactor product melting and mixing with stabilizer additives in post polymerization reactor "finishing" operations.

- Polymer compounding of multicomponent/two-phase polymer systems.
- Reactive polymer processing.

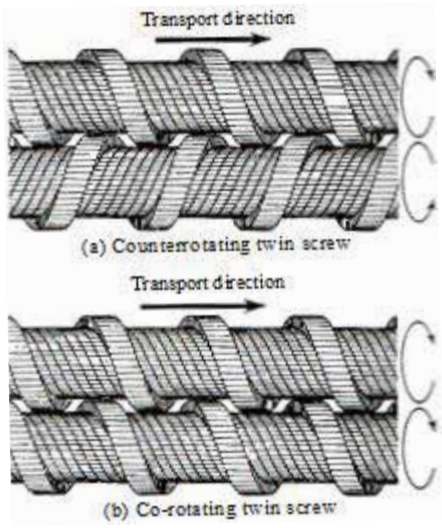

Figure 5 The counter- and co-rotating thin-flight (Tadmor, 2006)

4. Internal batch mixer

This machine has the ability to exert a high localized shear stress to the material being mixed (a nip- action) and a lower shear rate stirring (a homogenizing action). The effectiveness of dispersive mixing results from the combination of high shear stress and large shear deformation. There are two basic designs of rotor in internal mixers: nonintermeshing (e.g., Banbury, Boiling and Werner-Pfleiderer types) and intermeshing (e.g., Inter-mix and Werner-Pfleiderer types). Intermeshing rotors provide superior heat transfer and are therefore better for heat-sensitive compounds with long mixing cycles. However, in general, rotor design has little effect on internal mixer efficiency. This is probably a result of the importance of elongational flow being the result of converging flow lines irrespective of rotor design. Internal mixer design is a compromise to best accommodate the wide range of compounds typical of a manufacturing operation involving mixed product (Cheremisinoff, 1993).

5. Compression molding

Figure 6 shows the process of compression molding. The mold bottom half, containing one or more bottom cavities, is bolted to the bottom platen of the molding press. In this diagram an upward-closing press is shown. Compression molding can also be done in downward-closing presses. The mold halves are kept heated to about 150˚C, more or less, depending on the plastic being molded. A metered charge of molding compound, granular or preformed, is placed in the open bottom cavities. The press is then actuated to close, generally fast upward movement (200 to 800 in./min) until the molding material contacts the upper mold half. Then the closing speed is reduced (0 to 80 in./min) as the material in the cavities is heated by the mold and becomes fluid. As the mold continues to close, the material is forced to flow so as to fill the cavities. The metered charge contains about 3 to 5% more material than is required for the molded parts, including runner and cull. As the mold halves are moving together to fully close the cavities, the slight excess of material is squeezed out along the land surfaces, the flat areas sealing off the cavities and causing the plastic to be compressed for the polymerization or cure. The slight excess of material on the land area cures into a very thin flash, which is readily separated from the molded part following cure and removal of part from the mold (Hull, 2006).

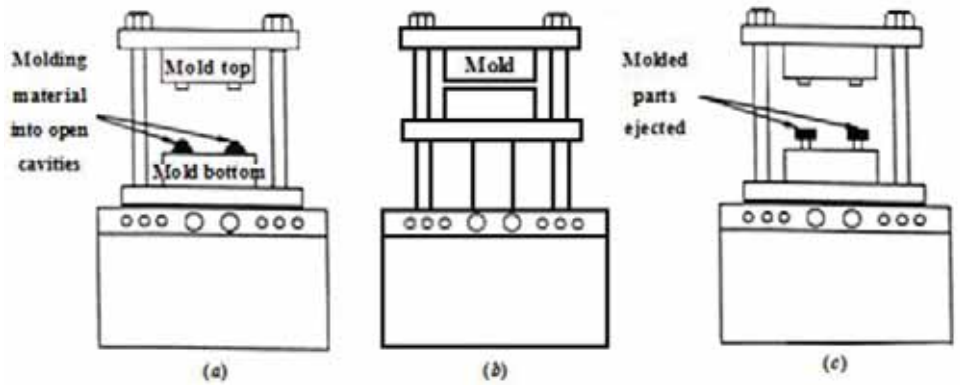

Figure 6 Compression molding sequence: (*a*) molding material is placed into open cavities; (*b*) the press closes the mold, compressing material in the hot mold for cure; (*c*) the press opens and molded parts are ejected from the cavities (Hull, 2006)

6. Mechanical properties

6.1 Tensile strength

A typical engineering stress-strain curve is shown in Figure 7. If the true stress, based on the actual cross-sectional area of the specimen, is used, it is found that the stress-strain curve increases continuously up to fracture (http://www.ndt-ed.org). Figure 8 shows the ultimate tensile strength (UTS) or, more simply, the tensile strength, is the maximum engineering stress level reached in a tension test. The strength of a material is its ability to withstand external forces without breaking. In brittle materials, the UTS will at the end of the linear-elastic portion of the stress-strain curve or close to the elastic limit. In ductile materials, the UTS will be well outside of the elastic portion into the plastic portion of the stress-strain curve. On the stress-strain curve above, the UTS is the highest point where the line is momentarily flat. Since the UTS is based on the engineering stress, it is often not the same as the breaking strength. In ductile materials strain hardening occurs and the stress will continue to increase until fracture occurs, but the engineering stress-strain curve may show a decline in the stress level before fracture occurs. This is the result of engineering stress being based on the original cross-section area and not accounting for the necking that commonly occurs in the test specimen. The UTS may not be completely representative of the highest level of stress that a material can support, but the value is not typically used in the design of components anyway. For ductile metals the current design practice is to use the yield strength for sizing static components. However, since the UTS is easy to determine and quite reproducible, it is useful for the purposes of specifying a material and for quality control purposes. On the other hand, for brittle materials the design of a component may be based on the tensile strength of the material (http://www.ndt-ed.org).

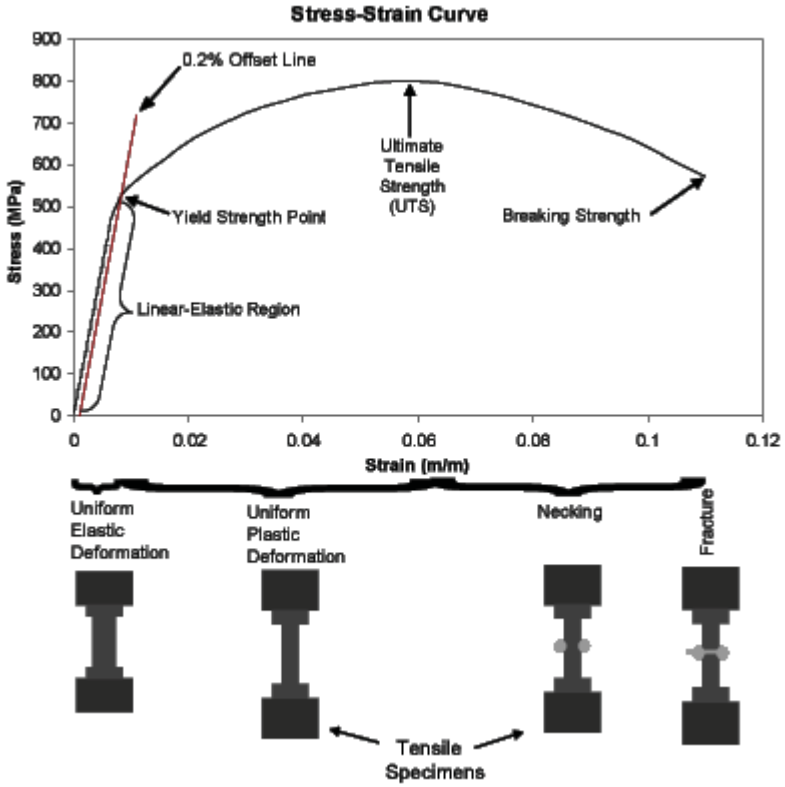

Figure 7 A typical engineering stress-strain curve (http://www.ndt-ed.org)

6.2 Elastic behavior

If only small deformations are considered and the solid material will return to its original shape when the force is relieved, then the deformation is called elastic. In elastic deformations all of the mechanical energy that was put into the material by the applied force to cause the deformation is held within the material and is then used to cause the material to return to its original shape and position. A common example would be a spring that is deformed slightly, thus imparting potential energy to the spring, which is then available within the spring to cause it to return to its original shape. Another way of saying this is that energy to returned or recovered. Energy is always recovered in elastic deformations (Brent Strong, 2006)

6.3 Yield Point

In ductile materials, at some point, the stress-strain curve deviates from the straight-line relationship and Law no longer applies as the strain increases faster than the stress. From this point on in the tensile test, some permanent deformation occurs in the specimen and the material is said to react plastically to any further increase in load or stress. The material will not return to its original, unstressed condition when the load is removed. In brittle materials, little or no plastic deformation occurs and the material fractures near the end of the linear-elastic portion of the curve. With most materials there is a gradual transition from elastic to plastic behavior, and the exact point at which plastic deformation begins to occur is hard to determine. Therefore, various criteria for the initiation of yielding are used depending on the sensitivity of the strain measurements and the intended use of the data. For most engineering design and specification applications, the yield strength is used. The yield strength is defined as the stress required to produce a small, amount of plastic deformation. The offset yield strength is the stress corresponding to the intersection of the stress-strain curve and a line parallel to the elastic part of the curve offset by a specified strain (in the US the offset is typically 0.2% for metals and 2% for plastics). Even though the yield strength is meant to represent the exact point at which the material becomes permanently deformed, 0.2% elongation is considered to be a tolerable amount of sacrifice for the ease it creates in defining the yield strength. Some materials such as gray cast iron or soft copper exhibit essentially no linear-elastic behavior. For these materials the usual practice is to define the yield strength as the stress required to produce some total amount of strain (http://www.ndt-ed.org).

- True elastic limit is a very low value and is related to the motion of a few hundred dislocations. Micro strain measurements are required to detect strain on order of 2 x 10 -6 in/in.
- Proportional limit is the highest stress at which stress is directly proportional to strain. It is obtained by observing the deviation from the straight-line portion of the stress-strain curve.
- Elastic limit is the greatest stress the material can withstand without any measurable permanent strain remaining on the complete release of load. It is

determined using a tedious incremental loading-unloading test procedure. With the sensitivity of strain measurements usually employed in engineering studies (10 - 4in/in), the elastic limit is greater than the proportional limit. With increasing sensitivity of strain measurement, the value of the elastic limit decreases until it eventually equals the true elastic limit determined from micro strain measurements.

- Yield strength is the stress required to produce a small-specified amount of plastic deformation. The yield strength obtained by an offset method is commonly used for engineering purposes because it avoids the practical difficulties of measuring the elastic limit or proportional limit (http://www.ndt-ed.org).

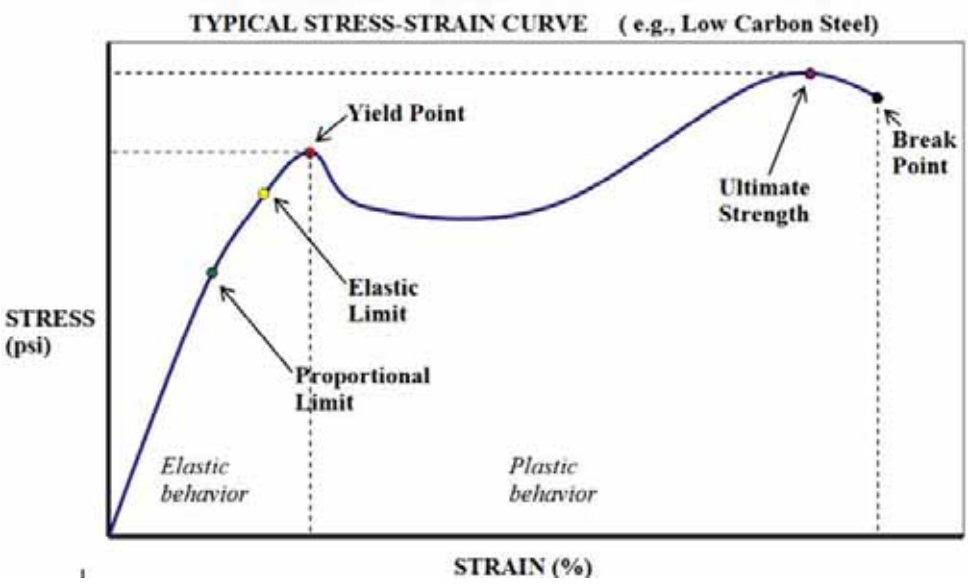

Figure 8 Example of stress-strain curve (www.gxsc.typepad.com).

6.4 Measures of Ductility

Figure 9 shows the ductility of polymer in stress-strain curve. The ductility of a material is a measure of the extent to which a material will deform before fracture. The amount of ductility is an important factor when considering forming operations such as rolling and extrusion. It also provides an indication of how visible overload damage to a component might become before the component fractures. Ductility is also used a quality control measure to assess the level of impurities and proper processing of a material. The conventional measures of ductility

are the engineering strain at fracture (usually called the elongation) and the reduction of area at fracture. Both of these properties are obtained by fitting the specimen back together after fracture and measuring the change in length and cross-sectional area. Elongation is the change in axial length divided by the original length of the specimen or portion of the specimen. It is expressed as a percentage. Because an appreciable fraction of the plastic deformation will be concentrated in the necked region of the tensile specimen, the value of elongation will depend on the gage length over which the measurement is taken. The smaller the gage length the greater the large localized strain in the necked region will factor into the calculation. Therefore, when reporting values of elongation, the gage length should be given. One way to avoid the complication from necking is to base the elongation measurement on the uniform strain out to the point at which necking begins. This works well at times but some engineering stress-strain curve are often quite flat in the vicinity of maximum loading and it is difficult to precisely establish the strain when necking starts to occur. Reduction of area is the change in cross-sectional area divided by the original cross-sectional area. This change is measured in the necked down region of the specimen. Like elongation, it is usually expressed as a percentage (http://www.ndt-ed.org).

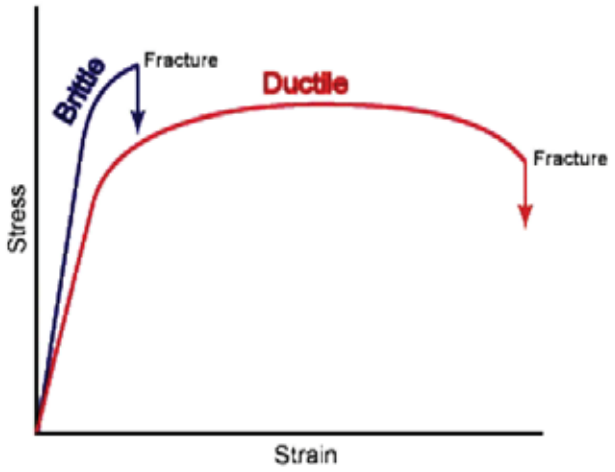

Figure 9 Ductility of polymers in stress-strain curve (http://www.ndt-ed.org)

Impact strength

Generally, the toughness of a material is much more important when the force is applied suddenly in an impact rather than over a relatively long period of time, as it is done in the stress-strain experiment. Therefore, a property called impact toughness (sometimes called impact strength) is defined as the energy absorbed by a material upon sudden impact. Impact toughness is strongly dependent upon the ability of the material to internally move or deform to accommodate the impact. This movement is related to elongation or strain. Therefore, materials that exhibit high elongation are often tough, especially if they also have good strength. However, the modulus is usually low in these materials (low stiffness). Hence, materials with high elongation and low modulus are called tough, and material with low elongation and high modulus are called brittle (the opposite of toughness). High molecular weight favors high toughness. These results from the combination of higher strength and better sharing of the impact force along the polymer chain by causing more atoms to rotate, vibrate, and stretch to absorb the energy of the impact. Crystallinity gives higher strength but lower toughness unless the nature of the backbone changes. For instance, even though nylon is crystalline, the ability of this material to absorb energy by passing the energy from one molecule to another through intermolecular forces makes it very tough. Crosslinking of a brittle polymer will usually decrease toughness because of the increased limitation of motion within the polymer mass caused by the intermolecular bonds, but crosslinking of a flexible polymer will increase impact toughness because of the greater ability to the polymer to transfer the eneygy (Brent Strong, 2006).

The Izod and Charpy tests (ASTM D 256) utilize a pendulum-impact testing device (illustrated in Figure 10). The sample is clamped in the sample holder either vertically (for Izod) or horizontally (Charpy) and may have a notch cut in it to initiate the rupture. In the Charpy and Izod tests, the pendulum will generally break the sample and continue its path beyond the impact point. Some of the energy in the pendulum will be absorbed in the breaking of the sample; therefore, it will not swing as high after the impact as before the impact. The reduction in height (potential energy) can be related directly to the energy absorbed by the sample. A pointer, which

is pulled by the pendulum and then stops at the maximum height, records the maximum height of the swing. Hence, the energy absorbed from the impact can be measured from the height of the pointer. This energy absorbed is a measure of the toughness of the sample. The samples are typically $\frac{1}{8} \times \frac{1}{2} \times 2$ inches but can be of other thicknesses up to $\frac{1}{2}$ inch. The thickness strongly influences the test results, so precise thickness measurement is required. The results are usually expressed as impact toughness (Izod or Charpy) with units of foot-pound/inch or J/m (Brent Strong, 2006).

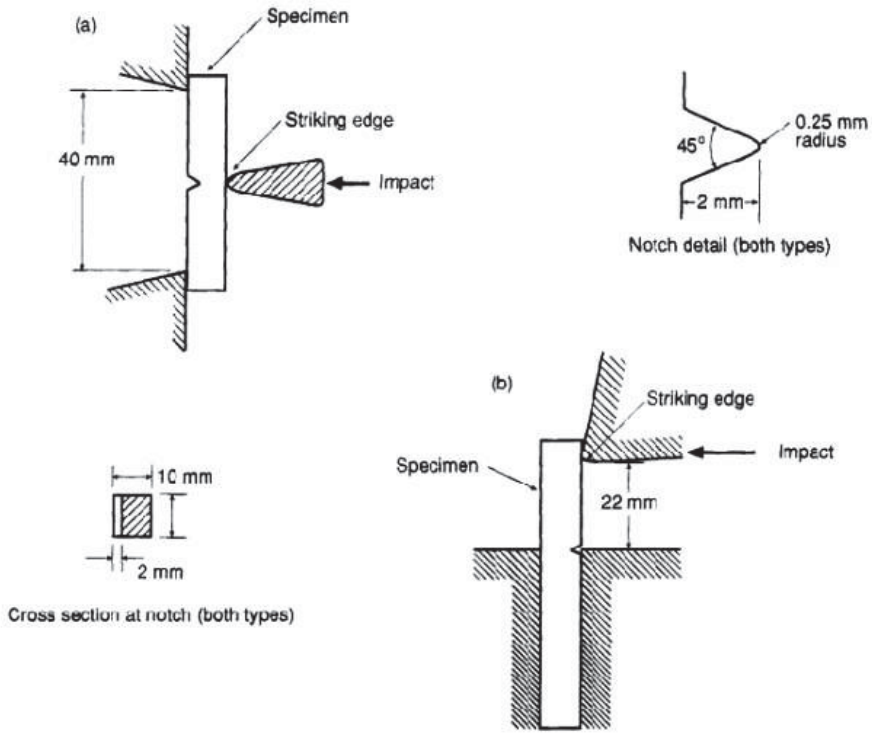

Figure 10 Specimens and loading configurations for (a) Charpy V-Notch and (b) Izod Tests (www.civilx.unm.edu)

7. Thermal properties

TGA is one of the members of the family of thermal analysis techniques used to characterize a wide variety of materials. TGA provides complimentary and supplementary characterization information to the most commonly used thermal

technique, DSC. TGA measures the amount and rate (velocity) of change in the mass of a sample as a function of temperature or time in a controlled atmosphere. The measurements are used primarily to determine the thermal and/or oxidative stabilities of materials as well as their compositional properties. The technique can analyze materials that exhibit either mass loss or gain due to decomposition, oxidation or loss of volatiles (such as moisture). It is especially useful for the study of polymeric materials, including thermoplastics, thermosets, elastomers, composites, films, fibers, coatings and paints. TGA measurements provide valuable information that can be used to select materials for certain end-use applications, predict product performance and improve product quality. The technique is particularly useful for the following types of measurements:

- Compositional analysis of multi-component materials or blends
- Thermal stabilities
- Oxidative stabilities
- Estimation of product lifetimes
- Decomposition kinetics
- Effects of reactive atmospheres on materials
- Filler content of materials
- Moisture and volatiles content (www.depts.washington.edu).

The example graph is obtained by TGA is shown in Figure 11.

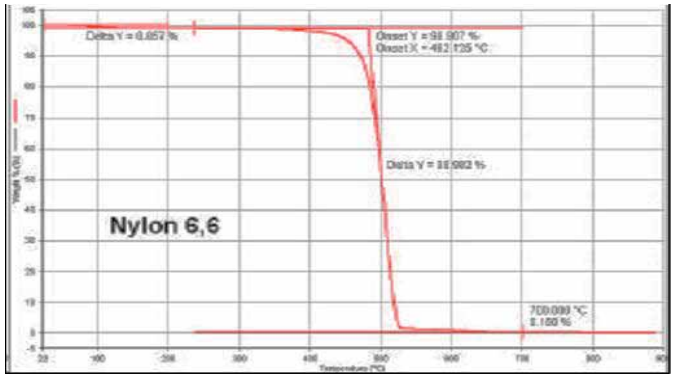

Figure 11 TGA results obtained for nylon 6, 6 bristles showing thermal degradation (www.depts.washington.edu)

In DSC, the thermal properties of a sample are compared against a standard reference material which has no transition in the temperature range of interest, such as powdered alumina. Each is contained in a small holder within an adiabatic enclosure as illustrated in Figure 12 (www.plc.cwru.edu).

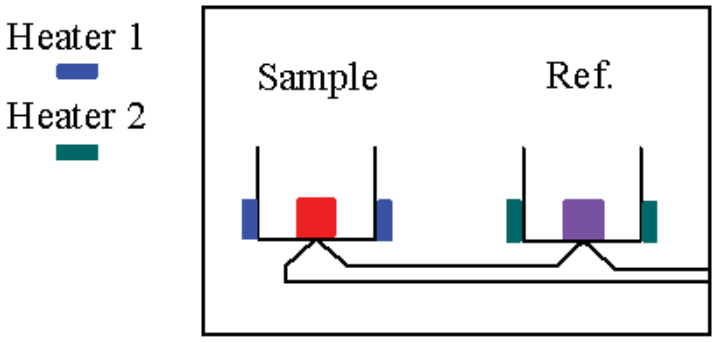

Figure 12 Sample and reference contained in a small holder within an adiabatic enclosure (www.plc.cwru.edu)

The temperature of each holder is monitored by a thermocouple and heat can be supplied electrically to each holder to keep the temperature of the two equal. A plot of the difference in energy supplied to the sample against the average temperature, as the latter is slowly increased through one or more thermal transitions of the sample yields important information about the transition, such as latent heat or a relatively abrupt change in heat capacity. The glass transition process is illustrated in the Figure 13 for a glassy polymer which does not crystallize and is being slowly heated from below glass transition temperature (T_g) (www.plc.cwru.edu).

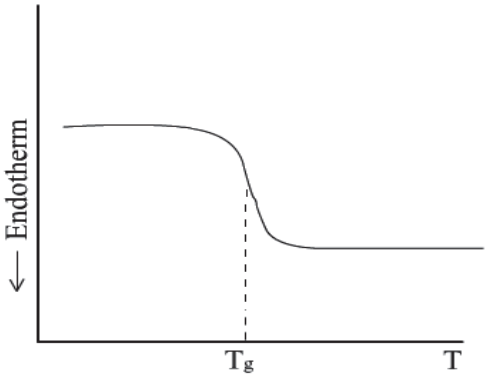

Figure 13 The glass transition process (www.plc.cwru.edu)

Here, the drop marked T_g at its midpoint represents the increase in energy supplied to the sample to maintain it at the same temperature as the reference material, due to the relatively rapid increase in the heat capacity of the sample as its temperature is raised through T_g. The addition of heat energy corresponds to this endothermal direction. A melting process is also illustrated in Figure 14 for the case of a highly crystalline polymer which is slowly heated through its melting temperature (www.plc.cwru.edu):

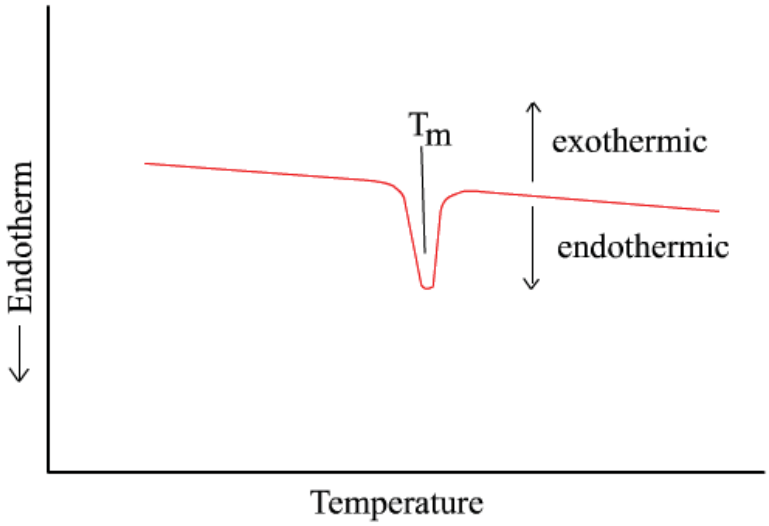

Figure 14 A melting temperature processes of DSC (www.plc.cwru.edu)

Again, as the melting temperature (T_m) is reached, an endothermal peak appears because heat must be preferentially added to the sample to continue this essentially constant temperature process. The peak breadth is primarily related to the size and degree of perfection of the polymer crystals. If the process were reversed so that the sample was being cooled from the melt, the plot would be inverted. In that case, as both are being cooled by ambient conditions, even less heat would need to be supplied to the sample than to the reference material, in order that crystals can form. This corresponds to an exothermal process. Use of the DSC will be illustrated again in the section on liquid crystals in connection with the identification of their phase transitions. An interesting exercise for the reader would be to predict the general form of a DSC plot for a semicrystalline polymer which has been rapidly quenched from the melt to a temperature below T_g. In the DSC plot, assume the temperature is slowly

increased from this value below T_g to a value well above, thus allowing for significant increases in the chain mobility as temperatures above T_g are reached so that some crystallization can begin, well before the melting point is reached (www.plc.cwru.edu).

8. Electrical properties

The basic electrical properties of all materials are related to the ease of formation of a conductive path through or along the surface of the material, such as metals, the sea of electrons that bind the metal ions together can move freely throughout the metal structure and thus provide a conductive path. Metals are, therefore, highly conductive. In other materials, charged atoms (ions) can move freely within a solution, such as salt dissolved in water. These, too, are conductors. The electrons and ions in plastics and ceramics are much more restricted except in some special cases of conductive polymers. Therefore, plastics are not usually conductive to electricity but are, instead, insulators. Some caution should be exercised, however, in using the terms conductor and insulators to describe any particular material because the terms are really comparative in nature and not absolute. For instance, most plastics would normally be considered as insulators but that is only as compared to common conductor such as metals. A specific plastic material could be considered a limited conductor if compared to some other plastic material with much lower conductivity. Polyvinylchloride (PVC) is, for instance, an insulator when compared to copper but is a conductor, or at least is more conductive, when compared to polytetrafluoroethylene (PTFE). Several electrical properties measure the tendency of a material to form a conductive path under different conditions. The most common of these properties are resistivity, dielectric strength, arc resistance, dielectric constant, and dissipation factor (Brent Strong, 2006). But in this research will discuss only dielectric constant.

Dielectric constant

Dielectric constant or permittivity is a measure of how well the insulative material will act as a dielectric in a capacitor. This constant is defined as the capacitance of the material in question compared (by ratio) with the capacitance of a vacuum. A high dielectric constant indicates that the material is highly insulative, thus permitting the use of small (thin) dielectric material in capacitors. Dielectric constants are dependent upon temperature and the frequency of the alternating electric field that is applied to the sample. The test for dielectric constant or permittivity is ASTM D 150. In the test, a carefully conditioned sample is placed between plates that are then charged, as they would be in a capacitor. The leakage current is measured and compared to the situation that would exist were a vacuum to exist between the plates. Nonpolar polymers would generally have a dielectric constant in the 2-3 range; polar polymer can range up to 7. (Pure water, by comparison, has a dielectric constant of 80.) Some applications require a high dielectric constant (such as a microwave dish), whereas others require a low dielectric constant (such as a capacitor). In either case, the ability of the plastic material to dissipate the charge placed upon it is also important. This property is called the dissipation factor (Brent Strong, 2006).

CHAPTER 3

LITTELATURE REVIEW

This chapter contains the research review of polymer composites properties, compatibilizing agents for polymer composites and zinc oxide synthesis.

1. Polymer composites properties

Cho *et al.* (2001) studied the properties of Nylon 6/organoclay nanocomposites. The composites were prepared by using a conventional twin screw extruder. They found that the organoclay was well exfoliated into the nylon 6 matrix when compounded with the twin screw extruder. The mechanical properties of the organoclay nanocomposites were significantly increased with marginal decrease of ductility and showed much greater values than glass fiber composites.

Chi-Ming *et al.* (2002) used Irganox 1010 as anti-oxidant in PP filled with $CaCO_3$ nanocomposites. They found that the notched fracture toughness of PP/$CaCO_3$ nanocomposites had substantially higher than pure PP. The nanoparticles were distributed in the PP matrix uniformly and little particle agglomeration at 4.8 and 9.2 vol%, this should maximize the interfacial interaction between the nanoparticles and the polymer. The DSC results indicated the presence of a small amount of β phase PP after the addition of the $CaCO_3$ nanoparticles. In addition, the crystallization temperature of PP was increased by approximately 10°C, when $CaCO_3$ was added to the PP, implying that the $CaCO_3$ nanoparticles were a very effective nucleating agent. Fractography of the broken specimens from the J-integral tests suggested that the nanoparticles introduced a massive number of stress concentration sites in the matrix and promoted cavitation at the particle-matrix boundary when loaded. The cavities, in

turn, released the plastic constraint and trigger large-scale plastic deformation of the matrix, which consumed tremendous fracture energy.

Zuiderduin *et al.* (2003) studied the effect of particle sizes and surface treatment of $CaCO_3$ on toughening property of PP. They used stearic acid to treatment $CaCO_3$. They found that the modulus of the composites increased, while the yield stress was lowered with filler content. The particle content and particle size showed no effect on the thermal properties. The stearic coating on the particle surface showed a large positive effect on the impact strength may be due to the improved dispersion of the $CaCO_3$ particles. Aggregates of particles had an effect on the impact behavior of the composites. The smaller particle sizes showed coarse morphologies and this lowered the toughening efficiency. Moreover, they found the molecular weight of the PP matrix had an effect on the toughening properties.

Bose *et al.* (2004) studied the effects of adding mica with variable particle size on the mechanical, thermal, electrical and rheological properties of nylon-6 was investigated. Composites of nylon-6 with varying concentrations (viz. 5 to 40 weights %) of mica were prepared by twin screw extrusion. The composites showed improved mechanical, thermal as well as electrical properties on addition of filler. It was also observed that mechanical and electrical properties as well as thermal properties were increased with decrease in particle size.

Chatterjee *et al.* (2006) prepared PP filament incorporating 1% carbon nanofibre by using conventional fibre processing equipment and drawn to a high draw ratio using 'Gradient Drawing' system. Nanocomposite filament at 1% loading of carbon nano fibres had tensile modulus of 16.8 GPa and tensile strength of 770 MPa at room temperature. These samples also had dynamic modulus values of 29 GPa at K70 8C. For neat PP filaments, the corresponding values were tensile modulus of 16.4 GPa and tensile strength of 670 MPa and dynamic modulus of 20 GPa. Nanocomposite filament properties were related to the presence of large number of oriented amorphous molecules and relatively low crystallinity. Further, the nanofibres

act as reinforcements to improve dynamic modulus and possibly bridge the microvoids, thereby enhancing the tensile strength.

Yang *et al.* (2006) studied the morphologies and mechanical properties of PP with different intrinsic toughness filled with four sizes of $CaCO_3$ particles (25, 4, 1.8 and 0.07 μm). It was cleared that the PP matrix and filler size had key effects on improvement of mechanical properties of PP matrix. It was found that, the yield strength, the flexural strength and modulus of composites filled with $CaCO_3$ 0.07 μm were lower than composites filled with other sizes of particles but it had the best toughening effect to improve the impact strength of PP matrix.

Zhao *et al.* (2006) studied the photo-degradation characteristics for ZnO nanoparticle filled PP nanocomposites. By paying attention to the evolution of the carbonyl absorption bands from fourier transform infrared spectroscopy (FTIR) analysis, it has been observed that UV irradiation induced significant photo-degradation for unfilled PP. However, with the incorporation of ZnO nanoparticles into the PP matrix found that the extent of photodegradation was significantly reduced. This is due to the superior UV light screening effects offered by the ZnO nanoparticles. Wide angle x-ray diffraction (WAXD) measurements showed that β-form PP crystal had been induced in the PP/ZnO nanocomposites. An interesting observation from this study was that β-form PP crystal was also induced in unfilled PP due to UV irradiation. UV-irradiation induced degradation caused a significant dropped in the ductility for unfilled PP. With the incorporation of ZnO nanoparticles, the ductility, and the tensile strength were recovered to some extent. The ZnO content filled in treated nanocomposites had higher elongation at break value in the UV irradiation. It was also observed that surface cracks were induced by photo-degradation, and the Talysurf surface profile measurements indicated that the severity of the surface cracks were significantly reduced in the ZnO/PP nanocomposites.

Avella *et al.* (2007) studied the mechanical properties of PMMA filled with modified $CaCO_3$ nanoparticles. They grafted polybutylacrylate (PBA) chains onto $CaCO_3$ nanoparticle surface. They found that homogeneous and find dispersion of nanoparticles into PMMA as well as strong interfacial adhesion between the two

phases. Both unmodified and modified $CaCO_3$ were responsible for an increase of the Young's modulus and significantly improved the abrasion resistance of PMMA.

Golebiewski *et al.* (2007) studied the thermo oxidative and thermal stability of PP nanocomposite with highly exfoliated montmorillonite (MMT) by simultaneous measurements by DSC and TGA methods in a wide temperature range. In this studied, they used PP-g-MA as compatibilizer for PP/MMT nanocomposites. They found that in oxygen-free atmosphere the thermal degradation of PP in nanocomposites was strongly inhibited up to the temperature of 420˚C and the degradation beginning with 300˚C. Exfoliated clay platelets modified with alkylammonium salt exhibited a strong stabilizing effect on PP macromolecules in oxygen-free atmosphere.

Lu *et al.* (2007) studied wood-(nylon 12) composites and compared them with wood-PP composites and wood- high density polyethylene (HDPE) composites in terms of mechanical properties, thermal properties and interfacial morphology. They found that wood-(nylon 12) composites had higher modulus of rupture, elasticity and tensile strength than nylon 12, wood-PP composites and wood-HDPE composites. They explained that wood increased the crystallization temperature and the degree of crystallinity of nylon 12 in wood-(nylon 12) composites. The improved in mechanical properties can be explained that the good interfacial adhesion between wood and nylon 12 and the increased transcrystallinity of nylon 12 by wood.

Mittal (2007) prepared PP nanocomposites with different volume fractions of the obtained organo-montmorillonite (OMMT) and the effect of the modified clay on the gas barrier and mechanical properties was studied. WAXRD and transmission electron microscopy (TEM) were used to investigate the microstructure obtained. Thermal behavior of the composites analyzed by TGA was observed to enhance significantly with the filler volume fraction. The gas permeation through the nanocomposite films markedly decreased with augmenting the filler volume fraction. The decrease in the gas permeation was even more significant than through the composites with ammonium treated MMT. Better thermal behavior of the organic modification owing to the delayed onset of degradation hindered the interface

degradation along with detrimental side reactions with polymer itself. Transmission electron microscopic studies indicated the presence of mixed morphology i.e., single layers and the tactoids of varying thicknesses in the composites. The crystallization behavior of PP remained unaffected with OMMT addition. A linear increase in the tensile modulus was observed with filler volume fraction owing to partial exfoliation of the clay.

Sharma *et al.* (2009) studied dielectric behavior of polyaniline (PANI)/ZnO composite. They found that dielectric constant of PANI/ZnO composite film was found to be smaller than the PANI film. The decrease of dielectric constant in PANI–ZnO films as compared to PANI was attributed to the interfaces formed between ZnO particles and PANI.

2. Compatibilizing agents for polymer composites

O' Donnell *et al.* (1995) studied the effect of PP-g-MA on mechanical properties of PP/liquid-crystalline polymer (PP/LCP). In this research, three LCPs were used. One LCP was a poly(ester amide) and the other two LCPs were copolyesters. They found that the addition of PP-g-MA to the PP phase leaded to significant mechanical property improvements in PP/LCP blends. The tensile strength for all three PP/LCP blends increases as the content of PP-g-MA was increased. These increases were dependent upon the particular LCP. It appeared that the properties of the copoly(ester amide), Vectra B950 LCP which can undergo strong hydrogen bonding, were strongly affected by the concentration of PP-g-MA. The addition of PP-g-MA to PP/LCP blends revealed increased dispersion of the LCP phase, reduced interfacial tension between the phases and enhanced adhesion, which were characteristics of compatibilized thermoplastic blends. The use of PP-g-MA in these PP/LCP blends leaded to improved tensile properties as opposed to improved impact strength and toughness observed in thermoplastic blends. The addition of PP-g-MA to these blends leaded to a finer dispersion of LCP within the matrix but with a more fibrillar structure being formed, which leaded to reinforcement of the matrix.

Chun *et al.* (2002) studied tensile performance and fractured surfaces of PP filled with silica with average diameter of 15 nm. They modified nano-silica (SiO_2) by grafting nano-SiO_2 with styrene and ethyl acrylate. They found that tensile tests showed the nanoparticles can simultaneously provide PP with stiffening, strengthening and toughening effects at a rather low filler content. The presence of grafting polymers on the nanoparticles improved the tailorability of the composites.

Lee *et al.* (2005) studied a partially intercalated/exfoliated PE/clay nanocomposite was successfully synthesized using the melt-intercalation method with PP-g-MA compatibilizer and a swelling agent. The x-ray diffraction (XRD) analysis and TEM observations depicted partially intercalated/exfoliated, well-dispersed nanoclays in the composite. The mechanical and gas barrier properties improved as the clay content increased. Dynamic mechanical analysis (DMA) tests also showed the good reinforcing effects of the nanoclays and good processability of the nanocomposites. However, introducing nanoclays decreased the temperature for the onset of thermal decomposition.

Modesti *et al.* (2005) studied the influence of processing conditions on the nanocomposites structure, i.e. intercalated or exfoliated, and on the enhancement of mechanical properties of PP nanocomposites. These nanocomposites were prepared using the melt intercalation technique in a co-rotating intermeshing twin screw extruder. In order to optimise processing conditions, both screw speed and barrel temperature profile were changed. The role of the compatibilizer (PP-g-MA) was also studied. The results showed that the barrel temperature was a very important parameter: using lower processing temperature, the apparent melt viscosity and, consequently, the shear stress were higher and, therefore, the exfoliation of the clay was promoted. Even using optimized processing conditions, exfoliation of clay can be achieved only when a high compatibility between polymer and clay exists: the PP nanocomposites containing MA show an exfoliated structure and a sensible enhancement of mechanical properties while PP nanocomposites without compatibilizer showed a structure mainly intercalated and a lower improvement of mechanical properties.

Ljungberg *et al.* (2006) studied the quality of dispersion of cellulose whiskers on properties of nanocomposite films of isotactic PP. They used PP as polymer matrix and three types of cellulose whisker. The first type of whiskers had no surface modification. The second type was a whiskers grafted with PP-g-MA. The final type was novel surfactant-modified coated whiskers. They found that the second type whiskers had better dispersion than the first type whiskers but the third type whiskers had the best dispersion. The high dispersion quality induced enhanced mechanical properties at large deformation at room temperature.

Hee-Soo *et al.* (2007) studied the effect of types of PP-g-MA on the interfacial adhesion properties of bio-flour-filled PP composites. They used five different PP-g-MA types with different %MA. They found that the enhanced interfacial adhesion, mechanical and thermal stability of the PP-g-MA -treated composites was strongly dependent on the high amount of MA graft (%) and the PP-g-MA molecular weight. The morphological properties of the PP-g-MA-treated composites showed strong bonding and a paucity of pulled-out traces from the matrix in the two phases.

Yang *et al.* (2007) studied the effect of compatibilizing agents on mechanical properties and morphology of a lignocellulosic material-thermoplastic polymer composite. Using rice-husk flour as the reinforcing filler and PP as the thermoplastic matrix polymer, a particle-reinforced composite was prepared, and its mechanical and morphological properties examined as a function of the amount of compatibilizing agent used. In the sample preparation, four levels of filler loading (10, 20, 30 and 40 wt%) and three levels of compatibilizing agent content (1, 3 and 5 wt%) were used, and in the tensile test, six test temperatures (-30, 0, 20, 50, 80 and 110 °C) and five crosshead speeds (2, 10, 100, 500 and 1500 mm/min) were used. The tensile strengths of the composites decreased as the filler loading increased, but the tensile properties were significantly improved with the addition of the compatibilizing agent. Both the notched and unnotched Izod impact strengths were almost the same with the addition of compatibilizing agent. A morphological study revealed that the positive effect of compatibilizing agent on interfacial bonding.

Suryadiansyah *et al.* (2008) studied the effect of two compatibilizers (ethylene diamine dilaurate (EDD) and PP-g-MA on mechanical properties, water absorption, morphology and thermal properties of Sio_2-filled PP composites. They found that both of compatibilizer improved Young's modulus, the tensile strength, impact and flexural strength, and water absorption resistance with increasing compatibilizer content. For compared with two compatibilizers, EDD had higher impact and flexural strength but lower tensile strength, Young's modulus and water absorption resistance than MAPP. Thermal analysis results indicated that the addition of EDD or MAPP slightly increased the thermal stability of PP/Sio_2 composites and had higher heat fusion and crystallinity than similar composites but without compatibilizer.

Ravindra Reddy *et al.* (2010) studied the physical properties of PP filled with wheat straw and organo-clay composites. They used MD-353D as compatibilizer (PP-g-MA from Dupont). The composite samples were prepared through melt blending method using a co-rotating twin-screw extruder. They found that the increase in wheat straw increased the flexural modulus and reduced the resistance for water absorption. The increase in PP-g-MA coupling agent also increased the flexural modulus and the resistance for water absorption this may due to the addition of coupling agent increased the interfacial adhesion between the fibers and polymer matrix which was evidenced further from increased flexural modulus. Further, increasing organo-clay slightly increased the flexural modulus and reduced the resistance to water absorption.

De la Orden *et al.* (2010) studied the effect of two coupling agents on the discoloration of composites made from cellulose and PP. They used polyethylenimine (PEI) and PP-g-MA as coupling agents. They found that both PP-g-MA and PEI increased the browning, but the two mechanisms were clearly different. The coupling agent increased the fibre-matrix adhesion, which increased the frictional degradation of cellulose during the melt processing of the composites. This increased frictional degradation favours the following degradation and discoloration processes.

Franco-Marquès *et al.* (2011) studied the influence of the intrinsic parameters of different PP-g-MA coupling agents to determine the effect of its acid number as

well as molecular weight in mechanical properties of composites reinforced with low cost reinforcements. They found that high functionalized PP-g-MA coupling leaded to important improvements in mechanical stresses and also a lower capacity of water absorption due to the formation of thinner interfaces. The high molecular weight PP-g-MA agents had higher mechanical strength than plain polymer matrix that conducted to an interesting increased in unnotched Charpy impact strength attributed to a low dispersion of the coupling agent in the matrix during mixing process keeping microdomains that help to avoid crack propagation.

3. Zinc oxide synthesis

Lili *et al.* (2005) prepared ZnO nanorods by hydrothermal method with synthesized $ZnCl_2 \cdot 4Zn(OH)_2$ as precursors in an autoclave. They found that morphologies of the nanorods were controlled by various reaction conditions with cetyltrimethylammonium bromide (CTAB) as modifying agent. The UV-Vis spectra indicated that the as-prepared ZnO nanorods had absorption of visible light as well as ultraviolet light.

Tonto *et al.* (2006) studied the preparation of ZnO nanorod by solvothermal reaction of zinc acetate in various alcohols. They used four types of alcohol eg. 1-butanol, 1-hexanol, 1-octanol and 1-decanol. They found that average diameter and length of the nanorods increased with an increase in reaction temperature or the initial concentration of zinc acetate. The aspect ratio of the product depended upon type of alcohol used as the reaction medium. The aspect ratio of ZnO nanorods increased with molecular chain of alcohol increased.

Young Joon *et al.* (2006) studied ZnO nanoparticles and its nano-crystalline particles on the photocatalytic degradation of methylene blue. They synthesized ZnO and its nano-crystalline particles by sprayed droplets of an aqueous zinc nitrate solution by flame spray pyrolysis and spray pyrolysis assisted with an electrical furnace. By this method, they had ZnO with average particles diameter of 20 nm and they found that photoactivity of the ZnO nanoparticles of 20 nm was higher than that

of the ZnO nano-crystalline particles of 20 nm in mean grain size. The efficiency of photodegradation of methylene blue using two kind of ZnO photocatalyst has been found to increase with increase in catalyst loading and decrease in initial concentration regardless of particle morphology.

Chang-Chun *et al.* (2008) studied the synthesis of nano-sized ZnO powders by direct precipitation method. They used the precipitated from method via reaction between zinc nitrate ($Zn(NO_3)_2$) and ammonium carbonate ($(NH_4)_2CO_3$) in aqueous solution as precursor. The precursors were calcined at a temperature of 550˚C for 2 h in the muffle furnace to obtain the nano-sized ZnO particles. They found that nano-sized ZnO particles were of pure wurtzite structures with the average crystalline sizes in 35.2 nm. The direct precipitation process for the fabrication of the nano-sized ZnO powders was well repeatable and easy controlled. The further improvement in experimental condition for the nano-sized ZnO particles with superfine grain size, good distribution, large specific surface area, and less agglomeration synthesized by direct precipitation is under way.

Shuang *et al.* (2008) studied one step method to synthesize nano/micron-sized ZnO sphere. They used the solution between zinc nitrate hexahydrate ($Zn(NO_3)_2 \cdot 6H_2O$) and triethanolamine (TEA). The mixed solution was transferred into a Teflon-lined autoclave and maintained at 160˚C for 2 h without stirring after that the products were dried at 60 ˚C. They found that ZnO spheres formed by the agglomeration of nano-particles have been synthesized by a hydrothermal method. Volume ratios of TEA to H_2O have been used to control the diameter of ZnO spheres.

Singh *et al.* (2008) studied the sensing response of ZnO nanoparticles and nanorods to ethanol vapours has been reported in this paper. ZnO powder has been synthesized as nanoparticles and nanorods by following a chemical route. The reaction temperature was found to be playing a critical role in the selective synthesis of morphologically distinct nanostructures. Synthesized ZnO powder was characterized by using TEM and XRD techniques. ZnO samples were deposited as thick films to act as gas sensors and their comparative response to ethanol vapors was investigated at different temperatures and concentrations. In this work the effect of

sintering temperature on the particle-size and sensor-sensitivity was also studied. The studies revealed that particle-size increases with the sintering temperature while sensitivity decreases. The investigations also revealed that sensing response of ZnO nanoparticles is exceptionally higher than that of ZnO nanorods.

Wei *et al.* (2008) studied synthesized ZnO rods by wet chemical method. They used bare glass as substrate for prepared ZnO rods using wet chemical method. They used different experimental parameter, such as the reactant concentration and the growth time. They found that the ratio of the length to diameter decreased with increasing the reaction concentration but increased weakly with the growth time.

CHAPTER 4

EXPERIMENTAL PROCEDURE

This chapter describes the research experimental procedure for sample preparation, materials and characterization of PP/ZnO composites without and with compatibilizer.

1. Materials

Pure PP (Mophen HP400K) was produced by HMC Polymer Co., Ltd with the melt flow rates 4 dg/min. PP-g-MA, Fusabond MZ-109D with MA content 0.55 wt% and MD-353D with MA content 1.305 wt% as compatibilizers were supplied by Chemical Innovation Co.,Ltd. The melt flow rates of the compatibilizers are 120 g/10 min and 450 g/10min, respectively. Zinc stearate with molecular weight 632 g/mol, was purchased from S.R.LAB Co.,Ltd. ZnO sphere in a form of a white powder with average particle sizes of 71 nm and 250 nm was purchased from Aldrich and S.R. LAB Co., Ltd, respectively. ZnO with rod shape and ZnO with sphere shape 100 nm were synthesized in our laboratory.

2. Synthesis of ZnO nanorod and nanoshpere

ZnO nanorods were synthesized by simple chemical route method, starting with a 0.2 M solution of zinc chloride ($ZnCl_2$) in DI water, adding ammonium hydroxide (NH_4OH) dropwise at room temperature with continuous stirring to yield precipitates of zinc hydroxide (ZnOH). The precipitates obtained were separated from a rest of the liquid by filtering and were dried into powder at 120 ˚C. The powder thus obtained was crushed and sintered in an air at the temperatures of 400 ˚C for 3 hours (Singh, 2008).

ZnO nanospheres 100 nm were synthesized by 0.2 M solution of $ZnCl_2$ in DI water, NH_4OH was dropped in the solution at 50 ˚C with continuous stirring to yield precipitates of ZnOH. The precipitates obtained were separated from a rest of the liquid by filtering and were dried into powder at 120 ˚C. The powder thus obtained was crushed and sintered in an air at the temperatures of 400 ˚C for 3 hours (Singh, 2008).

3. Preparation of the nanocomposites

Pure PP pellets, PP-g-MA (MZ-109D and MD-353D) pellets, zinc stearate and ZnO particles were dried in an oven at 100 ˚C for 3 hours before mixing.

3.1 PP/ZnO composites were prepared by a twin screw extruder

Figure 15-17 show the experimental steps for PP/ZnO composites by using a twin screw extruder in this research. The PP/ZnO composites were melted compounding in a twin screw extruder without and with compatibilizer at temperatures in a range of 160-210 ˚C and a screw rotation rate of 50 rpm as shown in Figure 19. The extrudates were palletized at the die exit. After compounding, the composites were compression molded into a standard dumb-bell tensile bars and rectangular bars by using compression molding as shown in Figure 20. Hot-press procedures involved preheating at 190 ˚C for 5 min followed by compressing for 15 min at same temperature, and subsequent cooling under pressure for 10 min.

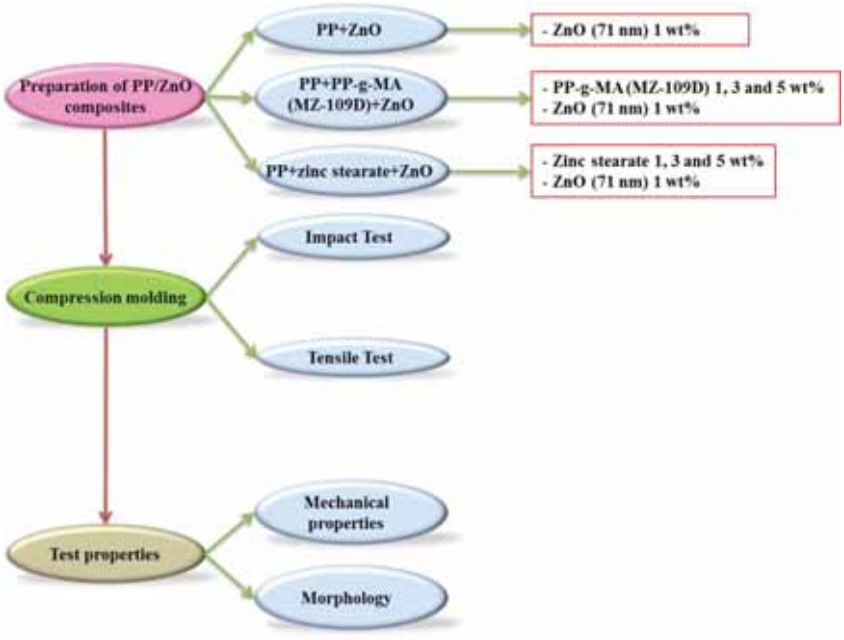

Figure 15 Schematic diagram displays the experimental procedure for the comparison between two types of dispersing agent

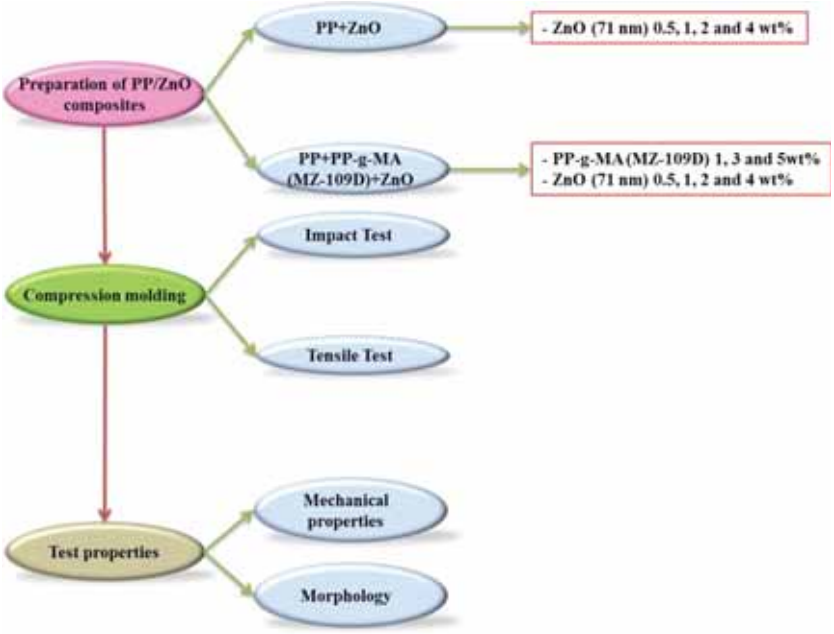

Figure 16 Schematic diagram displays the experimental procedure of the study of the suitable PP-g-MA content

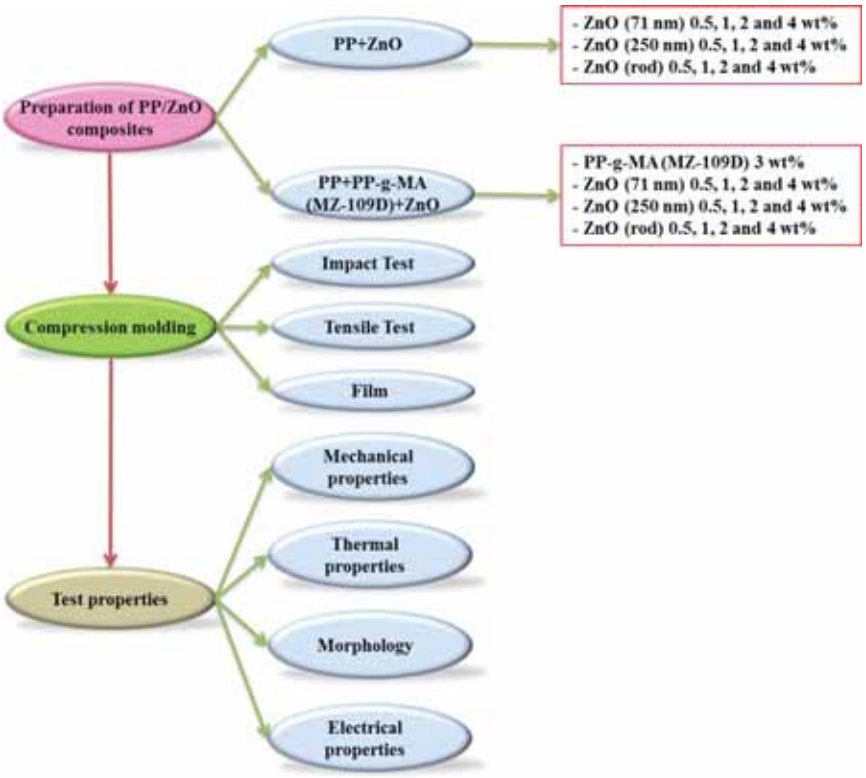

Figure 17 Schematic diagram displays the experimental procedure of the study of the effect of sizes and shapes of ZnO on the properties of PP/ZnO composites

3.2 PP/ZnO composites were prepared by an internal mixer

Figure 18 shows the experimental steps for PP/ZnO composites by using an internal mixer in this research. The PP/ZnO composites were prepared in an internal mixer at 190˚C and 50 rpm as shown in Figure 21. The first 5 minutes, PP and PP-g-MA were mixed in an internal mixer after that ZnO was added. Mixing was continued for another 5 min. At the end of 10 min, the composites were taken out and crushed in grider machine as shown in Figure 22. The composites were compression molded into a standard dumb-bell tensile bars and rectangular bars as shown by using compression moldimg as shown in Figure 20. Hot-press procedures involved preheating at 190˚C for 5 min followed by compressing for 15 min at same temperature, and subsequent cooling under pressure for 10 min.

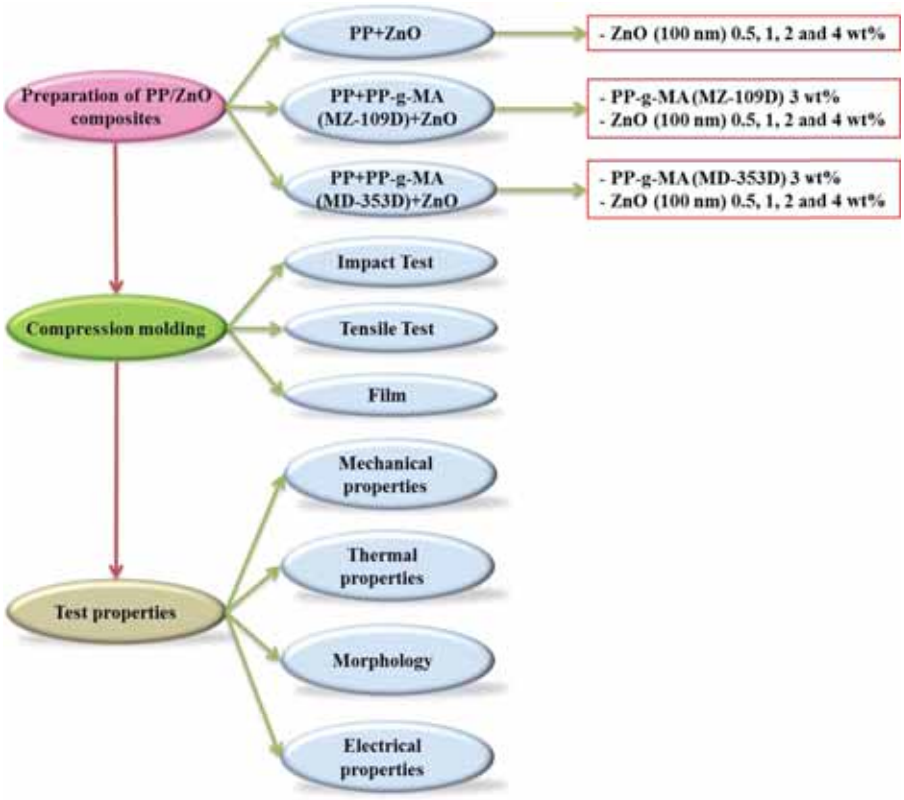

Figure 18 Schematic diagram displays the experimental procedure for the comparison between MA content of two types of PP-g-MA

Figure 19 Twin screw extruder (Thermo hake polylab system, model; PTW16/25D, Germany)

Figure 20 Compression molding machine

Figure 21 Internal mixer machine

Figure 22 Grider machine

4. Characterisation of ZnO nanorods and nanospheres

4.1 XRD observation

XRD patterns of powder were obtained using an X-ray diffractometer SIEMENS D5000 connected with a computer with Diffract ZT version 3.3 programs for fully control of the XRD analyzer. The experiments were carried out using Ni-filtered CuKα radiation. Scans were performed over the 2θ ranges from 20° to 80°. The crystalline size was estimated from line broadening according to the Scherrer equation and α-alumina was used as standard. This instrument has located at Center of Excellence on Catalysis and Catalytic Reaction, Chulalongkorn University. XRD patterns of synthesized ZnO were obtained by using Rigaku MiniFlex II. The experiments were carried out using Ni-filtered CuKα radiation. Scans were performed over the 2θ ranges from 4° to 90°. This instrument has located at Faculty of Science, Silpakorn University.

4.2 TEM observation

TEM is a conventional method to give detailed information about the shapes, the mean particle size and the size distribution of ZnO nanorods. The ZnO nanorod was observed using JEOL-JEM 200CX transmission electron microscope operated at 100 kV. This instrument has located at Central Laboratory and Greenhouse Complex, Kasetsart University.

4.3 SEM 0bservation

SEM with a MX 2000S Camscan, was taken to study the morphologies, shapes of ZnO and dispersion of ZnO particles in the matrix polymer that study the effect of type of dispersing agent as shown in Figure 23. This instrument has located at Faculty of science, Silpakorn University. The dispersion of ZnO particles in the matrix polymer and the impact fractured surface of the effect of MA contents on properties of PP/ZnO composites were observed by scanning electron microscope and X-ray microanalysis model XL 30 CP PHILIPS as shown in Figure 24. This instrument has located at Metallurgy and Materials Science Research Institute (MMRI), Chulalongkorn University.

Figure 23 Scanning electron microscope (MX 2000S Camscan Aalytical, England)

Figure 24 Scanning electron microscope (XL 30 CP PHILIPS)

4.4 Brunauer-Emmett-Teller (BET) observation

The BET equation is used primarily to determine the surface area from the physical adsorption of a gas on a solid surface. This analysis is beneficial in the estimation of surface area, micro-pore size and volume in for ZnO powders by using BET machine as shown in Figure 25.

Figure 25 Brunauer-Emmett-Teller

5. Characterization of PP/ZnO composites without and with PP-g-MA

5.1 Mechanical properties

Tensile tests were conducted according to ASTM D 638 with a universal tensile testing machine LR 50k from Lloyd instruments. The tensile tests were performed at a crosshead speed of 50.8 mm/min as shown in Figure 26. Charpy impact strength tests were performed according to ASTM D 256 at room temperature as shown in Figure 27. Each value reported represents the average of five samples.

5.2 Morphology

SEM was taken to study the morphology of the PP/ZnO nanocomposites with and without PP-g-MA to evaluate the dispersion quality of the ZnO particles. The impact fractured surface of PP/ZnO nanocomposites obtained from the impact test was examined. All specimens were coated with gold before SEM observations.

Figure 26 Universal tensile testing machine (LR 50K from Lloyd instruments)

Figure 27 Charpy impact strength tests (Zwick/material testing August-Nagelstr.11.D-89079 Ulm)

5.3 Thermal properties

Thermal stability of PP/ZnO composites were studied by TGA (Perkin Elmer instrument, TGA 7) as shown in Figure 28 this instrument was located at Faculty of Engineering and Industrial Technology, Silpakorn University. The PP/ZnO composites (71, 250 nm and rod) were studied by this equipment. The samples were cut into small pieces and then heated from 50˚C to 600˚C at a heating rate of 10˚C/min under a nitrogen atmosphere. For PP/ZnO 100 nm composites, we used DSC-TGA Q Series^{TM} instrument at Center of Excellence on Catalysis and Catalytic Reaction, Chulalongkorn University.

Thermal behavior of PP/ZnO composites were investigated by DSC (a Pyris I, Perkin Elmer, USA) as shown in Figure 29. The temperature calibration of DSC was done by measuring the melting temperature, crystallization temperature and %crystallinity of PP/ZnO composites. The samples of weight 3-5 mg were put in an aluminum pan. Samples were heated twice at a heating rate of 10˚C/min from 50˚C to 200˚C. Between the two heating cycles, a controlled cooling at a rate of 10˚C/min was performed. Details are shown as follows:

1. Hold for 1 min at 50˚C

2. Heat from 50˚C to 200˚C at 10˚C/min

3. Hold for 1 min at 200˚C

4. Cool from 200˚C to 50˚C at 10˚C/min

5. Hold for 1 min at 50˚C

6. Heat from 50˚C to 200˚C at 10˚C/min

7. Hold for 1 min at 200˚C

Figure 28 Thermogravimetric analysis (Perkin Elmer TGA 7)

Figure 29 Differential scanning calorimeter (Pyris I, Perkin Elmer, USA)

5.4 Electrical properties

Electrical properties of the polymer films were obtained via the capacitance method and were measured at room temperature and 1V with Agilent E 4980A Precision LCR Meter as shown in Figure 30. This instrument has located at Center of Excellence on Catalysis and Catalytic Reaction, Chulalongkorn University. The sample size was 1.5×1.5 cm^2. The dielectric constants of the films calculated from the following equation (1);

$$k = \frac{Ct}{\varepsilon_0 A} \tag{1}$$

Where C is the measured capacitance, t is the thickness of the sample, A is the area of the films, ε_0 is the permittivity of the free space (8.854 pF).

Figure 30 LCR meter equipment

CHAPTER 5

RESULTS AND DISCUSSION

The main topic of this research involves the properties of PP/ZnO composites without and with PP-g-MA compatibilizer that has various sizes (71, 100 and 250 nm) and shapes (sphere and rod) of ZnO. Furthermore, the comparison between two compatibilizers and two dispersing agents was investigated. The results and discussion were divided into five sections. In the first section, the characterization of ZnO nanorod and nanosphere were synthesized by simple chemical route. The second section discussed the type of dispersing agent that suitable for dispersion ZnO particles in the PP matrix. The suitable of PP-g-MA content in polymer composites was determined in the third section. The fourth section discussed the effect of the two compatibilizers which has the different percent of MA content (MZ-109D 0.55 wt% and MD-353D 1.305 wt%) on properties of PP/ZnO 100 nm composites. These composites were prepared by an internal mixer. The fifth section was determined the properties of PP/ZnO composites with different sizes and shapes of ZnO without and with PP-g-MA (MZ-109D), which were prepared by a twin screw extruder.

1. Characterization of ZnO

1.1 BET

This analysis is beneficial in the estimation of surface area, pore size and particle sizes. This research, mainly interested in particle sizes of ZnO sphere shapes was obtained from BET. The particle sizes were calculated from surface area was 71, 100 and 250 nm, respectively.

1.2 TEM

TEM is a conventional method to give detailed information about the shape, particle size distribution and average particle size. Figure 31 is presented TEM micrographs of ZnO. The particle size distribution of ZnO calculated from TEM was corresponding with BET. It can be seen that the ZnO purchased in the market (Figure 31(a) and (c)) has to vary shapes but the most shape was sphere shape. Our ZnO powder (Figure 31 (b) and (d)) that was synthesized in our laboratory could see that ZnO powders had a sphere shape and rod shape, according to the particle size and morphology in Figure 31.

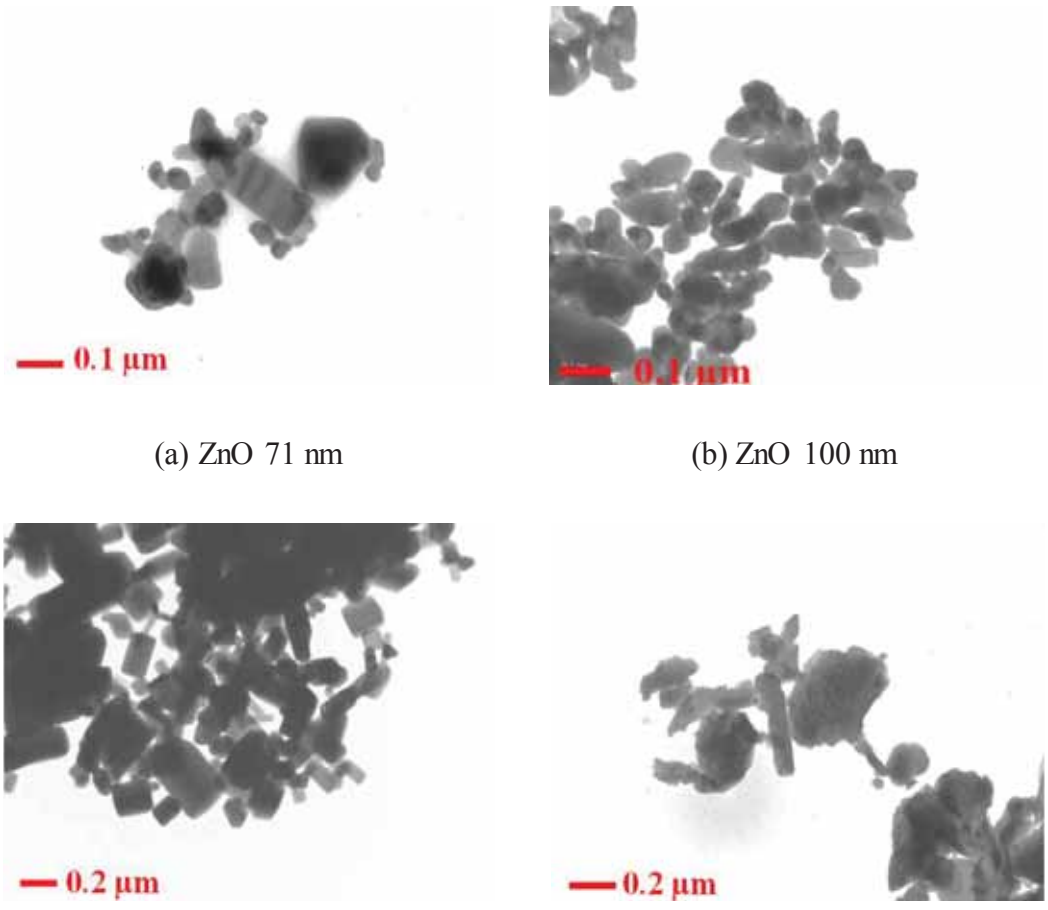

(a) ZnO 71 nm (b) ZnO 100 nm

(c) ZnO 250 nm (d) ZnO rod

Figure 31 TEM micrographs of ZnO

1.3 SEM

Figure 32 shows the SEM images of ZnO 71, 100, 250 nm and ZnO rod, respectively. From the images of ZnO, sphere shape morphology with an average diameter of 71, 100 and 250 nm and rod-like morphology with an average breadth of 100 nm and an average length of 360 nm was observed. It was found that ZnO 71 nm had higher agglomeration than ZnO 100, 250 nm and rod.

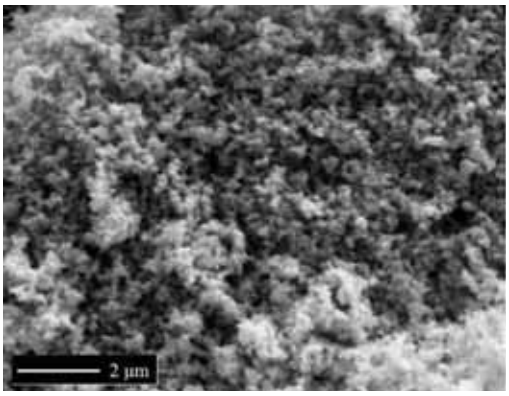

(a) ZnO 71 nm

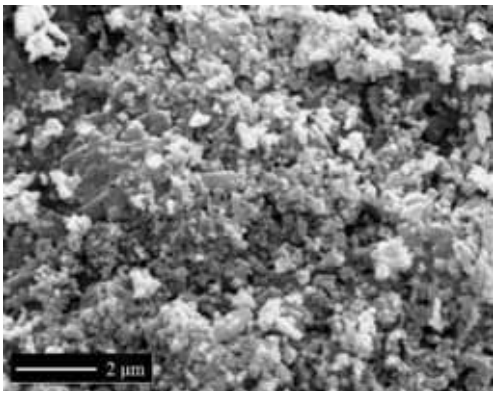

(b) ZnO 100 nm

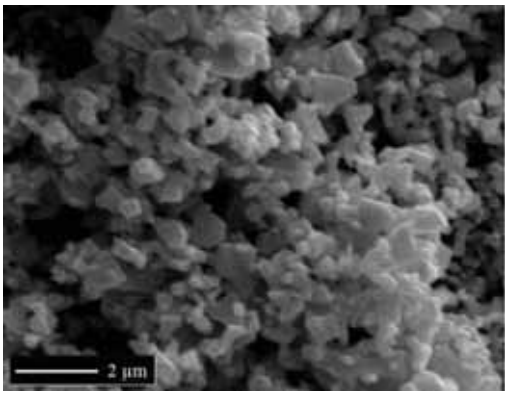

(c) ZnO 250 nm

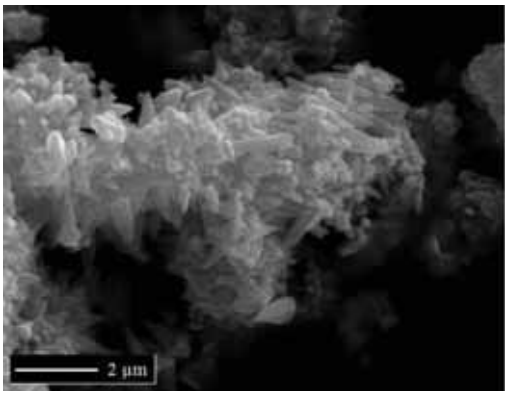

(d) ZnO rod

Figure 32 SEM micrographs of ZnO

The summarized of particle sizes of ZnO both by purchased and synthesized in our laboratory were shown in Table 1.

Table 1 ZnO particle sizes obtained by BET and TEM

Samples	BET (nm)	TEM (nm)
ZnO commercial nanopowder (Aldrich)	71	~71
ZnO synthesized by chemical route method (sphere)	100	~100
ZnO commercial micropowder (Ajax Finechem)	250	~250
ZnO synthesized by chemical route method (rod)	-	diameter~100 nm length~360 nm

1.4 XRD

Figure 33 shows the XRD patterns of standard peak of ZnO, commercial ZnO, ZnO sphere and ZnO rod, respectively. The XRD was taken out to find the crystalline phase and structure of the particles, it was found that the diffraction pattern plot showed the ZnO main peaks at 2θ = 31.7º, 34.4º, 36.2º, 47.5º, 56.5º, 62.8º, 66.4º, 67.9º, 69º, 72.5º and 76.9º (Ashkarran A. A., 2009) which was agreement with the standard XRD peak following JCPDS card no. 36-1451 (Zhigang J., 2008) confirmed that the synthesized materials were ZnO of the hexagonal wurtzite phase.

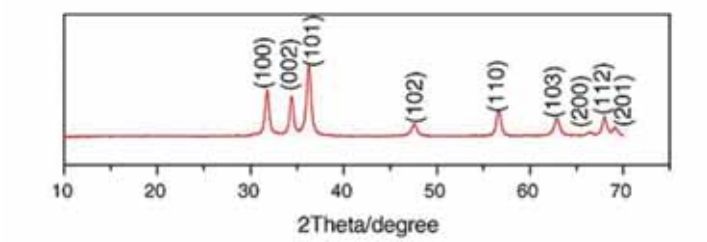

(a) Standard ZnO peak

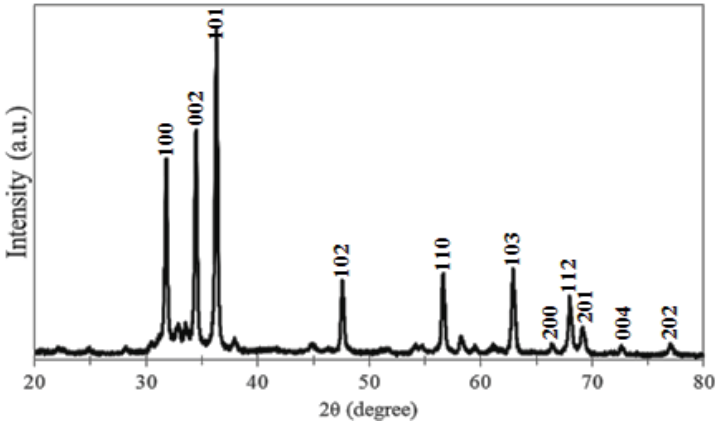

(b) ZnO 71 nm was prepared by simple chemical route method

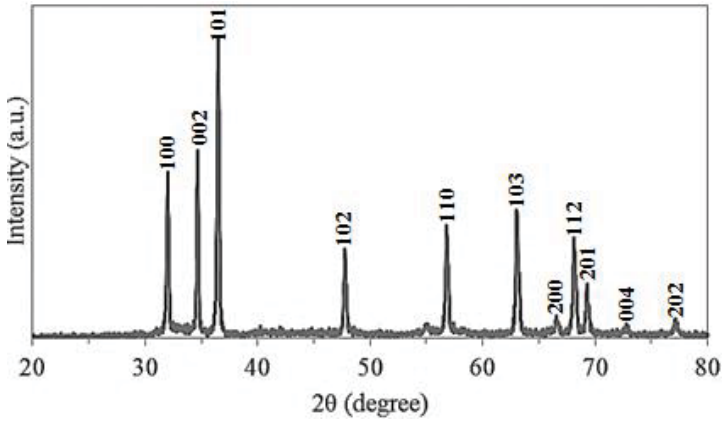

(c) ZnO rod was prepared by simple chemical route method

Figure 33 XRD patterns of (a) standard peak of ZnO (b) ZnO 71 nm was prepared at 50 ºC with sintered at 400 ºC and (c) ZnO rod was prepared at room temperature with sintered at 400 ºC

2. Effect of types of dispersing agent (PP-g-MA (MZ-109D) and zinc stearate) on dispersion and mechanical properties of PP/ZnO nanocomposites

This section we used PP-g-MA and zinc stearate as dispersing agent to compare the dispersion of ZnO nanoparticles (71 nm) in the PP matrix and mechanical properties of PP/ZnO composites without and with dispersing agent at 1 wt% of ZnO content. The dispersing agent content was 1, 3 and 5 wt%.

2.1 Dispersion of ZnO 71 nm in PP matrix without and with dispersing agent

The morphologies of the impact fractured surface specimen of PP/ZnO nanocomposites filled with different dispersing agent were examined by SEM. Figure 34 and 35 show the micrographs of the impact fractured surface PP/ZnO nanocomposites filled with PP-g-MA and zinc stearate at 1, 3 and 5 wt%, respectively. It was observed that the dispersion of ZnO in PP matrix without dispersing agent was poor and formed large aggregates. Figure 34 shows the dispersion of ZnO filled with PP-g-MA was good and contained few aggregates. While the dispersion of ZnO filled with zinc stearate was relatively good, only few small aggregates existed as shown in Figure 35. It can be seen that the addition of dispersing agent improved interfacial adhesion and the dispersion of ZnO in PP matrix. The strong agglomerate makes it difficult to disperse uniformly the nanoparticles in the matrix. The ZnO aggregates may influence the tensile properties of PP nanocomposites. The crack initiation and propagation zones that shown in Figure 34 and 35. It can be seen that the propagation zone has two different regions, a narrow stable crack growth region and a region of unstable crack growth. The narrow stable crack growth region lies immediately after the crack initiation site. The unstable crack growth region has cleavage type of fracture in the middle and thread like fibrils along the edges. Cleavage is associated with low-energy brittle fracture, which has been bright reflecting facets. The edges of the unstable crack growth region have a thread like fibrils (Saminathan *et al.*, 2008).

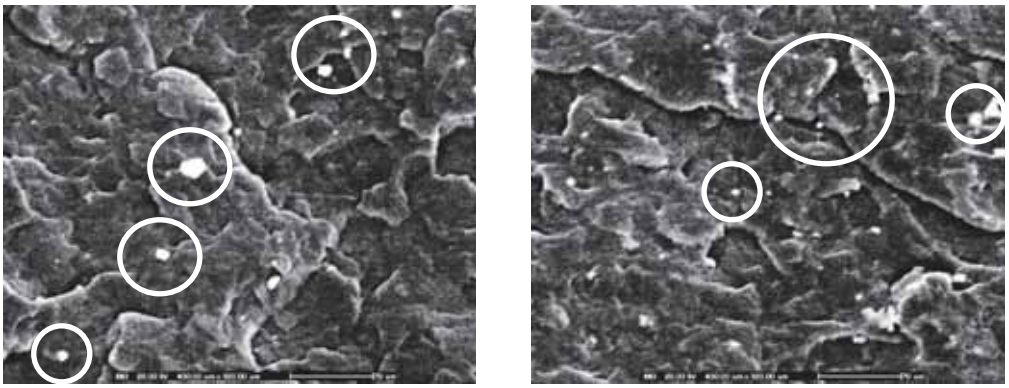

(a) PP-g-MA 0 wt%

(b) PP-g-MA 1 wt%

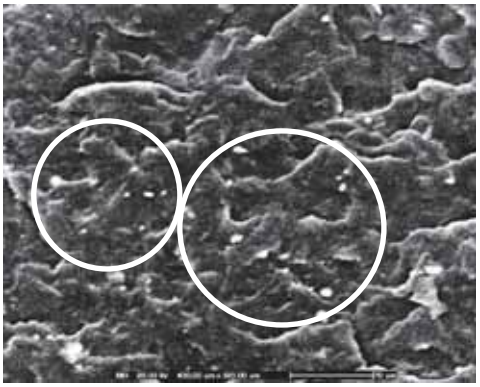

(c) PP-g-MA 3 wt%

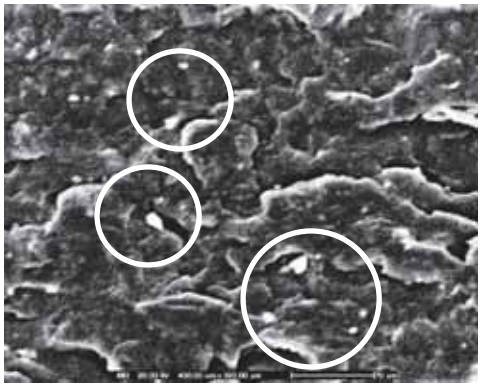

(d) PP-g-MA 5 wt%

Figure 34 SEM micrographs of the composites of PP and ZnO 71 nm (1 wt%) at various PP-g-MA contents

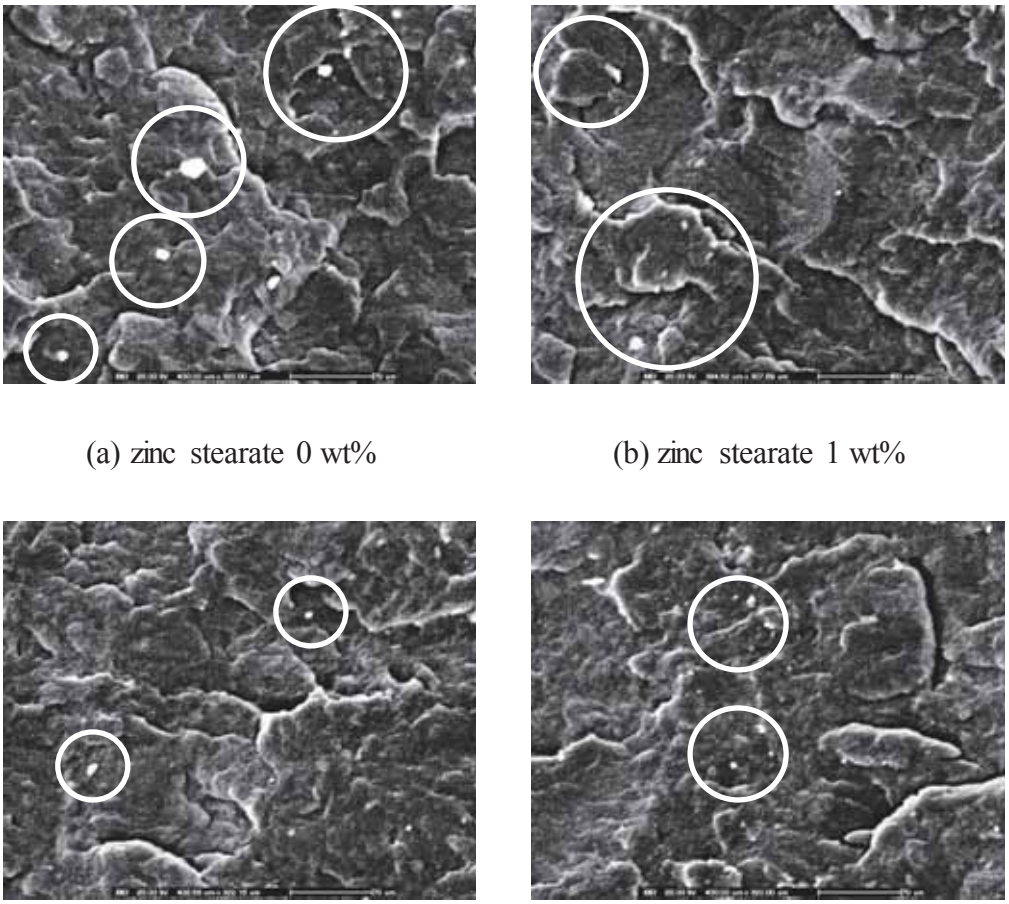

(a) zinc stearate 0 wt% (b) zinc stearate 1 wt%

(c) zinc stearate 3 wt% (d) zinc stearate 5 wt%

Figure 35 SEM micrographs of the composites of PP and ZnO 71 nm (1 wt%) at various zinc stearate contents

2.2 Mechanical properties

The Young's modulus of PP/ZnO composites at various types of dispersing agent is shown in Figure 36. The Young's modulus of the PP/ZnO nanocomposites without PP-g-MA or zinc stearate was higher than PP/ZnO composites with PP-g-MA or zinc stearate. After adding PP-g-MA, the Young's modulus of PP/ZnO nanocomposites slightly increased with increasing PP-g-MA content. The Young's modulus of PP/ZnO nanocomposites with zinc stearate slightly increased with increasing zinc stearate content and higher than the nanocomposites

with PP-g-MA but at 5 wt% the Young's modulus of PP/ZnO nanocomposites with PP-g-MA slightly higher than the nanocomposites with zinc stearate.

Figure 37 shows the tensile strength of PP/ZnO nanocomposites without and with dispersing agent. The tensile strength of PP/ZnO nanocomposites without dispersing agent had been lower than the nanocomposites with PP-g-MA at 1 wt% and slightly lower than the nanocomposites with zinc stearate at 1 wt% content. After adding PP-g-MA, the tensile strength increased with increasing PP-g-MA content and higher than the nanocomposites without dispersing agent and with zinc stearate. The tensile strength of PP/ZnO nanocomposites with zinc stearate dropped with increasing zinc stearate content. It is shown that PP-g-MA more improved on the tensile strength of PP than zinc stearate.

The stress at break of PP/ZnO nanocomposites is shown in Figure 38. It was found that the stress at break of the nanocomposites with PP-g-MA or zinc stearate was higher than the nanocomposites without dispersing agent. The stress at break of PP/ZnO nanocomposites with PP-g-MA was higher than the nanocomposites with zinc stearate. With zinc stearate, the stress at break of PP/ZnO nanocomposites increased with 3 wt% of zinc stearate and dropped with 5 wt% content.

Figure 39 shows impact strength of PP/ZnO nanocomposites without and with PP-g-MA or zinc stearate. It can be seen that impact strength of PP/ZnO nanocomposites without dispersing agent slightly higher than the nanocomposites with PP-g-MA or zinc stearate at 3 wt%. The impact strength of PP/ZnO nanocomposites increased significantly after adding PP-g-MA 3wt%, and it was higher impact strength than the nanocomposites without dispersing agent and with zinc stearate. The adding 5 wt% content of PP-g-MA, the impact strength dropped and higher than the nanocomposites without dispersing agent and with zinc stearate. The impact strength of the nanocomposites filled zinc stearate dropped with increasing zinc stearate content. From the dispersion of ZnO particles and mechanical properties of PP/ZnO nanocomposites can be explained that the increased interfacial area in the nanocomposite with PP-g-MA was better than zinc stearate.

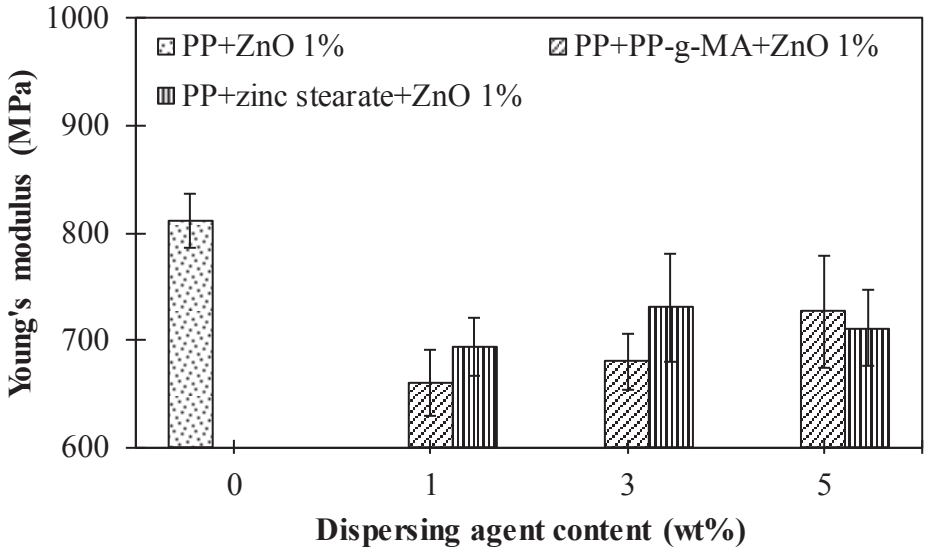

Figure 36 Young's modulus of the PP/ZnO nanocomposites at two types of dispersing agent contents

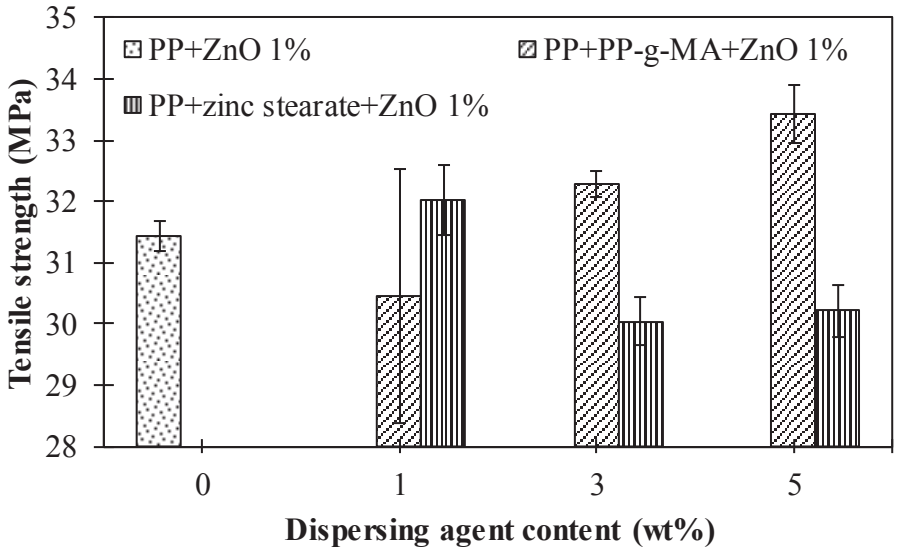

Figure 37 Tensile strength of the PP/ZnO nanocomposites at two types of dispersing agent contents

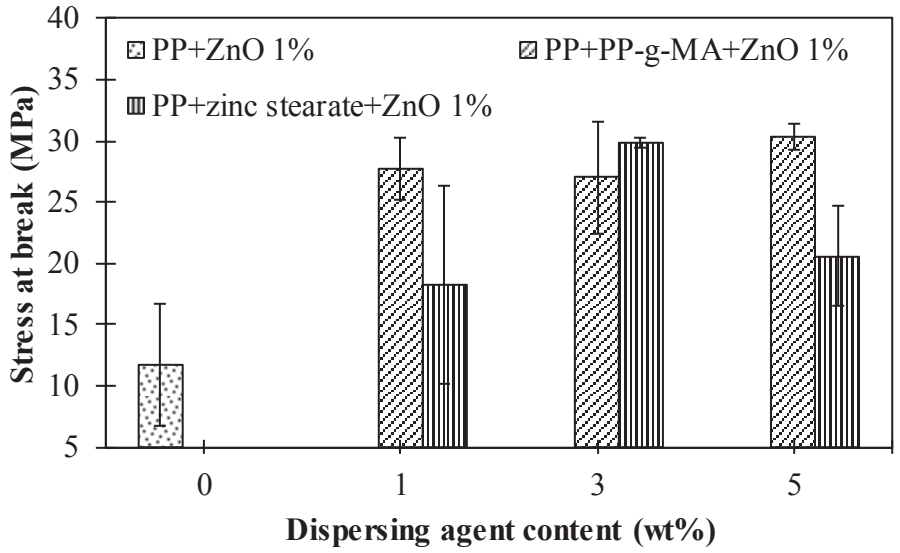

Figure 38 Stress at break of the PP/ZnO nanocomposites at two types of dispersing agent contents

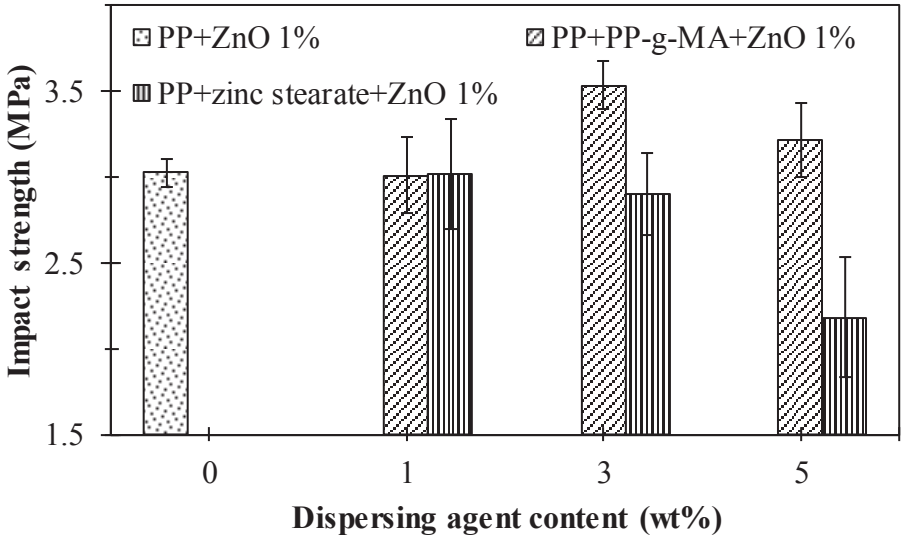

Figure 39 Impact strength of the PP/ZnO nanocomposites at two types of dispersing agent contents

3. Effect of PP-g-MA compatibilizer (MZ-109D) content on the properties of PP/ZnO composites

3.1 Dispersion of ZnO 71 nm in PP matrix without and with PP-g-MA compatibilizer

Figure 40 shows SEM micrographs of the nanocomposites of PP and ZnO 71 nm without PP-g-MA at the magnification of x300. The results showed that the dispersion of ZnO in PP matrix was poor and formed large aggregates. The agglomeration of ZnO nanoparticle in PP matrix increased with increasing ZnO content. Addition of ZnO high content had an effect of the strong agglomerates made it difficult to disperse uniformly in the matrix. The ZnO aggregates may influence on the mechanical properties of PP/ZnO nanocomposites. Figure 41-43 show the dispersion of ZnO 71 nm in PP matrix and the impact fractured surface of the PP/ZnO nanocomposites after adding PP-g-MA compatibilizer. It was found that the dispersion of particles with PP-g-MA compatibilizer was better than without PP-g-MA compatibilizer. The interaction compatibility between ZnO and PP matrix would be improved by adding PP-g-MA compatibilizer. The content of compatibilizer had an effect on the dispersion and aggregates of ZnO nanoparticles in PP matrix. Increased in compatibilizer content made good disperse and low aggregates of ZnO nanoparticles. The addition of 1 wt% of PP-g-MA had higher aggregates and lower disperses than 3 and 5 wt% of PP-g-MA, but 3 wt% had a better disperse and low aggregate than 5 wt% that was observed in Figure 42 and 43. The properties of nanocomposites were strongly dependent on the state of dispersion of nanoparticles in the polymeric matrix (Chinellato *et al.*, 2010) so PP-g-MA content at 3 wt% was suitable than 5 wt% because it has given a better dispersion.

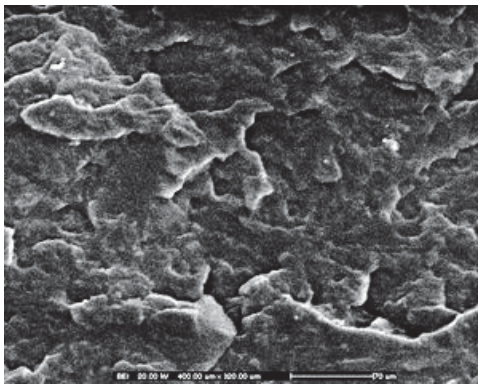

(a) PP

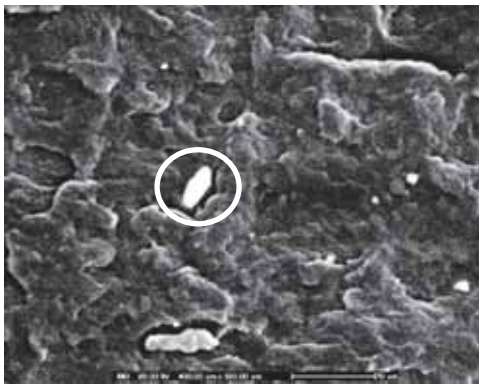

(b) ZnO (71 nm) 0.5 wt%

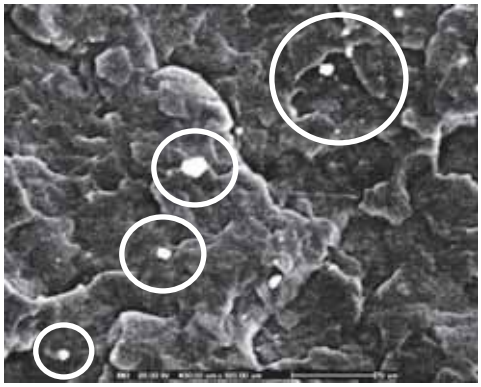

(c) ZnO (71 nm) 1 wt%

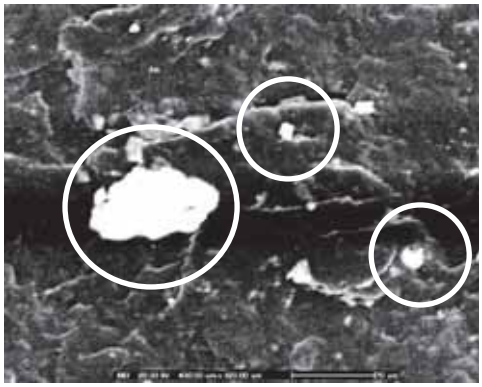

(d) ZnO (71 nm) 2 wt%

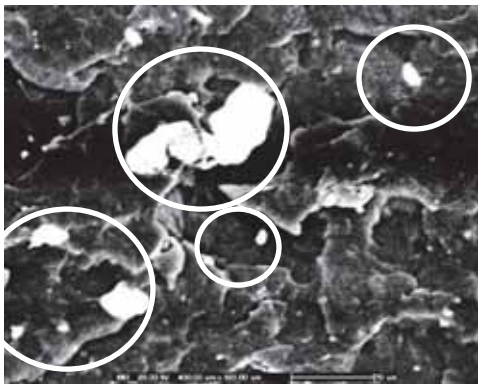

(e) ZnO (71 nm) 4 wt%

Figure 40 SEM micrographs of the nanocomposites of PP and ZnO 71 nm

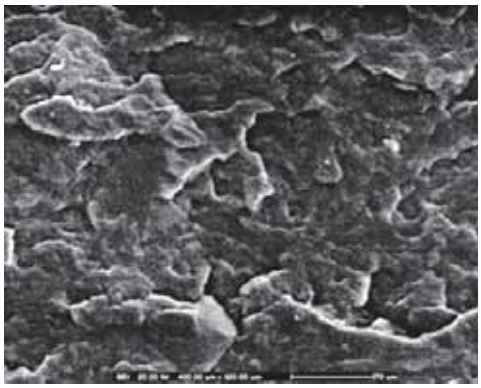

(a) PP

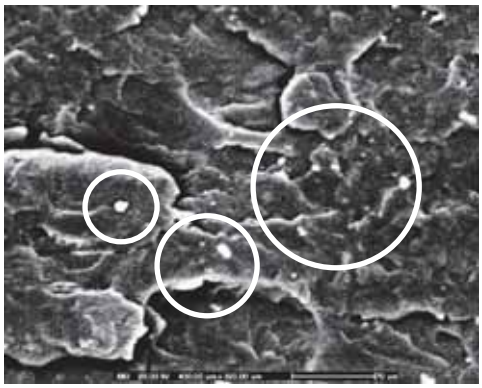

(b) ZnO (71 nm) 0.5 wt%

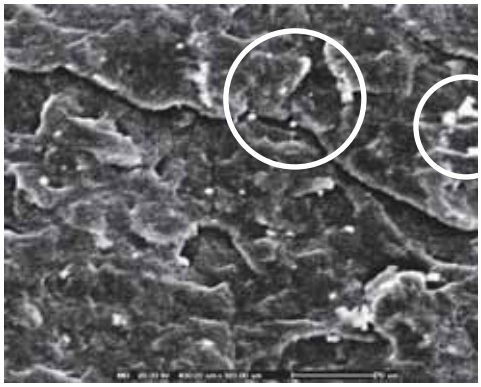

(c) ZnO (71 nm) 1 wt%

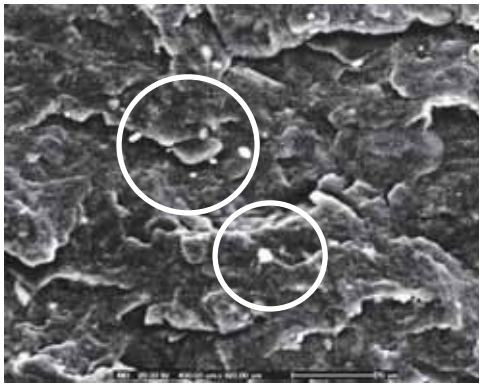

(d) ZnO (71 nm) 2 wt%

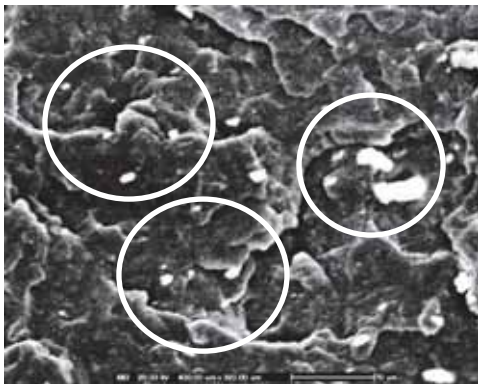

(e) ZnO (71 nm) 4 wt%

Figure 41 SEM micrographs of the nanocomposites of PP and ZnO 71 nm after adding PP-g-MA 1 wt%

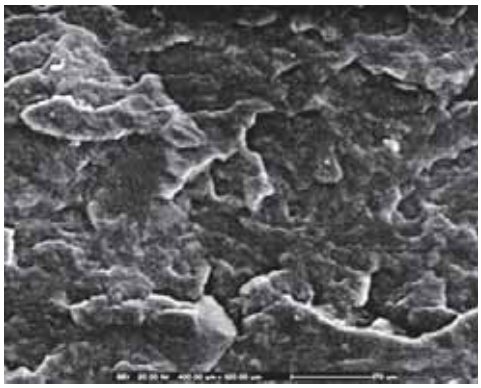

(a) PP

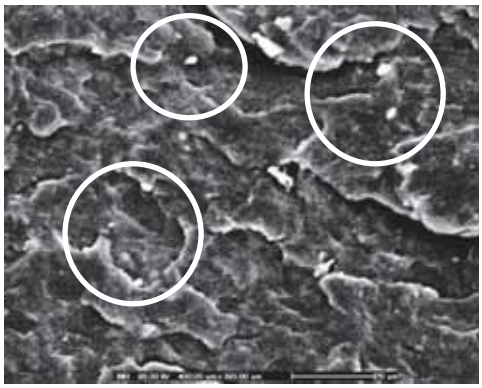

(b) ZnO (71 nm) 0.5 wt%

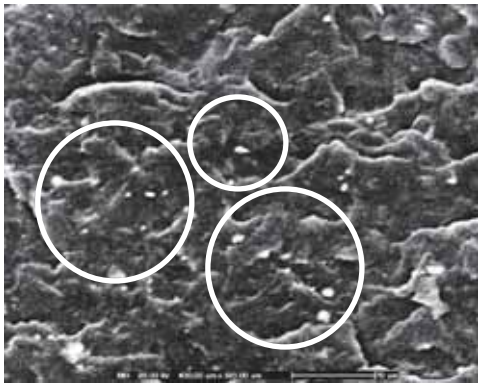

(c) ZnO (71 nm) 1 wt%

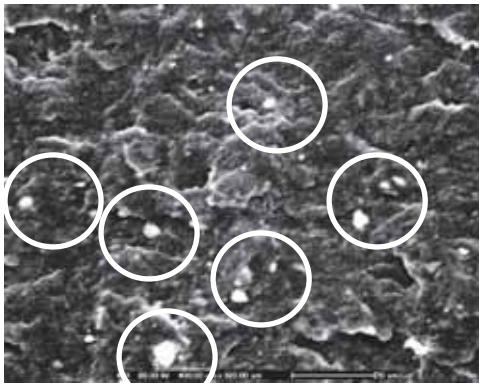

(d) ZnO (71 nm) 2 wt%

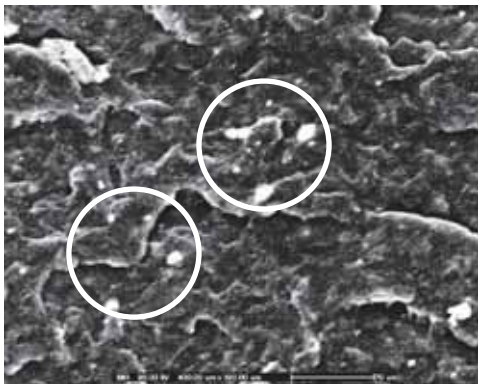

(e) ZnO (71 nm) 4 wt%

Figure 42 SEM micrographs of the nanocomposites of PP and ZnO 71 nm after adding PP-g-MA 3 wt%

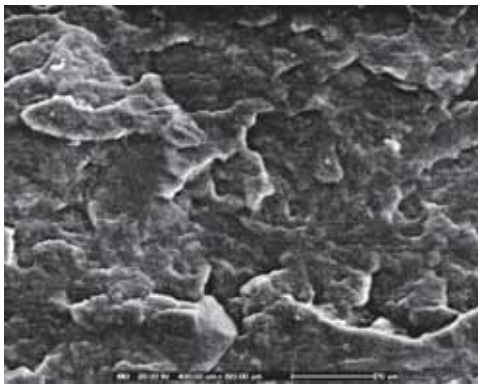

(a) PP

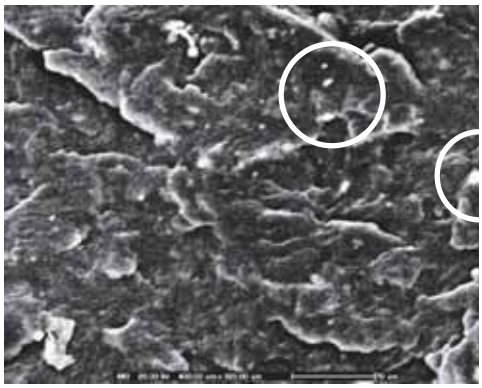

(b) ZnO (71 nm) 0.5 wt%

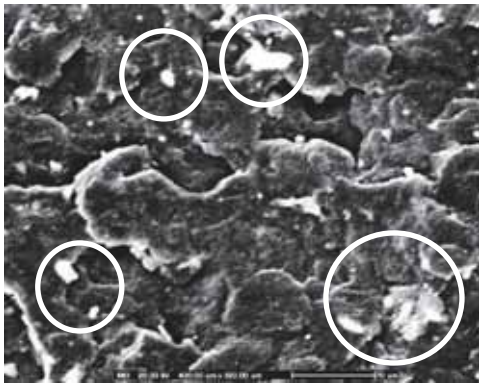

(c) ZnO (71 nm) 1 wt%

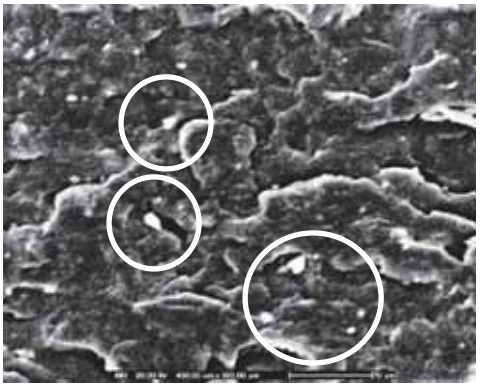

(d) ZnO (71 nm) 2 wt%

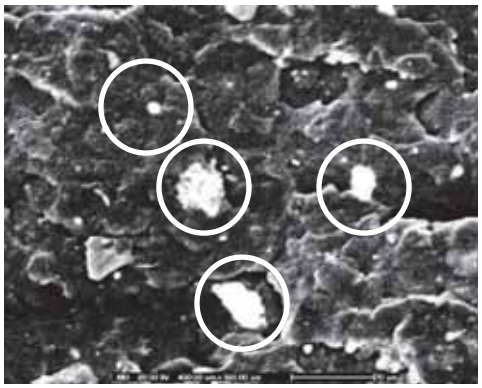

(e) ZnO (71 nm) 4 wt%

Figure 43 SEM micrographs of the nanocomposites of PP and ZnO 71 nm after adding PP-g-MA 5 wt%

3.2 Mechanical properties

(1) Young's modulus

Figure 44 shows Young's modulus of PP/ZnO 71 nm nanocomposites with various PP-g-MA compatibilizer contents. The result found that Young's modulus of PP/ZnO 71 nm nanocomposites without PP-g-MA did not change clearly with increasing ZnO content compared with PP. After adding PP-g-MA 1 wt%, Young's modulus of the nanocomposites decreased and lower than pure PP and the nanocomposites without PP-g-MA. At PP-g-MA 3 wt%, Young's modulus was lower than the nanocomposites without PP-g-MA and slightly increased with increasing ZnO content. For PP-g-MA 5 wt%, it also found as same as 3 wt% of PP-g-MA but Young's modulus was slightly higher than PP-g-MA 1 and 3 wt%.

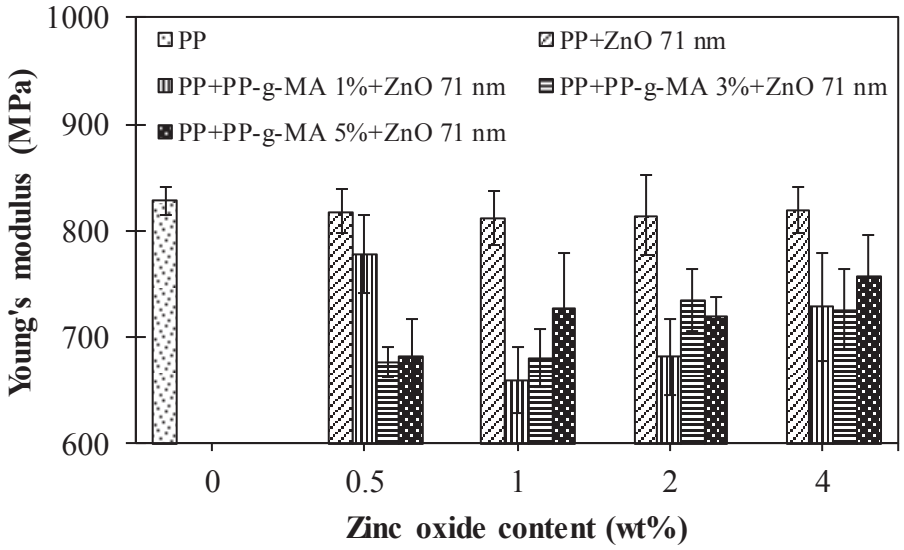

Figure 44 Young's modulus of the PP/ZnO nanocomposites without and with PP-g-MA at various ZnO contents

(2) Tensile strength

Tensile strength of PP/ZnO 71 nm nanocomposites after adding 1, 3 and 5 wt% of PP-g-MA compatibilizer contents compared with pure PP is shown in Figure 45. Tensile strength of PP/ZnO nanocomposites without adding compatibilizer slightly increased with increasing ZnO content. When adding PP-g-MA 1 wt%, the tensile strength trended to increase with increasing ZnO content and slightly higher than the nanocomposites without PP-g-MA. At 3 wt% of PP-g-MA, tensile strength increased with increasing ZnO content and higher than the nanocomposites without PP-g-MA and PP-g-MA 1 wt%. For PP-g-MA 5 wt%, tensile strength increased and higher than other nanocomposites at 0.5-1 wt% of ZnO and dropped more than 1 wt% of ZnO content. High content of compatibilizer improved the tensile strength.

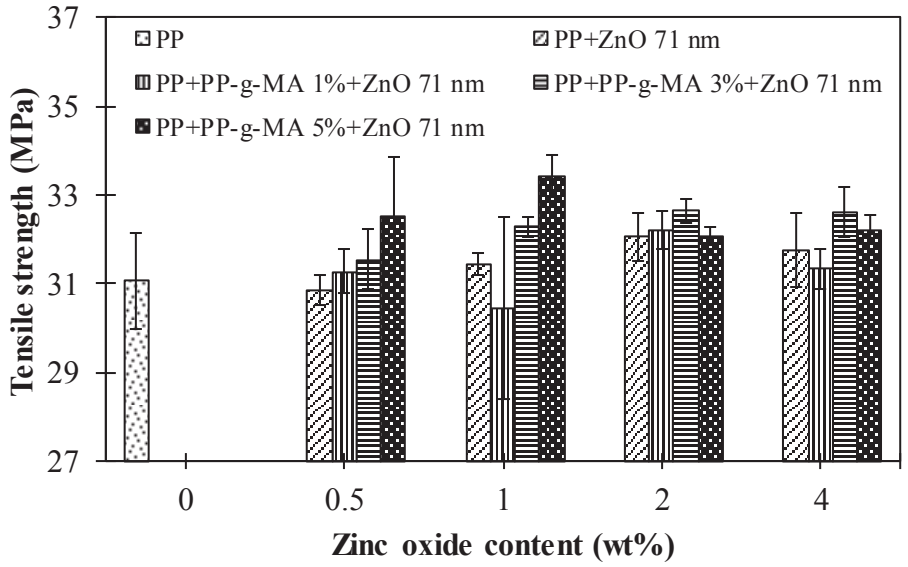

Figure 45 Tensile strength of the PP/ZnO nanocomposites without and with PP-g-MA at various ZnO contents

(3) Stress at break

Stress at break of PP/ZnO 71 nm nanocomposites after adding 1, 3 and 5 wt% of PP-g-MA compatibilizer compared with pure PP is shown in Figure 46. Stress at break of PP/ZnO nanocomposites without PP-g-MA dropped with ZnO content at 0.5-2 wt% compared with PP but stress at break increased at 4 wt%. After adding PP-g-MA 1 wt%, it can be seen that stress at break higher than without PP-g-MA and increased with increasing ZnO content. At 3 wt% of PP-g-MA, stress at break increased with increasing ZnO content. For PP-g-MA 5 wt%, stress at break was the highest but not different with PP-g-MA 3 wt% at 4 wt% of ZnO content. The nanocomposites with PP-g-MA 3 wt% had stress at break higher than the nanocomposites with PP-g-MA 1 wt%. The stress at break of the nanocomposites after adding PP-g-MA was higher than trhe nanocomposites without PP-g-MA and pure PP. This may be due to the PP-g-MA improved the compatibility and interfacial area of ZnO nanoparticles in PP matrix as seen in Figure 41-43, the aggregates decreased with adding PP-g-MA.

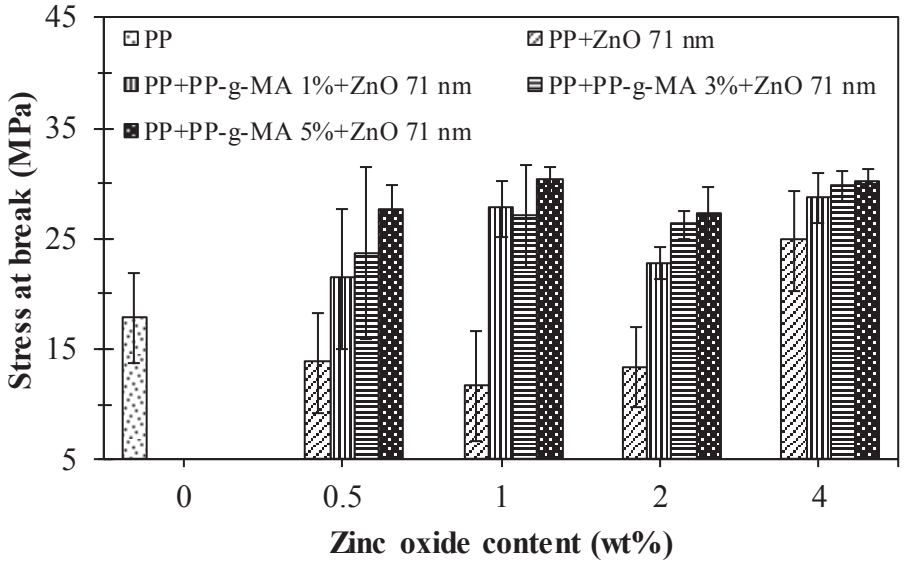

Figure 46 Stress at break of the PP/ZnO nanocomposites without and with PP-g-MA at various ZnO contents

(4) Impact strength

Impact strength of PP/ZnO nanocomposites after adding 1, 3 and 5 wt% of PP-g-MA compared with pure PP is shown in Figure 47. It can be seen that impact strength of PP/ZnO nanocomposites without PP-g-MA slightly dropped with increasing ZnO content. At 1 wt% of PP-g-MA, impact strength of the nanocomposites slightly increased at 0.5 wt% of ZnO content and dropped after adding ZnO more than 0.5 wt%, but it was slightly higher than the nanocomposites without PP-g-MA. At 3 wt% of PP-g-MA, impact strength of the nanocomposites slightly decreased at 0.5 wt% of ZnO content and increased at 1 wt% of ZnO content but impact strength dropped after adding ZnO more than 1 wt%. For 5 wt% of PP-g-MA, impact strength was lowest at 0.5 wt% of ZnO content. After adding ZnO more than 0.5 wt%, it can be seen that impact strength slightly increased.

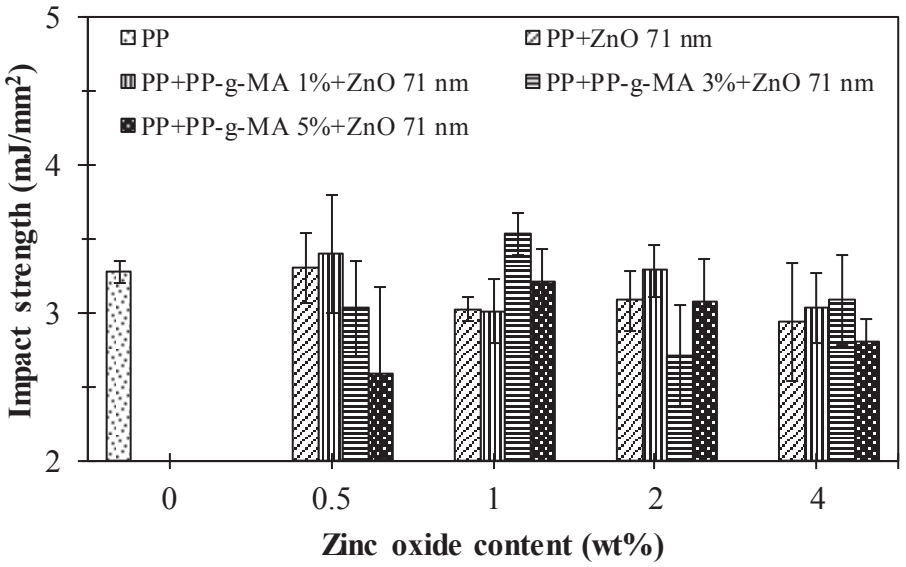

Figure 47 Impact strength values of PP/ZnO nanocomposites without and with PP-g-MA at various ZnO contents

From the morphology and mechanical properties of PP/ZnO 71 nm nanocomposites, the good dispersion was found when used PP-g-MA at 3 wt%. The mechanical properties of the composites of PP and ZnO 71 nm after adding PP-g-MA 5 wt%, was found the slightly higher in Young's modulus, tensile strength at 0.5-1 wt% of ZnO and higher in stress at break than the composites of PP/ZnO 71 nm after adding PP-g-MA 3 wt% but the impact strength of PP/ZnO 71 nm nanocomposites after adding PP-g-MA 5 wt% was lower than PP/ZnO 71 nm nanocomposites after adding PP-g-MA 3 wt%. The slightly different of mechanical properties between PP/ZnO 71 nm nanocomposites after adding PP-g-MA 5 wt% and 3 wt%, and a good dispersion of ZnO in the composites after adding PP-g-MA 3 wt% thus, we chose to use PP-g-MA 3 wt% for the composites of PP/ZnO 71 nm in this research.

4. The effect of PP-g-MA compatibilizer with different MA content (0.55 and 1.305 wt%) on the properties of PP/ZnO 100 nm composites by an internal mixer

In this section, we used PP-g-MA with different MA content (MZ-109D (0.55 wt%) and MD-353D (1.305 wt%)) and ZnO with average particle size is 100 nm was prepared in our laboratory. The PP/ZnO 100 nm composites without and with compa- tibilizer were prepared by an internal mixer.

4.1 Dispersion of ZnO 100 nm in PP matrix and fractured surface of the composites without and with PP-g-MA (0.55 and 1.305 wt%) compatibilizer

Figure 48-50 show SEM micrographs of the impact-fractured surface of PP/ZnO composites without and with PP-g-MA compatibilizer. The results found that the composites before adding compatibilizer showed the dispersion of ZnO particles in PP matrix was poor and formed large aggregates, addition of ZnO high content had an effect of the strong agglomerates and low dispersion. After adding MZ-109D

compatibilizer, the dispersion of ZnO particles was better dispersion and lower aggregates than PP/ZnO composites without PP-g-MA. When adding MD-353D compatibilizer, the dispersion of ZnO particles was better dispersion and lower aggregates than PP/ZnO composites without PP-g-MA. The crack initiation and propagation zones that shown in Figure 51-53. It can be seen that the propagation zone has two different regions, a narrow stable crack growth region and a region of unstable crack growth. The narrow stable crack growth region lies immediately after the crack initiation site. The unstable crack growth region has cleavage type of fracture in the middle and thread like fibrils along the edges. Cleavage is associated with low-energy brittle fracture, which has been bright reflecting facets. The edges of the unstable crack growth region have a thread like fibrils (Saminathan *et al.*, 2008).

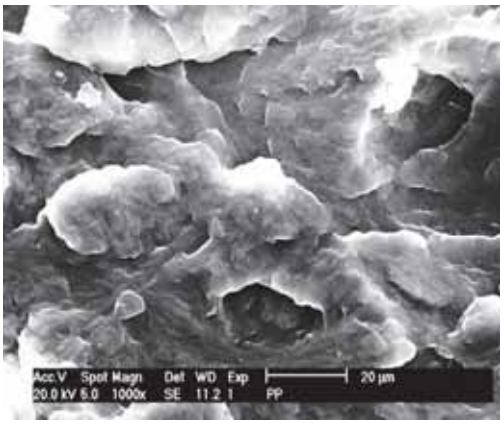

(a) PP

(b) ZnO (100 nm) 0.5 wt%

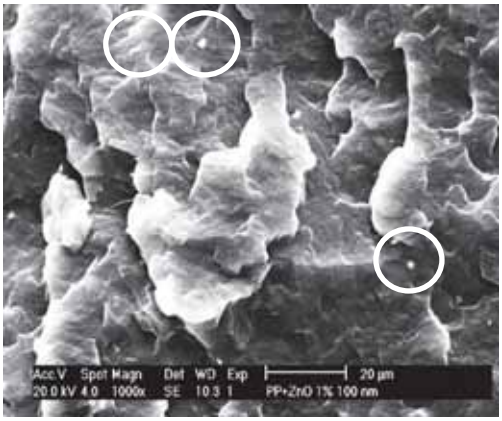

(c) ZnO (100 nm) 1 wt%

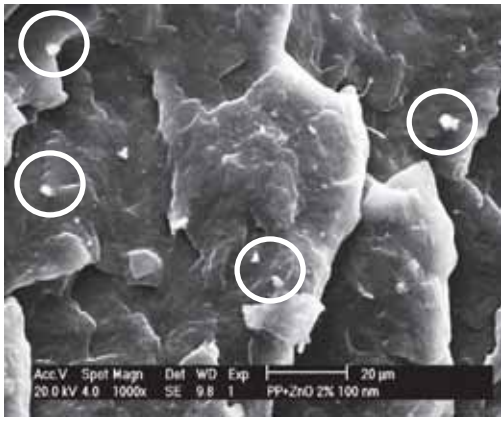

(d) ZnO (100 nm) 2 wt%

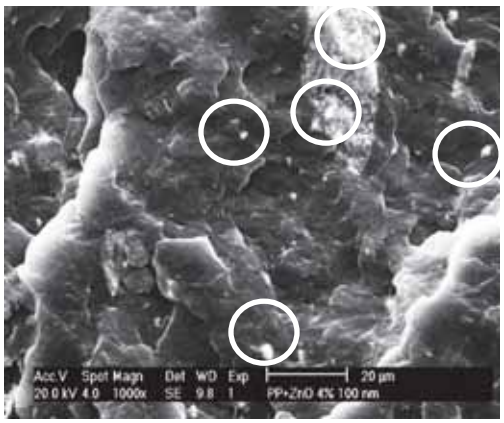

(e) ZnO (100 nm) 4 wt%

Figure 48 SEM micrographs of the composites of PP and ZnO 100 nm

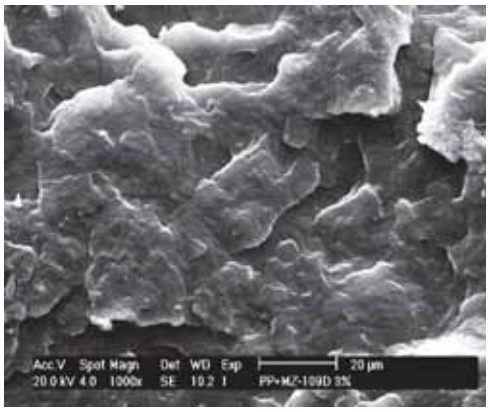

(a) PP

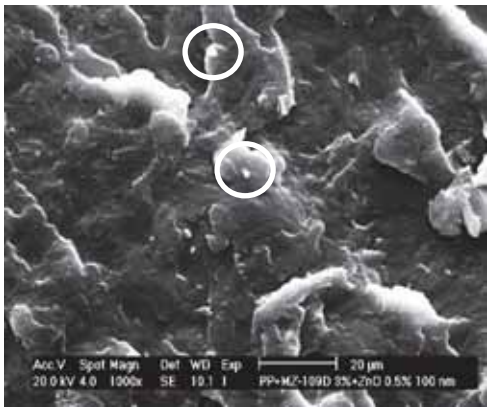

(b) ZnO (100 nm) 0.5 wt%

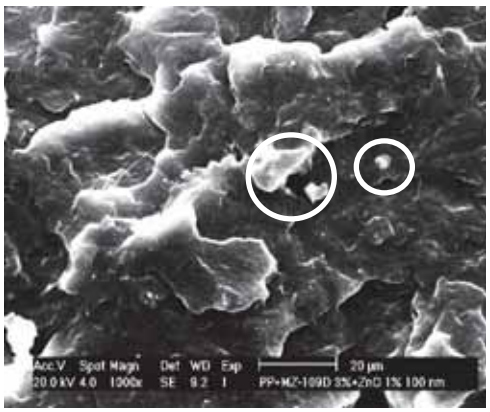

(c) ZnO (100 nm) 1 wt%

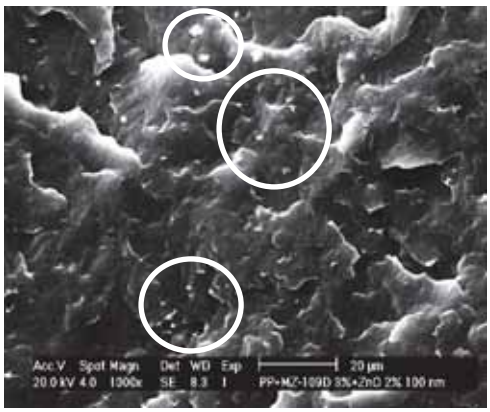

(d) ZnO (100 nm) 2 wt%

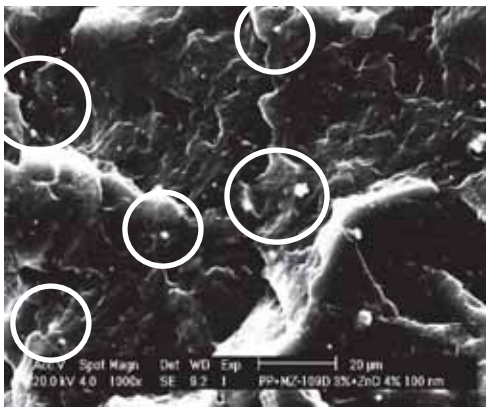

(e) ZnO (100 nm) 4 wt%

Figure 49 SEM micrographs of the composites of PP and ZnO 100 nm with MZ-109D 3 wt%

(a) PP

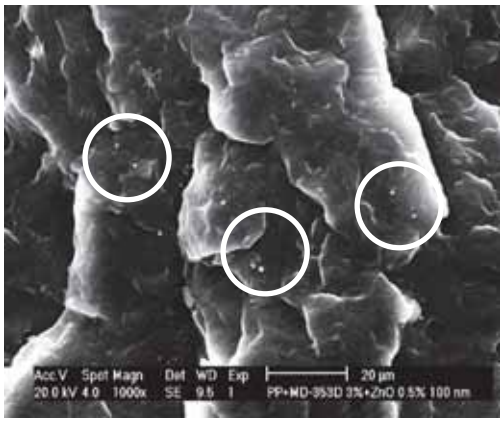

(b) ZnO (100 nm) 0.5 wt%

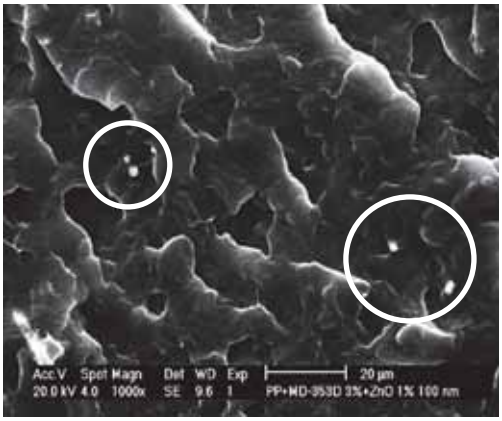

(c) ZnO (100 nm) 1 wt%

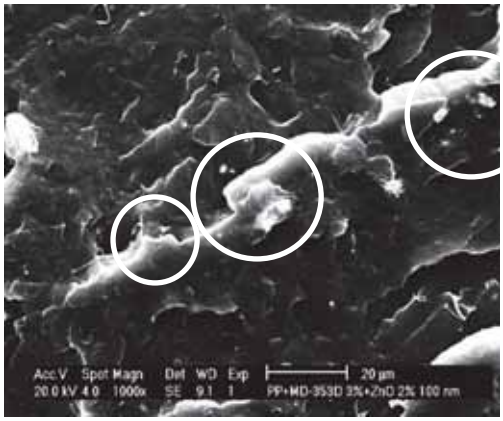

(d) ZnO (100 nm) 2 wt%

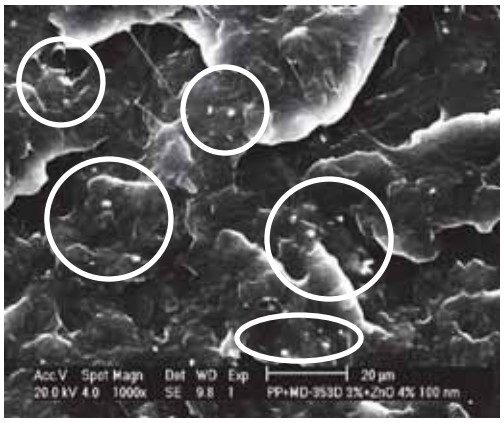

(e) ZnO (100nm) 4 wt%

Figure 50 SEM micrographs of the composites of PP and ZnO 100 nm with MD-353D 3 wt%

(a) PP

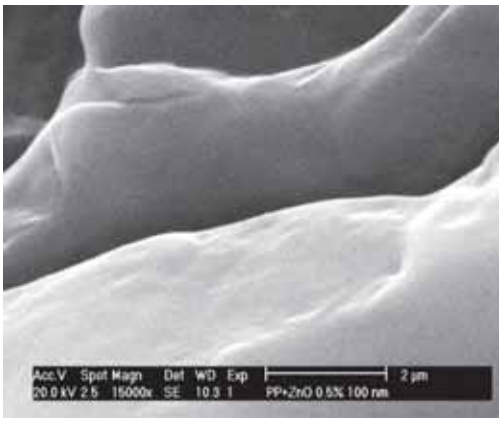

(b) ZnO (100 nm) 0.5 wt%

(c) ZnO (100 nm) 1 wt%

(d) ZnO (100 nm) 2 wt%

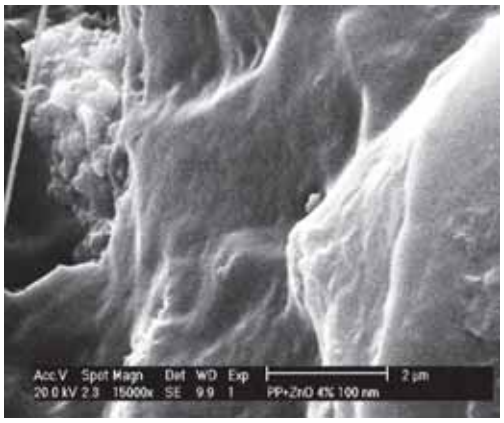

(e) ZnO (100 nm) 4 wt%

Figure 51 SEM micrographs of impact fractured-surface of PP/ZnO 100 nm composites

(a) PP

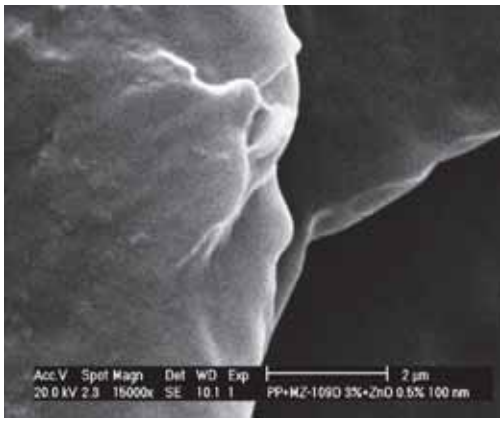

(b) ZnO (100 nm) 0.5 wt%

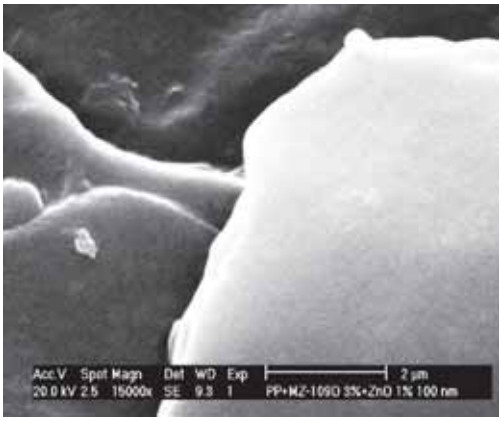

(c) ZnO (100 nm) 1 wt%

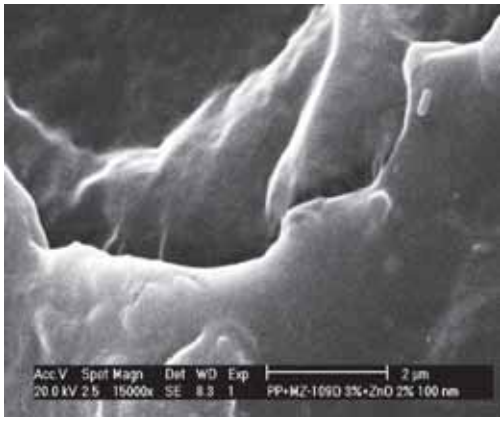

(d) ZnO (100 nm) 2 wt%

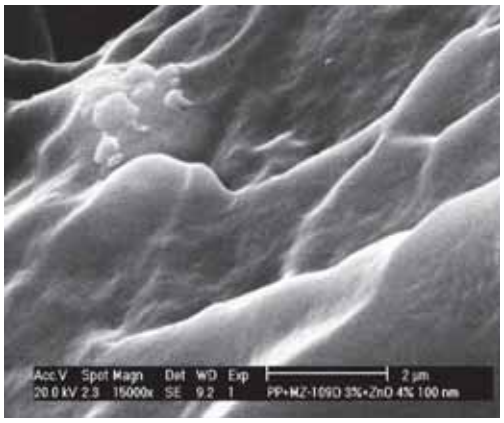

(e) ZnO (100 nm) 4 wt%

Figure 52 SEM micrographs of impact fractured-surface of PP/ZnO 100 nm composites with MZ-109D 3 wt%

(a) PP

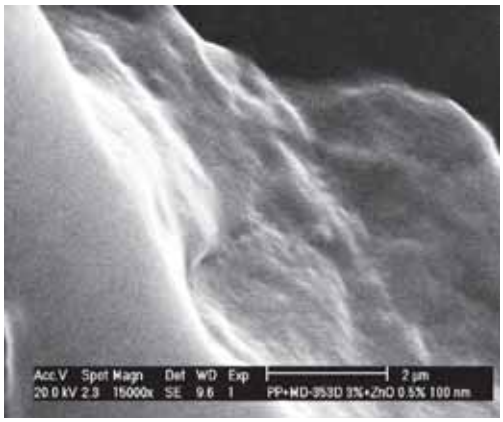

(b) ZnO (100 nm) 0.5 wt%

(c) ZnO (100 nm) 1 wt%

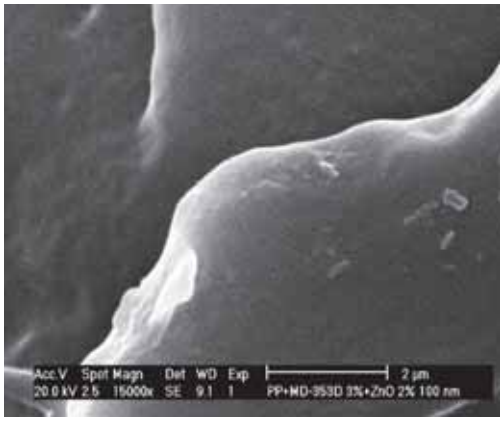

(d) ZnO (100 nm) 2 wt%

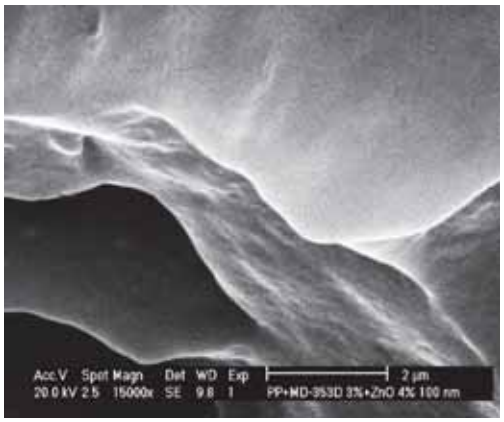

(e) ZnO (100 nm) 4 wt%

Figure 53 SEM micrographs of impact fractured-surface of PP/ZnO 100 nm composites with MD-353D 3 wt%

4.2 Thermal properties

(1) Melting temperature (T_m)

Figure 54 show the effect of types of PP-g-MA on T_m of PP/ZnO composites. Before adding PP-g-MA, the results found that the addition of ZnO 100 nm had not significantly changed T_m of the composites of PP/ZnO. After adding MZ-109D and MD-353D, the results also found that T_m did not change evidently with increasing ZnO content. It can be deduced that the crystallite size distribution of PP was hardly changed with the presence of ZnO (Nan-Ying, 2007).

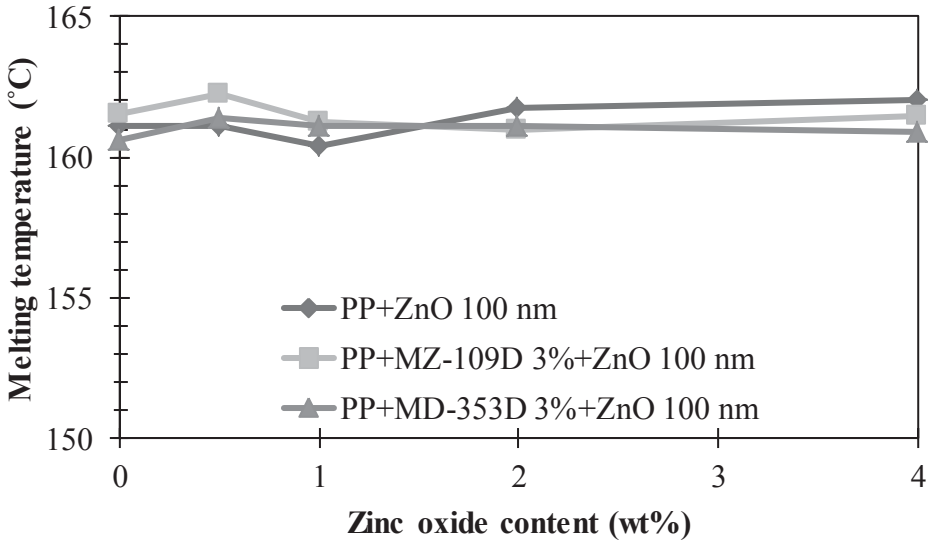

Figure 54 Melting temperatures of PP/ZnO composites without and with two types of PP-g-MA compatibilizer

(2) Crystallization temperature (T_c)

Figure 55 show the effect of types of PP-g-MA on T_c of PP/ZnO composites. The results found that before adding PP-g-MA, the addition of ZnO 100 nm in PP matrix slightly decreased T_c. When increasing ZnO content T_c had slightly increased. The composites after adding MZ-109D showed T_c had been slightly higher than PP/ZnO 100 nm composites without PP-g-MA and with MD-353D. Moreover T_c had slightly decreased with increasing ZnO content. PP/ZnO composites with MD-353D had slightly increased in T_c with increasing ZnO content and did not different in T_c between without PP-g-MA and with MD-353D. The results indicated that the efficiency of ZnO as a nucleating agent for PP crystallization, but mainly at high ZnO content (Nan-Ying, 2007).

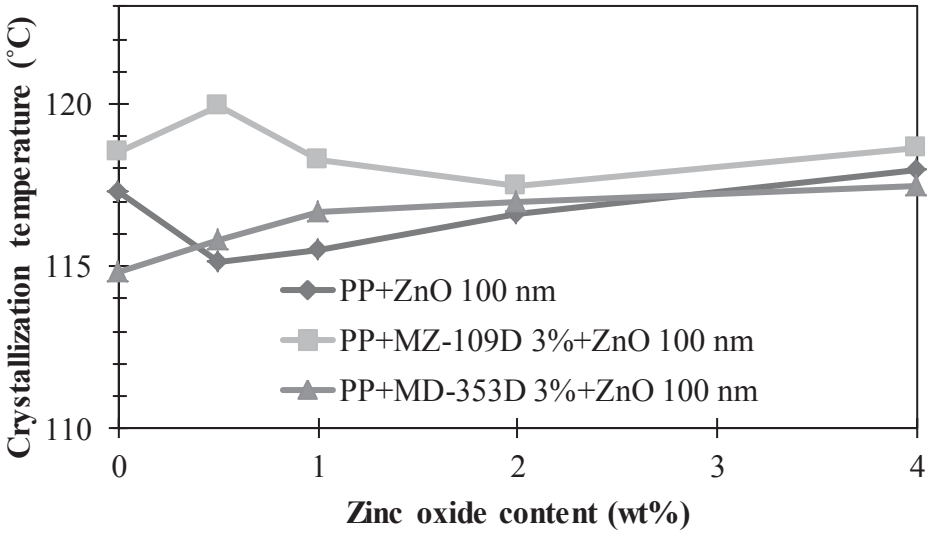

Figure 55 Crystallization temperatures of PP/ZnO composites without and with two types of PP-g-MA compatibilizer

(3) Percent crystallinity

Figure 56 show the effect of types of PP-g-MA on percent crystallinity of PP/ZnO composites. The results found that percent crystallinity of PP/ZnO composites without PP-g-MA had increased with ZnO content was 0.5 wt% and percent crystallinity was dropped after adding ZnO more than 1 wt%. Percent crystallinity of PP/ZnO 100 nm composites with MZ-109D also found as same as without PP-g-MA and higher percent crystallinity than without PP-g-MA. This may due to ZnO was a nucleating agent but at high content the agglomeration of ZnO particles reduced percent crystallinity of PP/ZnO composites. After adding MZ-109D, the ZnO particles had well dispersed so percent crystallinity increased. It can be explained that PP-g-MA enhanced crystallization temperature (Nan-Ying, 2007) and dispersion of ZnO particles so the percent crystallinity was improved. With MD-353D, percent crystallinity was dropped with increasing ZnO content but percent crystallinity increased at 4 wt% of ZnO.

(4) Decomposition temperature (T_d)

Figures 57-58 show the effect of types of PP-g-MA on T_d of PP/ZnO composites. T_d was measured by TGA and was calculated at 5 (T_{d5}) and 10 (T_{d10}) %weight loss of the composites. The results found that T_{d5} and Td_{10} of PP/ZnO composites without PP-g-MA increased with increasing ZnO content and were higher than the T_{d5} and Td_{10} of pure PP, which showed lower thermal stability than PP/ZnO composites. The PP/ZnO composites with MZ-109D had T_{d5} and Td_{10} lower than without PP-g-MA and with MD-353D and increased with increasing ZnO content. T_{d5} and T_{d10} of PP/ZnO composites with MD-353D had increased with increasing ZnO content but lower than PP/ZnO composites without PP-g-MA. It can be explained that ZnO 100 nm improved the thermal stability of PP.

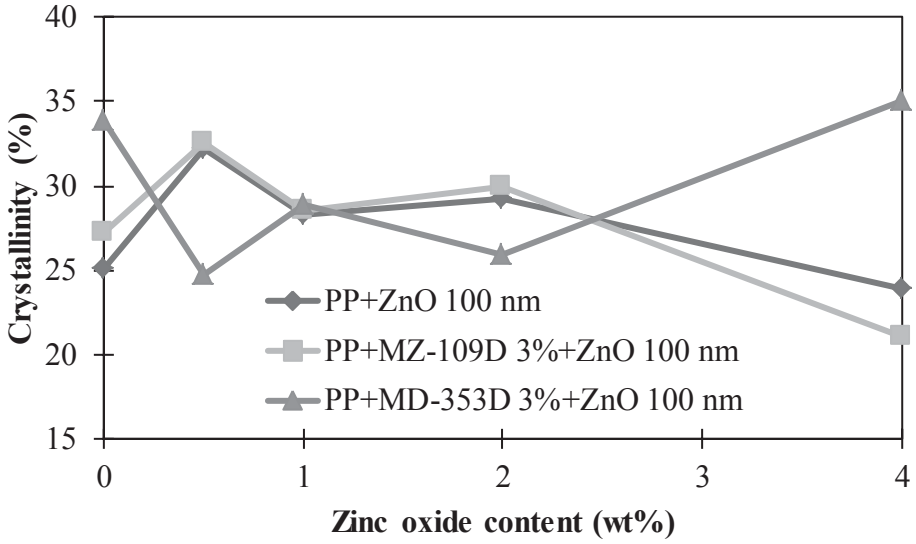

Figure 56 Percent crystallinity of PP/ZnO composites without and with two types of PP-g-MA compatibilizer

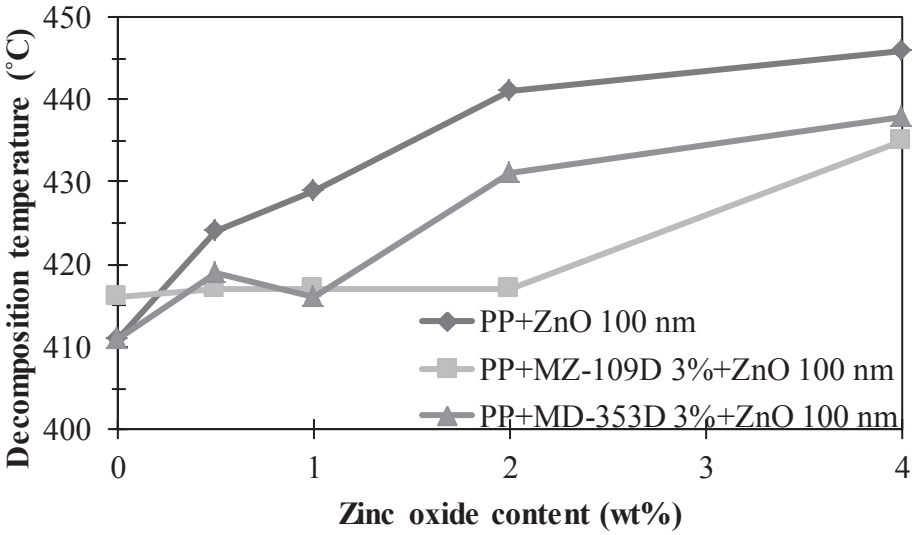

Figure 57 Decomposition temperature (T_{d5}) of PP/ZnO composites without and with two types of PP-g-MA compatibilizer

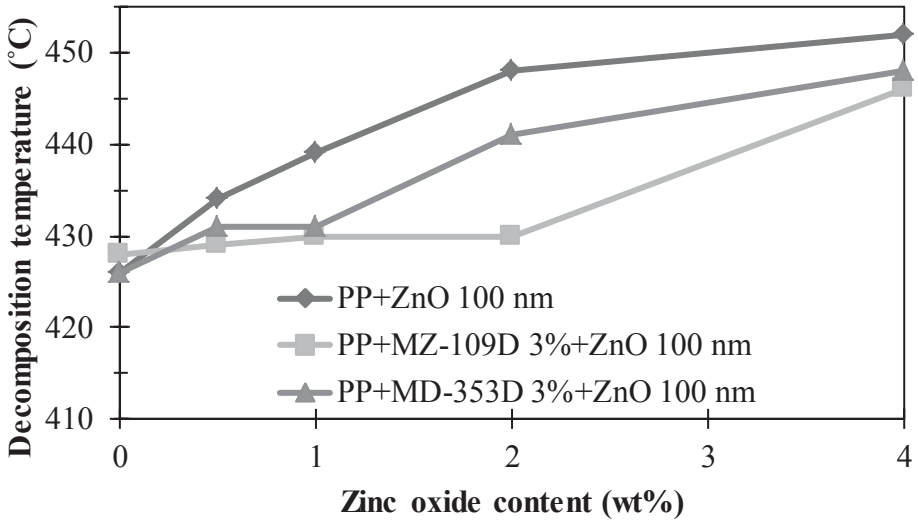

Figure 58 Decomposition temperature (T_{d10}) of PP/ZnO composites without and with two types of PP-g-MA compatibilizer

4.3 Mechanical properties

(1) Young's modulus

Figure 59 shows the Young's modulus of PP/ZnO composites without and with PP-g-MA. The results found that Young's modulus of PP/ZnO composites without PP-g-MA increased at 0.5-1 wt% of ZnO content and dropped after adding 2-4 wt% of ZnO content. After adding MZ-109D without ZnO, Young's modulus was lowered than pure PP. When adding ZnO in the composites between PP and MZ-109D, Young's modulus was increased with increasing ZnO content and higher than PP/ZnO without PP-g-MA and with MD-353D. PP/ZnO composites with MD-353D showed Young's modulus of the composites slightly lower than pure PP. After adding ZnO, Young's modulus of PP/ZnO composites increased with increasing ZnO content but lower than PP/ZnO composites with MZ-109D and higher than PP/ZnO composites without PP-g-MA after 2-4 wt% of ZnO content.

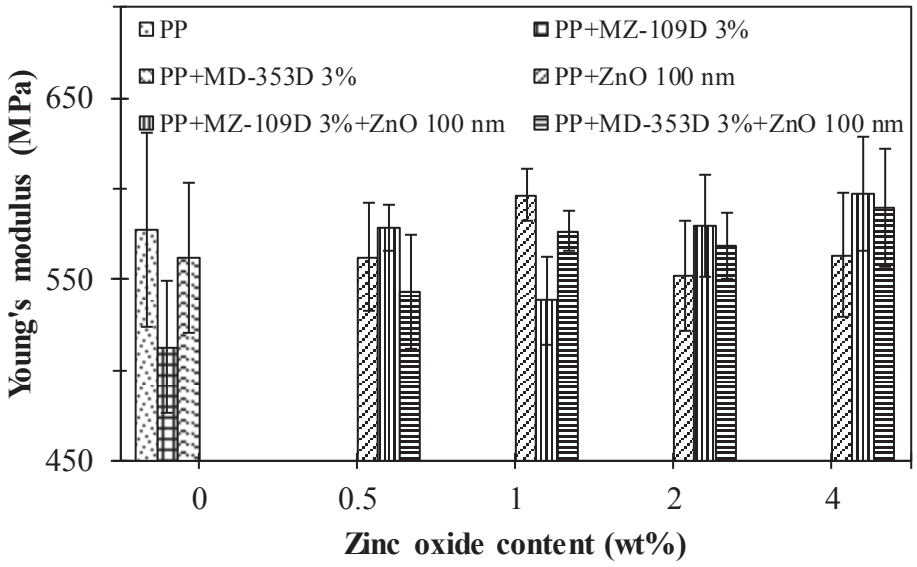

Figure 59 Young's modulus of PP/ZnO 100 nm composites without and with two types of PP-g-MA compatibilizer

(2) Tensile strength

Figure 60 shows tensile strength of PP/ZnO composites without and with PP-g-MA. The results found that tensile strength of PP/ZnO composites without PP-g-MA did not change clearly with ZnO content at 0.5-3 wt% and dropped at 4 wt% of ZnO content. After adding MZ-109D without ZnO, tensile strength of PP/ZnO composites was higher than PP. When adding ZnO, tensile strength increased with increasing ZnO content and dropped at 4 wt% of ZnO. Tensile strength of PP/ZnO composites with PP-g-MA lower than PP/ZnO composites without PP-g-MA. The composites after adding MD-353D without ZnO, tensile strength was higher than PP and not different with MZ-109D. Tensile strength of PP/ZnO composites with MD-353D increased with increasing ZnO content but lower than PP/ZnO without PP-g-MA and with MZ-109D composites.

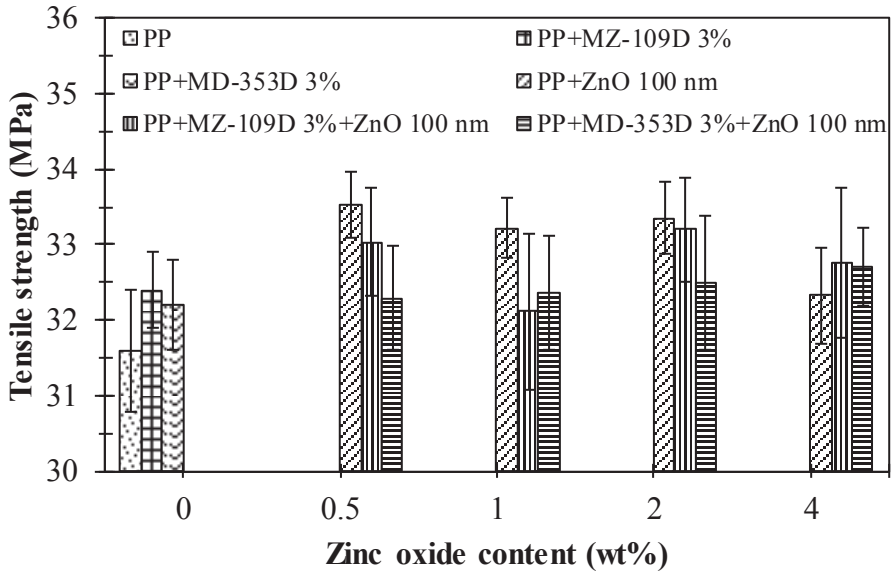

Figure 60 Tensile strength of PP/ZnO 100 nm composites without and with two types of PP-g-MA compatibilizer

(3) Stress at break

Figure 61 shows stress at break of PP/ZnO composites without and with PP-g-MA. The results found that stress at break of PP/ZnO composites without PP-g-MA increased with increasing ZnO content. The stress at break of the composites with MZ-109D increased with increasing ZnO content and higher than pure PP and the composites without PP-g-MA. The stress at break of the composites with MD-353D did not different clearly compared with PP/ZnO composites without MD-353D. The adding MD-353D increased the stress at break of the composites with increasing ZnO content and lower than PP/ZnO composites with MZ-109D.

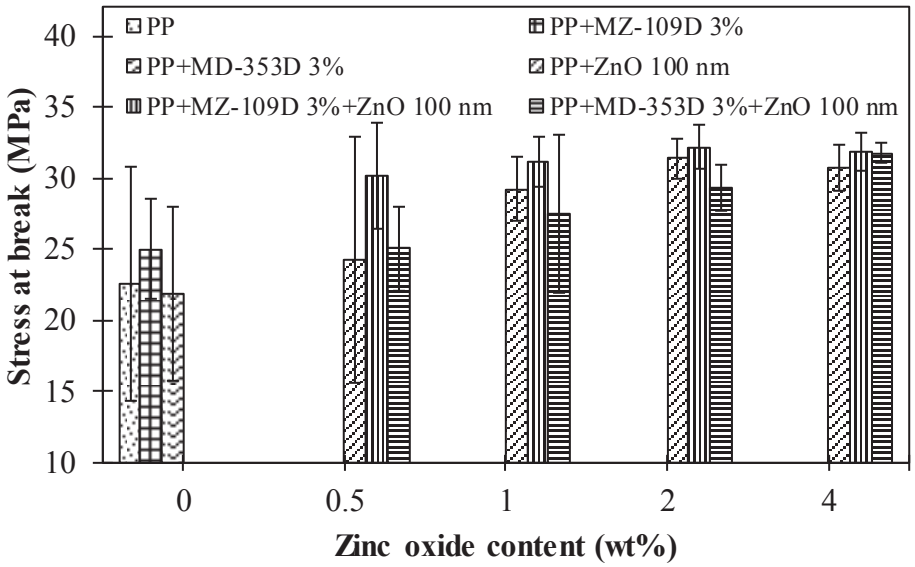

Figure 61 Stress at break of PP/ZnO 100 nm composites without and with two types of PP-g-MA compatibilizer

(4) Percent strain at break

Figure 62 shows the percent strain at break of PP/ZnO composites without and with PP-g-MA. The results found that the percent strain at break of PP/ZnO composites without PP-g-MA decreased with increasing ZnO content. PP/ZnO composites with MZ-109D showed the percent strain at break was higher than PP. The percent strain at break of the composites with MZ-109D decreased with increasing ZnO content and lower than PP/ZnO composites without PP-g-MA. PP/ZnO composites with MD-353D showed the percent strain at break was higher than PP and the composites with MZ-109D. The percent strain at break of the composites with MD-353D decreased with increasing ZnO content and lower than PP/ZnO composites without PP-g-MA but higher than PP/ZnO composites with MZ-109D.

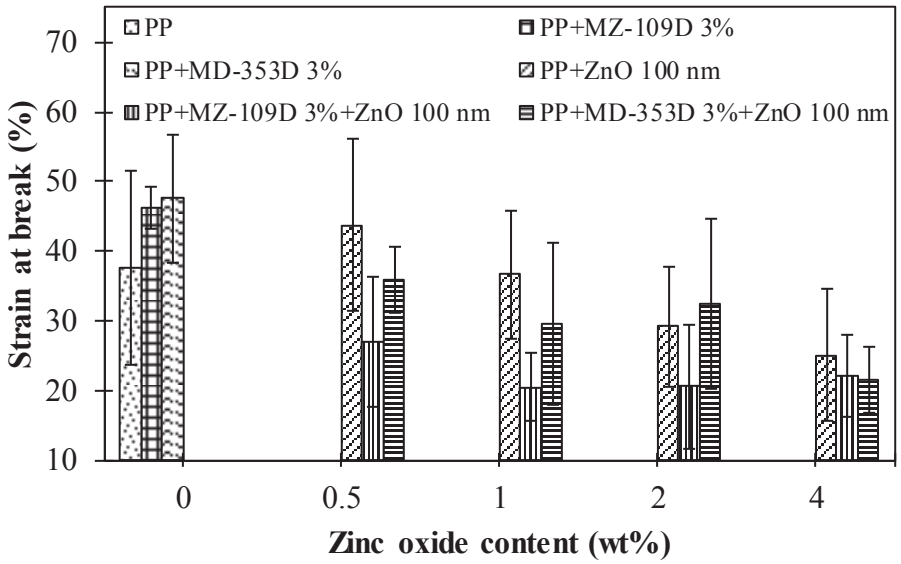

Figure 62 Percent strain at break of PP/ZnO 100 nm composites without and with two types of PP-g-MA compatibilizer

(5) Impact strength

Figure 63 shows impact strength of PP/ZnO composites without and with PP-g-MA. The results found that impact strength of PP/ZnO composites without PP-g-MA increased with increasing ZnO content at 0.5-2 wt% and dropped at 4 wt%. Adding MZ-109D, impact strength was lowered than PP. After adding ZnO, impact strength of PP/ZnO composites increased at 0.5-1 wt% of ZnO content and decreased after adding 2 wt% of ZnO content. The impact strength of the composites with MD-353D was lower than PP and slightly higher than the composites with MZ-109D. When added ZnO, impact strength of PP/ZnO composites with MD-353D increased with increasing ZnO content in the range of 0.5-1 wt% and dropped after adding ZnO content 2-4 wt%.

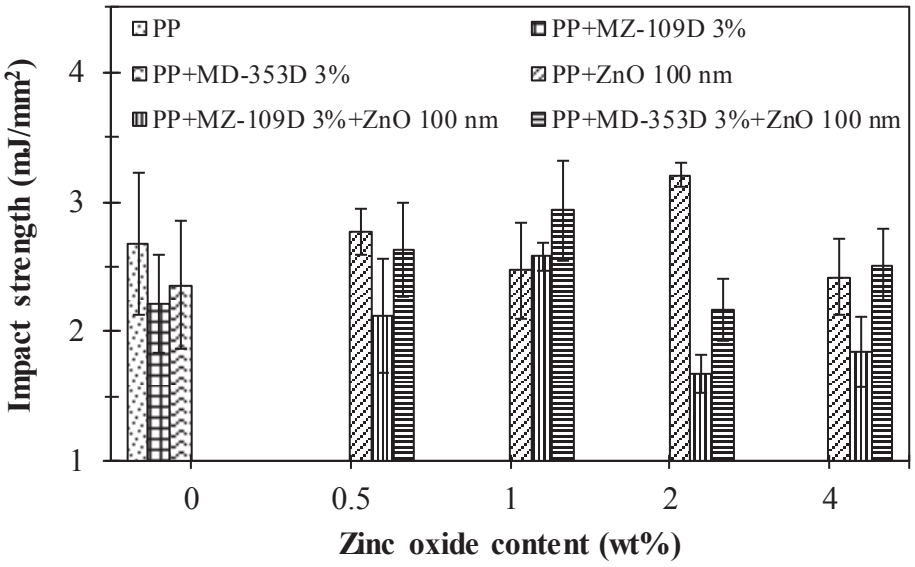

Figure 63 Impact strength of PP/ZnO 100 nm composites without and with two types of PP-g-MA compatibilizer

4.4 Electrical properties

Dielectric constant

Figure 64 shows the dielectric constant of PP/ZnO 100 nm composites without and with PP-g-MA prepared by an internal mixer. Before adding PP-g-MA, the results found that the dielectric constant of PP/ZnO composites slightly increased with increased ZnO content. After adding PP-g-MA, the results found that the dielectric constant of PP/ZnO composites filled with MZ-109D had slightly increased at 0.5-1 wt% and dropped after 2 wt% of ZnO while the composites filled with MD-353D the dielectric constant did not change evidently. It was found that the dielectric constant of PP/ZnO composites with MZ-109D had been slightly higher than without PP-g-MA and PP/ZnO composites with MD-353D at 0.5-1 wt% but after 2 wt% the dielectric constant of PP/ZnO composites without PP-g-MA trend to be higher than PP/ZnO composites filled with MZ-109D or MD-353D.

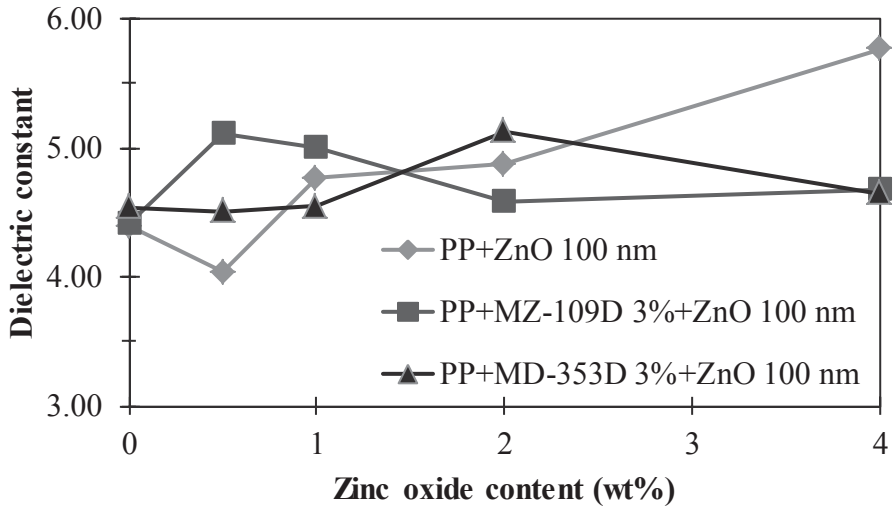

Figure 64 Dielectric constant of PP/ZnO composites without and with two types of PP-g-MA compatibilizer

5. Properties of PP/ZnO composites without and with PP-g-MA (MZ-109D) at various sizes and shapes of ZnO

5.1 Effect of sizes of ZnO on properties of PP/ZnO composites without and with PP-g-MA (MZ-109D) compatibilizer

5.1.1 Dispersion and fractured surface of ZnO in PP matrix

The dispersion of ZnO particles in PP matrix and the impact fractured surface of PP/ZnO composites before and after adding PP-g-MA compatibilizer were examined by SEM. Figures 65 shows the dispersion of ZnO 71 and 250 nm in PP matrix without PP-g-MA. All of PP/ZnO composite samples with various sizes were found that the dispersion of ZnO in PP matrix without compatibilizer was poor and formed large aggregates, addition of ZnO high content had an effect of the strong agglomerates made it difficult to disperse uniformly the particles in the matrix. Comparison between ZnO 71 and 250 nm in Figure 65 and 66,

it was found that ZnO 71 nm had higher agglomeration than ZnO 250 nm this may due to the small particles had high surface area so it made high agglomeration.

Figure 67 and 68 show the composites after adding compatibilizer the dispersion of ZnO particles with different sizes was relatively good, only few aggregates existed of all ZnO samples. The presence of the 3 wt% PP-g-MA compatibilizer improved properties of PP. It can be seen that addition of compatibilizer improved interfacial adhesion and the dispersion of ZnO in PP matrix. The crack initiation and propagation zones that shown in Figure 69-72. It can be seen that the propagation zone has two different regions, a narrow stable crack growth region and a region of unstable crack growth. The narrow stable crack growth region lies immediately after the crack initiation site. The unstable crack growth region has cleavage type of fracture in the middle and thread like fibrils along the edges. Cleavage is associated with low-energy brittle fracture, which has been bright reflecting facets. The edges of the unstable crack growth region have a thread like fibrils (Saminathan *et al.*, 2008).

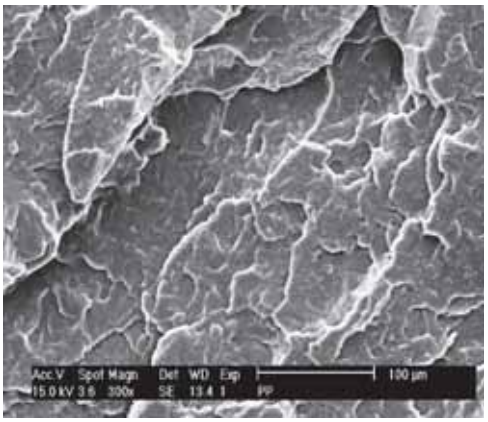

(a) PP

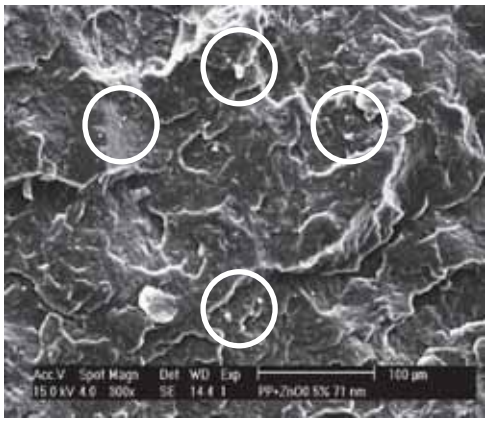

(b) ZnO (71 nm) 0.5 wt%

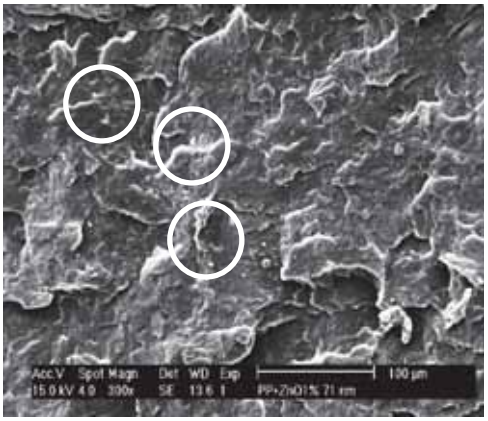

(c) ZnO (71 nm) 1 wt%

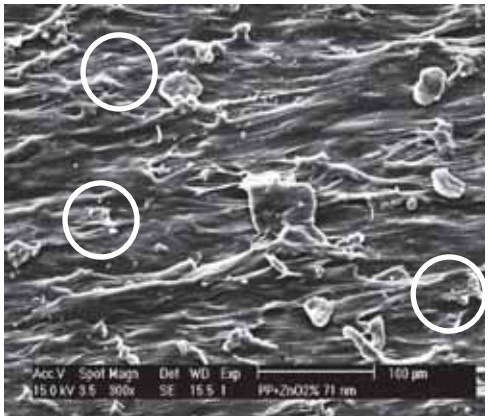

(d) ZnO (71 nm) 2 wt%

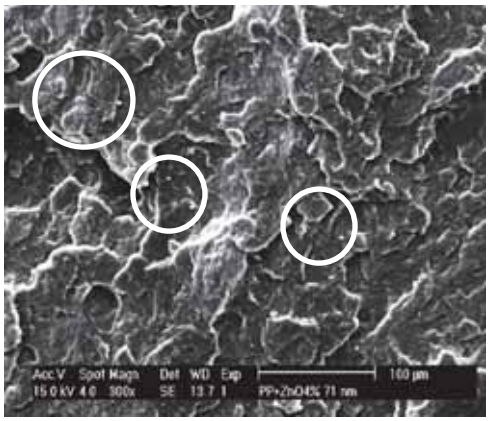

(e) ZnO (71 nm) 4 wt%

Figure 65 SEM micrographs of the composites of PP and ZnO 71 nm

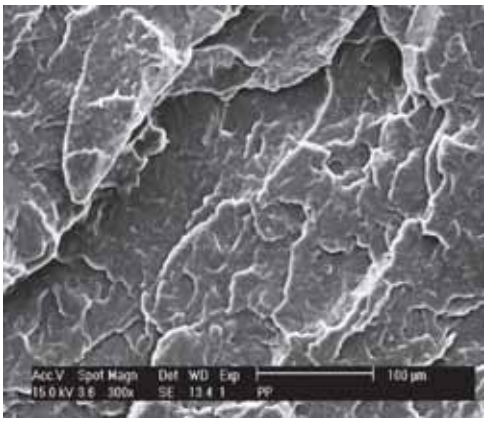

(a) PP

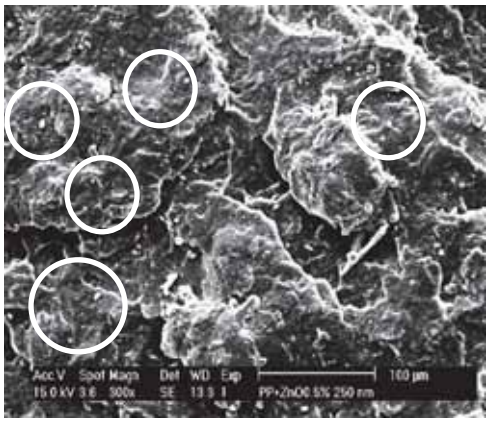

(b) ZnO (250 nm) 0.5 wt%

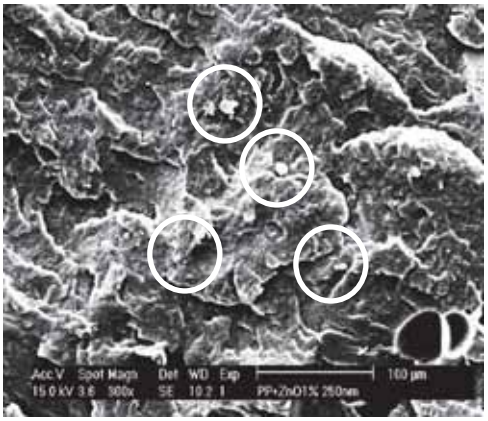

(c) ZnO (250 nm) 1 wt%

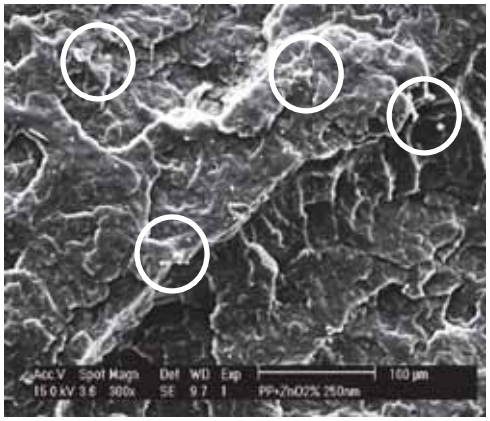

(d) ZnO (250 nm) 2 wt%

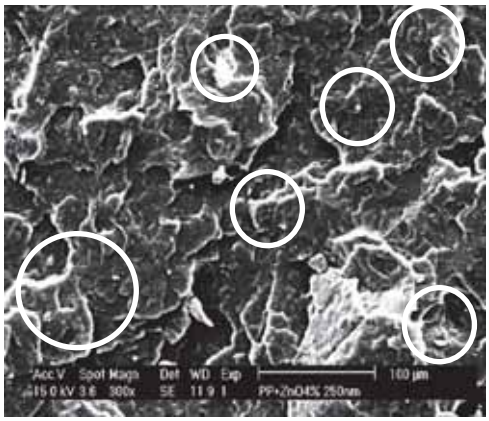

(e) ZnO (250 nm) 4 wt%

Figure 66 SEM micrographs of the composites of PP and ZnO 250 nm

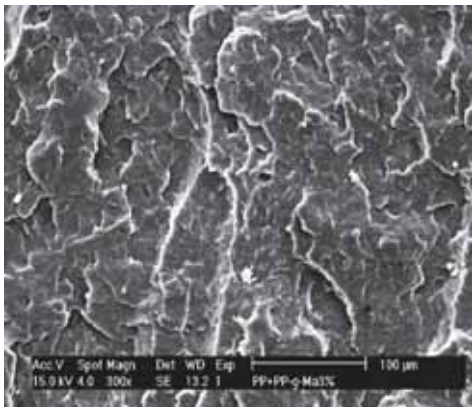

(a) PP

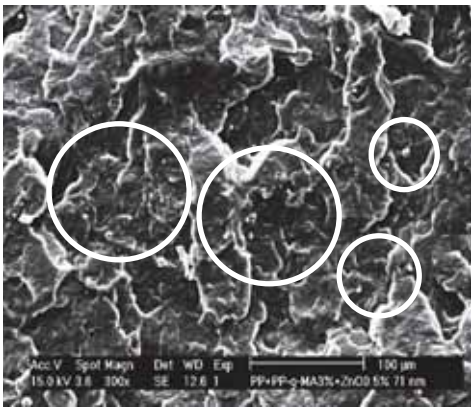

(b) ZnO (71 nm) 0.5 wt%

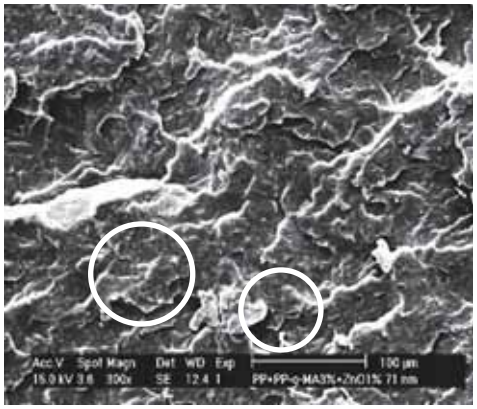

(c) ZnO (71 nm) 1 wt%

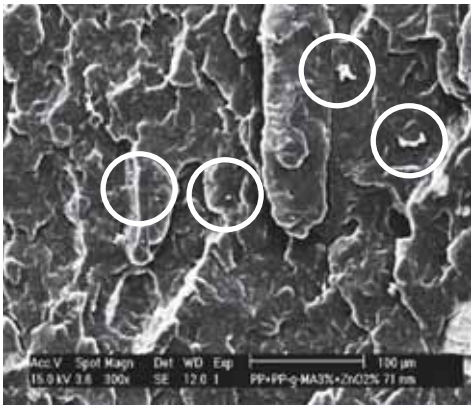

(d) ZnO (71 nm) 2 wt%

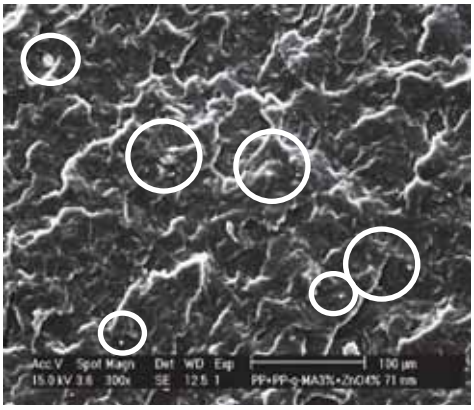

(e) ZnO (71 nm) 4 wt%

Figure 67 SEM micrographs of the composites of PP and ZnO 71 nm with PP-g-MA 3 wt%

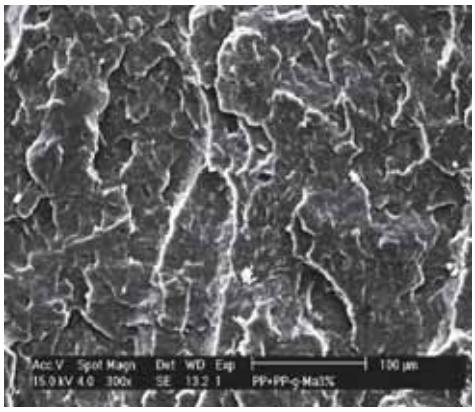

(a) PP

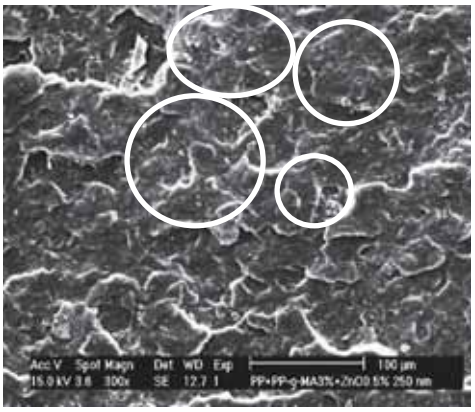

(b) ZnO (250 nm) 0.5 wt%

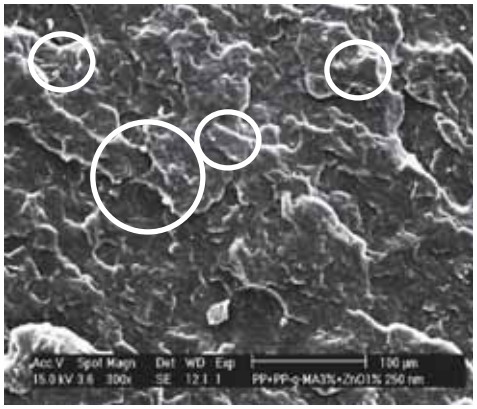

(c) ZnO (250 nm) 1 wt%

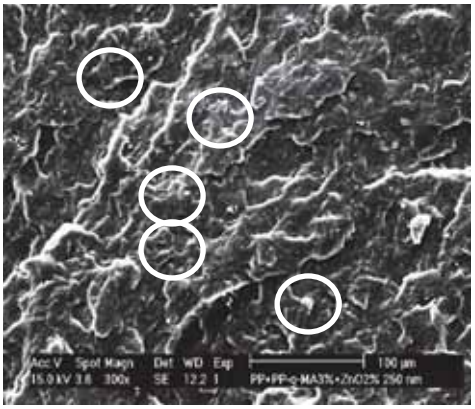

(d) ZnO (250 nm) 2 wt%

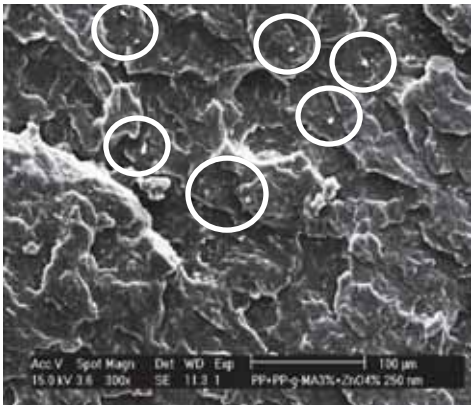

(e) ZnO (250 nm) 4 wt%

Figure 68 SEM micrographs of the composites of PP and ZnO 250 nm with PP-g-MA 3 wt%

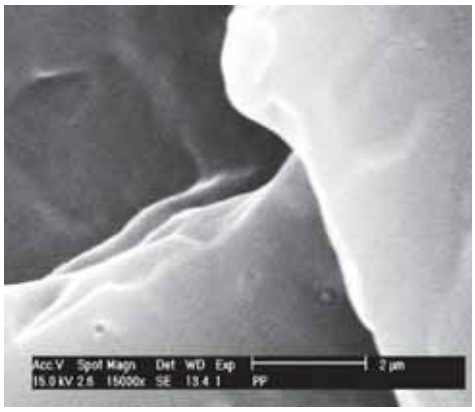

(a) PP

(b) ZnO (71 nm) 0.5 wt%

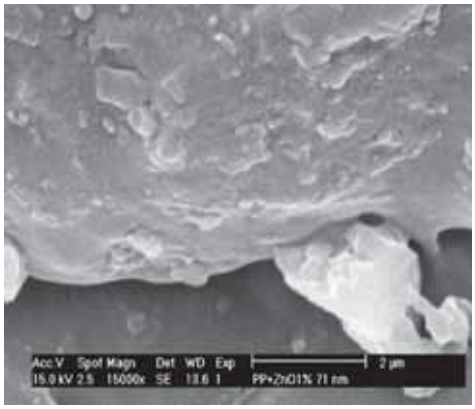

(c) ZnO (71 nm) 1 wt%

(d) ZnO (71 nm) 2 wt%

(e) ZnO (71 nm) 4 wt%

Figure 69 SEM micrographs of impact fractured-surface of PP/ZnO 71 nm composites

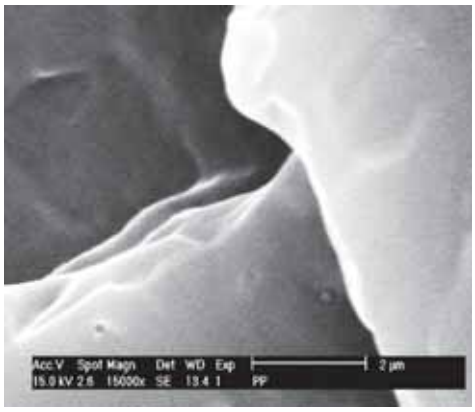

(a) PP

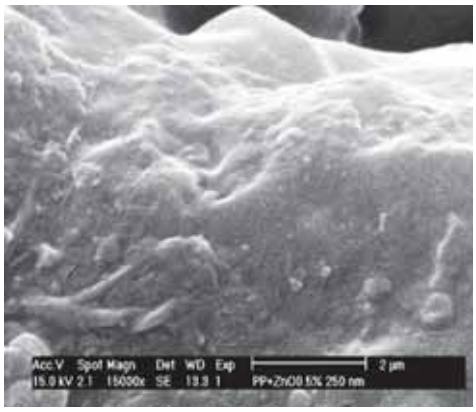

(b) ZnO (250 nm) 0.5 wt%

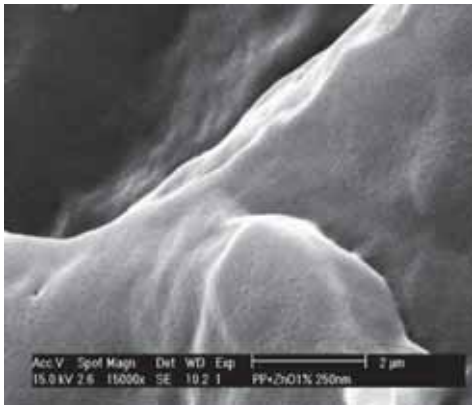

(c) ZnO (250 nm) 1 wt%

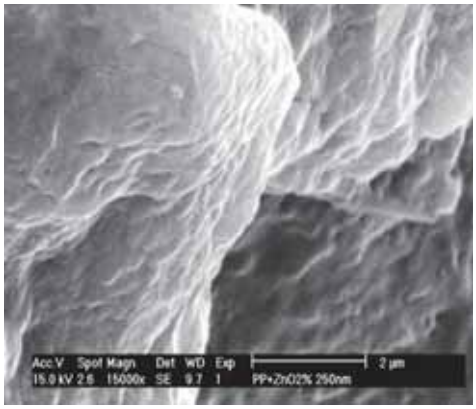

(d) ZnO (250 nm) 2 wt%

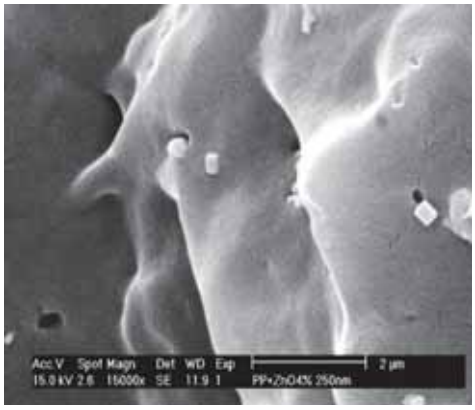

(e) ZnO (250 nm) 4 wt%

Figure 70 SEM micrographs of impact fractured-surface of PP/ ZnO 250 nm composites

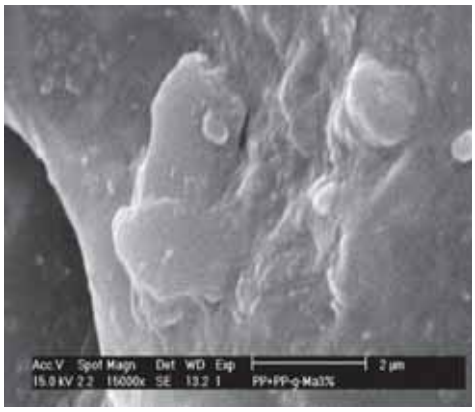

(a) PP

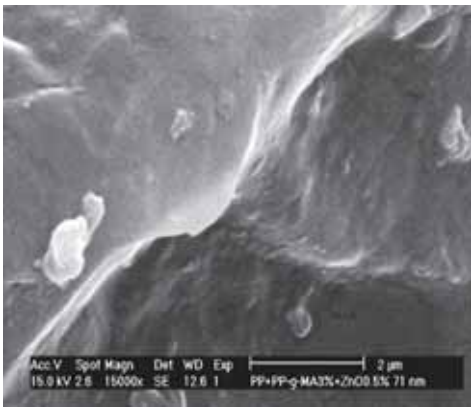

(b) ZnO (71 nm) 0.5 wt%

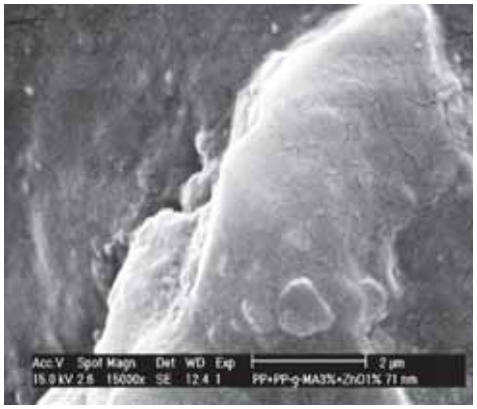

(c) ZnO (71 nm) 1 wt%

(d) ZnO (71 nm) 2 wt%

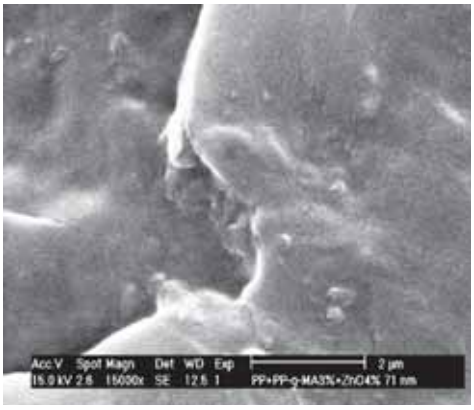

(e) ZnO (71 nm) 4 wt%

Figure 71 Impact fractured surface of the composites of PP and ZnO 71 nm with PP-g-MA 3 wt%

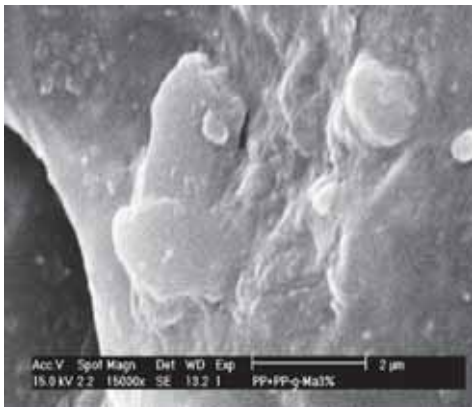

(a) PP

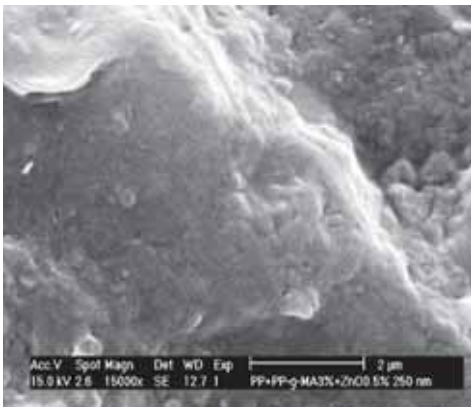

(b) ZnO (250 nm) 0.5 wt%

(c) ZnO (250 nm) 1 wt%

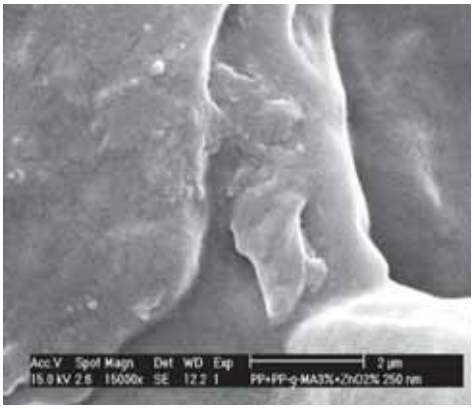

(d) ZnO (250 nm) 2 wt%

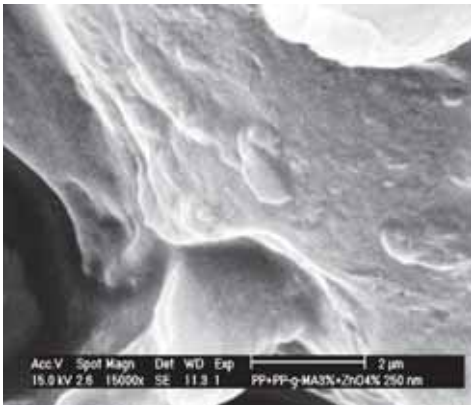

(e) ZnO 4 wt% 250 nm

Figure 72 Impact fractured surface of the composites of PP and ZnO 250 nm with PP-g-MA 3 wt%

5.1.2 Thermal properties

(1) Melting temperature (T_m)

Figure 73-74 and Table 2 show the effect of ZnO 71 and 250 nm on the T_m of PP/ZnO composites without and with PP-g-MA compatibilizer. Before adding PP-g-MA, the results found that the addition of ZnO 71 and 250 nm had not significantly changed the T_m of the composites of PP/ZnO. It can be deduced that the crystallite size distribution of PP was hardly changed with the presence of ZnO (Nan-Ying, 2007). After adding PP-g-MA, the results found that the T_m had a slightly increased with PP-g-MA compatibilizer. This can be explained that the presence of PP-g-MA had a slightly increased crystallite size distribution of PP (Nan-Ying, 2007).

(2) Crystallization temperature (T_c)

Figure 75-76 and Table 2 show the effect of ZnO 71 and 250 nm on T_c of PP/ZnO composites without and with PP-g-MA compatibilizer. The results found that before adding PP-g-MA the addition of ZnO 71 and 250 nm in PP matrix small increased in T_c with increasing ZnO content. PP/ZnO 250 nm composites had slightly higher T_c than PP/ZnO 71 nm composites. The results indicated that the efficiency of ZnO as a nucleating agent for PP crystallization, but mainly at high ZnO content (Nan-Ying, 2007). The corresponding of T_c with almost constant values was in good agreement with the isothermal crystallization results. After adding PP-g-MA, the results found a small increased in T_c from 115 ˚C to 118 ˚C. It can be explained that the incorporation of the compatibilizer improved the level of crystallinity of PP (Othman, 2006).

(3) Percent crystallinity

Figure 77-78 show the effect of ZnO 71 and 250 nm on the percent crystallinity of PP/ZnO composites without and with PP-g-MA compatibilizer. The results found that the percent crystallinity of PP/ZnO 71 nm composites without PP-g-MA had slightly increased with increasing ZnO content.

The percent crystallinity of PP/ZnO 250 nm composites slightly decreased with increasing ZnO content. PP/ZnO 71 nm composites had higher the percent crystallinity than PP/ZnO 250 nm composites due to ZnO 71 nm was better nucleating agent than ZnO 250 nm. After adding PP-g-MA, the results found that the percent crystallinity of PP/ZnO 71 nm and PP/ZnO 250 nm composites increased. The percent crystallinity of PP/ZnO 71 nm composites after adding PP-g-MA had been higher than PP/ZnO 250 nm composites after adding PP-g-MA at ZnO content of 0.5-1 wt%. After 1 wt% of ZnO content the percent crystallinity of PP/ZnO 250 nm composites with PP-g-MA had been higher than PP/ZnO 71 nm composites with PP-g-MA. It can be explained that PP-g-MA enhanced crystallization temperature (Nan-Ying, 2007) and dispersion of ZnO particles so the percent crystallinity was improved. The percent crystallinity of PP/ZnO 71 and 250 nm composites without and with PP-g-MA was 32±2.43 %, 32±1.85 %, 28±1.11 % and 28±4.39 %, respectively.

Table 2 Thermal behaviors of PP/ZnO composites without and with PP-g-MA at various sizes of ZnO

Sample	T_m (°C)	T_c (°C)
PP	161	115
PP+PP-g-MA 3%	162	118
PP+ZnO 71 nm	161±0.57	115±0.31
PP+ZnO 250 nm	161±0.24	115±0.73
PP+PP-g-MA 3%+ZnO 71 nm	162±0.34	118±1.41
PP+PP-g-MA 3%+ZnO 250 nm	162±0.80	118±0.27

(4) Decomposition temperature (T_d)

Figures 79-82 show the effect of ZnO 71 and 250 nm on the T_d of PP/ZnO composites without and with PP-g-MA compatibilizer. The T_d was measured by TGA and was calculated at 5 (T_{d5}) and 10 (T_{d10}) %weight loss of the composites. The results found that the T_{d5} and Td_{10} of PP/ZnO composites without PP-g-MA increased with increasing filler content and were higher than the T_{d5} and Td_{10} of pure PP, which showed lower thermal stability than PP/ZnO composites. The PP/ZnO 71 nm composites had the T_{d5} and Td_{10} higher than PP/ZnO 250 nm composites. It can be explained that ZnO 71 and 250 nm improved the thermal stability of PP because of the improvement in percent crystallinity of the PP/ZnO composites so it made more energy to break the crystalline bond. The composites after adding PP-g-MA showed the T_{d5} and Td_{10} of PP/ZnO 71 nm composites were higher than the composites without PP-g-MA at ZnO content more than 1 wt%. The T_{d5} and Td_{10} of PP/ZnO 250 nm composites with PP-g-MA were higher than the composites without PP-g-MA. It can be explained that PP-g-MA made a good dispersion of ZnO particles so the percent crystallinity improved.

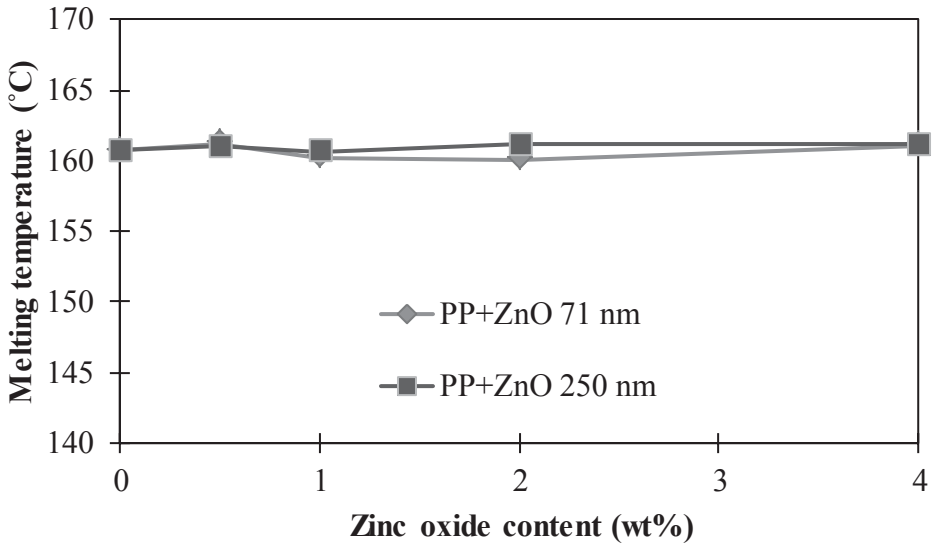

Figure 73 Melting temperatures of PP/ZnO composites without PP-g-MA at various particle sizes of ZnO

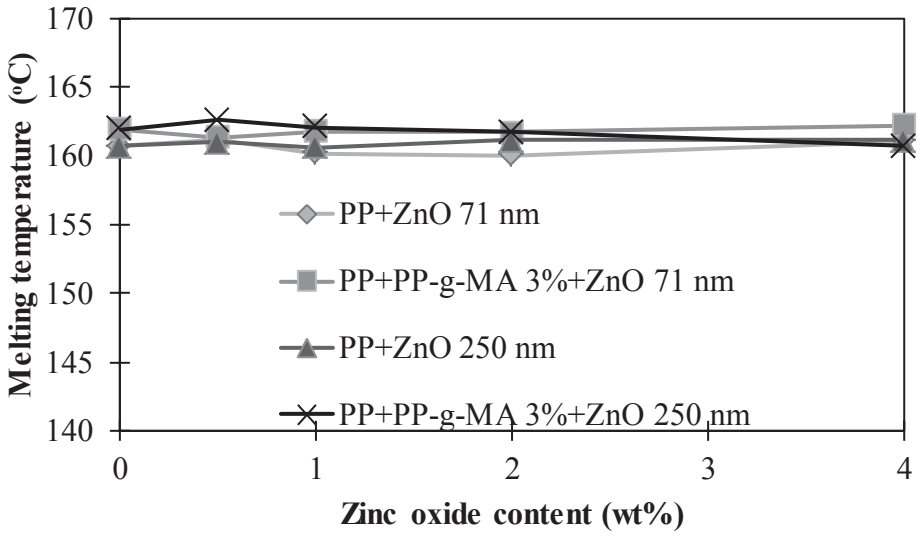

Figure 74 Melting temperature of PP/ZnO composites without and with PP-g-MA at various particle sizes of ZnO

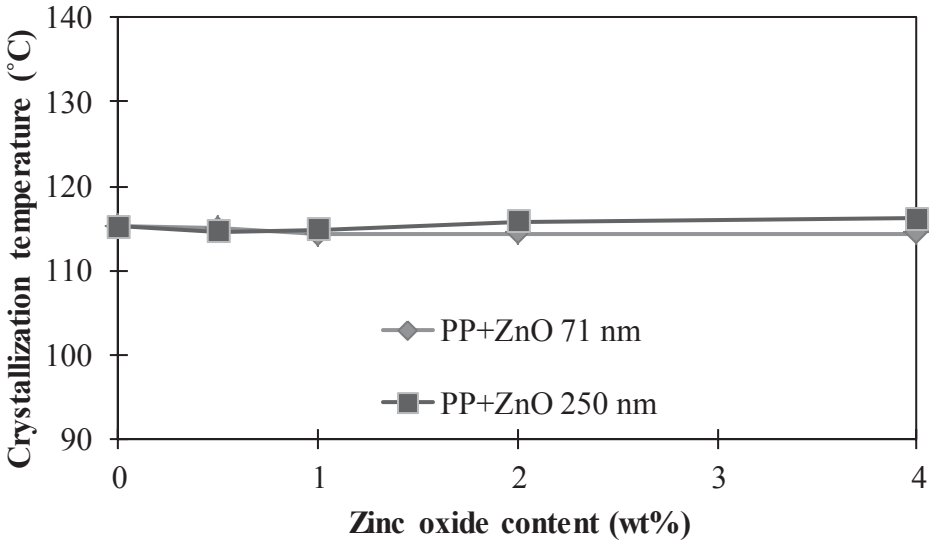

Figure 75 Crystallization temperatures of PP/ZnO composites without PP-g-MA at various particle sizes of ZnO

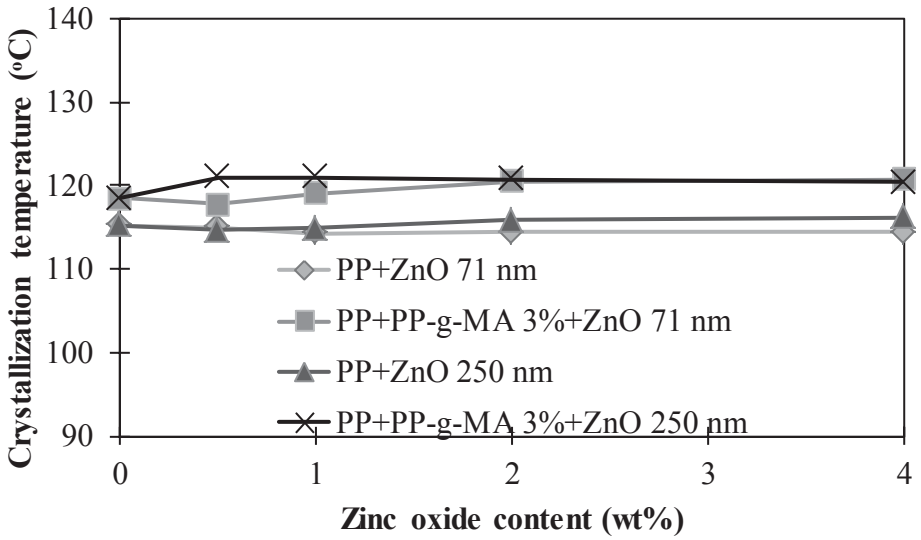

Figure 76 Crystallization temperature of PP/ZnO composites without and with PP-g-MA at various particle sizes of ZnO

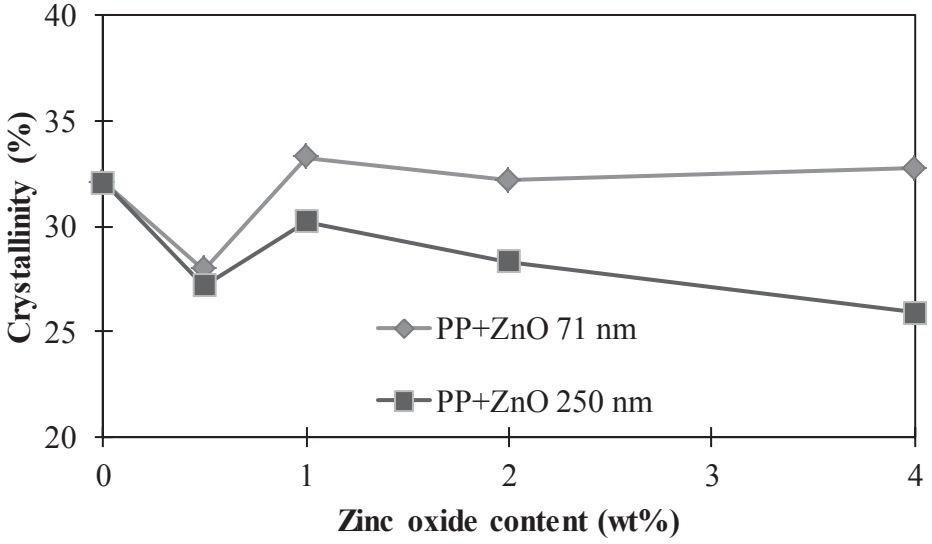

Figure 77 Percent crystallinity of PP/ZnO composites without PP-g-MA at various particle sizes of ZnO

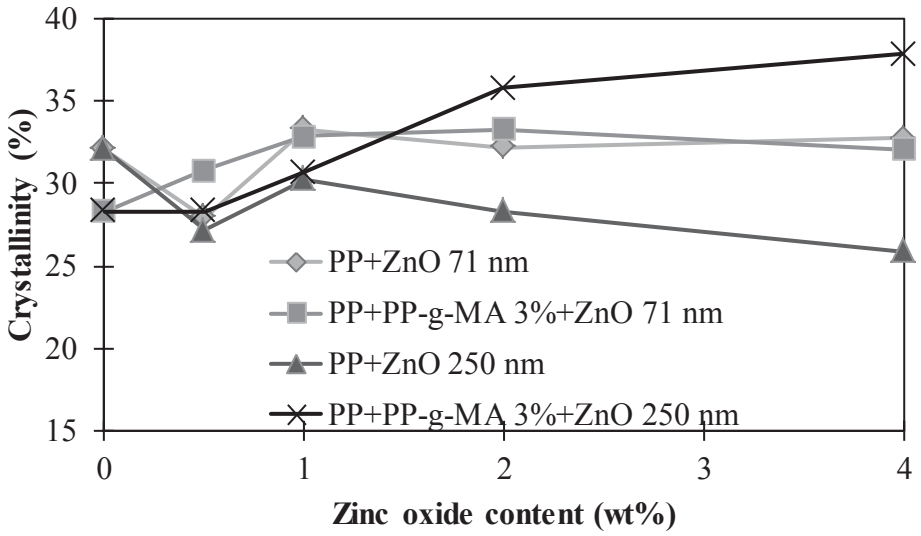

Figure 78 Percent crystallinity of PP/ZnO composites without and with PP-g-MA at various particle sizes of ZnO

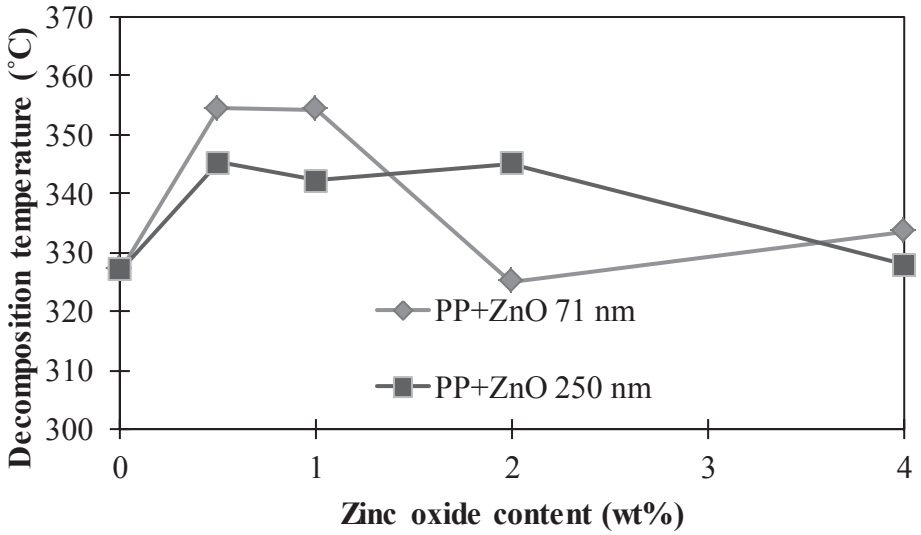

Figure 79 Decomposition temperature (T_{d5}) of PP/ZnO composites without PP-g-MA at various particle sizes of ZnO

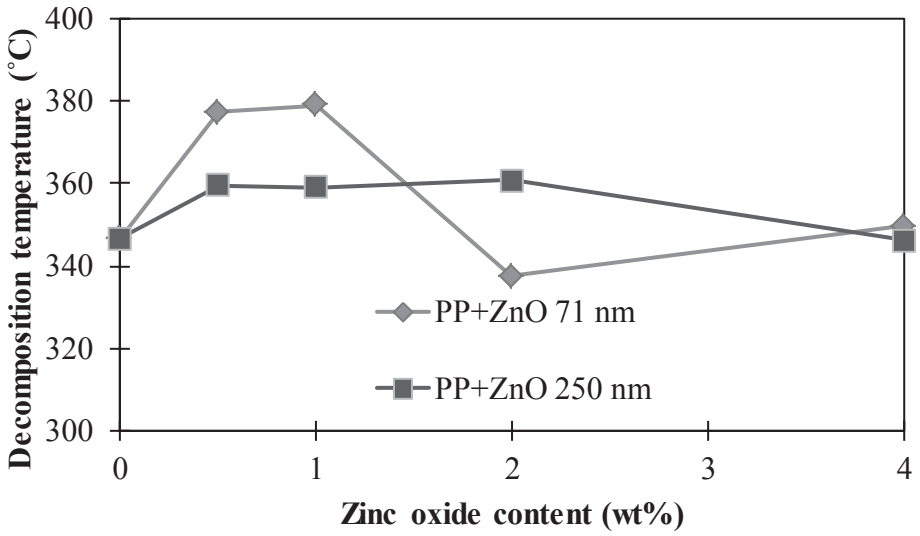

Figure 80 Decomposition temperature (T_{d10}) of PP/ZnO composites without PP-g-MA at various particle sizes of ZnO

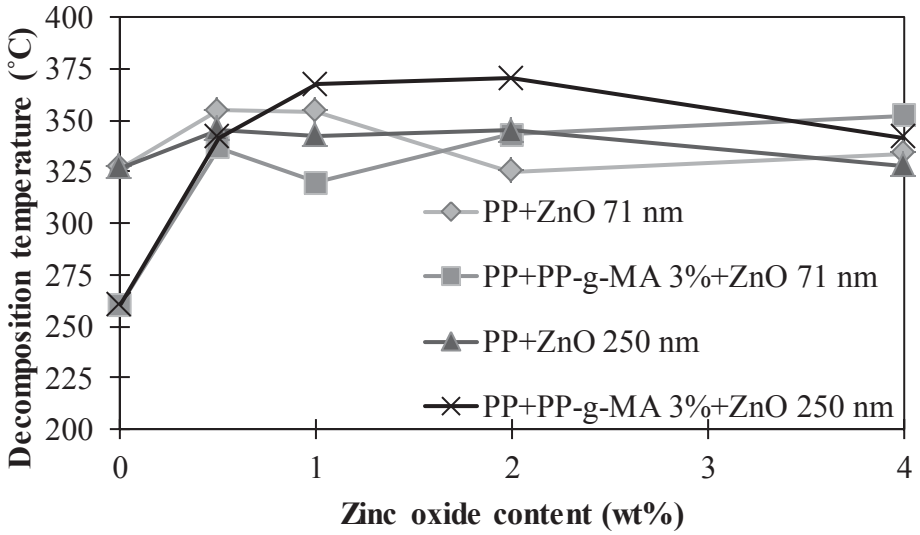

Figure 81 Decomposition temperature (T_{d5}) of PP/ZnO composites without and with PP-g-MA at various particle sizes of ZnO

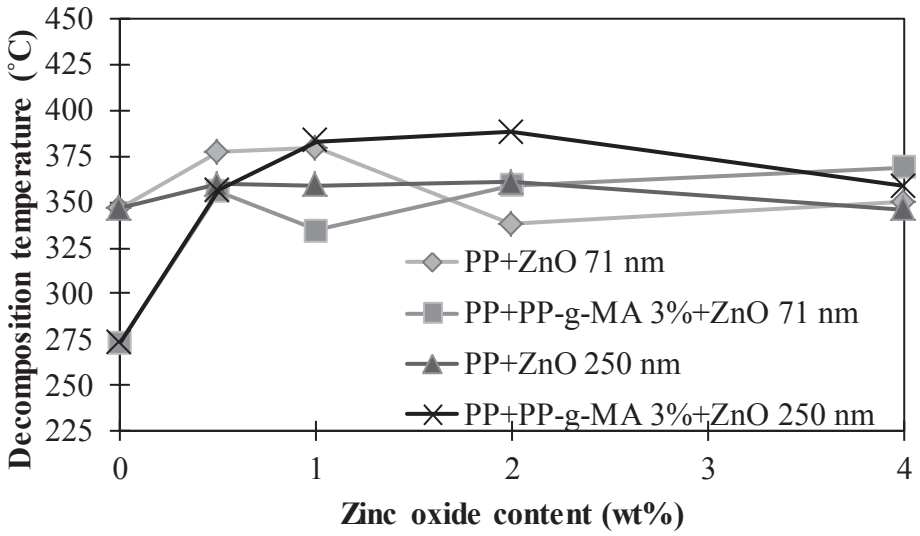

Figure 82 Decomposition temperature (T_{d10}) of PP/ZnO composites without and with PP-g-MA at various particle sizes of ZnO

5.1.3 Mechanical properties

(1) Young's modulus

Figure 83-84 show the effect of particle sizes of ZnO on Young's modulus of PP/ZnO composites without and with PP-g-MA compatibilizer. Before adding PP-g-MA, the results found that the Young's modulus of PP/ZnO 71 nm composites trend to be increased with increasing ZnO content. While Young's modulus of PP/ZnO 250 nm did not change evidently but a trend to be a slightly increased. This may due to the percent crystallinity of PP/ZnO 71 nm composites higher than PP/ZnO 250 nm composites so it led to more stiffness but lower toughness. After adding PP-g-MA, the results found that the Young's modulus of PP/ZnO 71 nm and PP/ZnO 250 nm composites increased higher than PP/ZnO composites before adding PP-g-MA. This can be explained that PP-g-MA enhanced interfacial adhesion (Hee-Soo, 2007) and reduced interfacial tension between the phases (O'Donnell, 1995) so the compatibility and dispersion of ZnO particles were

improved so the percent crystallinity increased, which made the composites more stiffness.

(2) Tensile strength

Figure 85-86 show the effect of particle sizes of ZnO on the tensile strength of PP/ZnO composites without and with PP-g-MA compatibilizer. Before adding PP-g-MA, the results found that the tensile strength of PP/ZnO 71 nm composites slightly increased after adding ZnO. The tensile strength of PP/ZnO 250 nm composites slightly increased at 0.5 wt% of ZnO particles into PP and then not changed with increasing ZnO content. PP/ZnO 250 nm composites had higher the tensile strength than PP/ZnO 71 nm composites. After adding PP-g-MA, the results found that the tensile strength of PP/ZnO 71 nm and PP/ZnO 250 nm composites with PP-g-MA had a slightly higher than the PP/ZnO 71 nm and PP/ZnO 250 nm composites without PP-g-MA. The increase in stiffness (Do Hoon *et al.*, 2007) due to the well dispersion increased the degree of crystallinity (Wacharawichanant *et al.*, 2008).

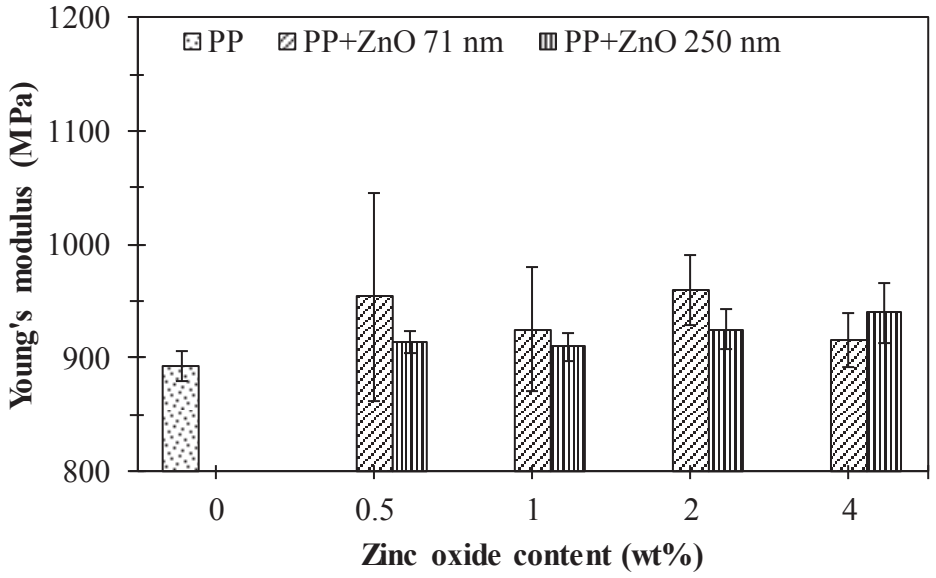

Figure 83 Young's modulus of PP/ZnO composites without PP-g-MA at various particle sizes of ZnO

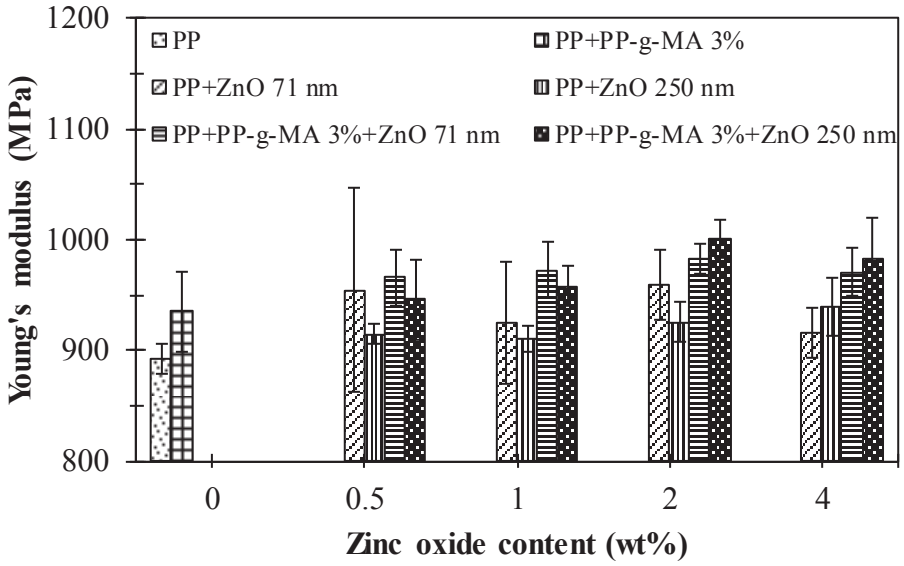

Figure 84 Young's modulus of PP/ZnO composites without and with PP-g-MA at various particle sizes of ZnO

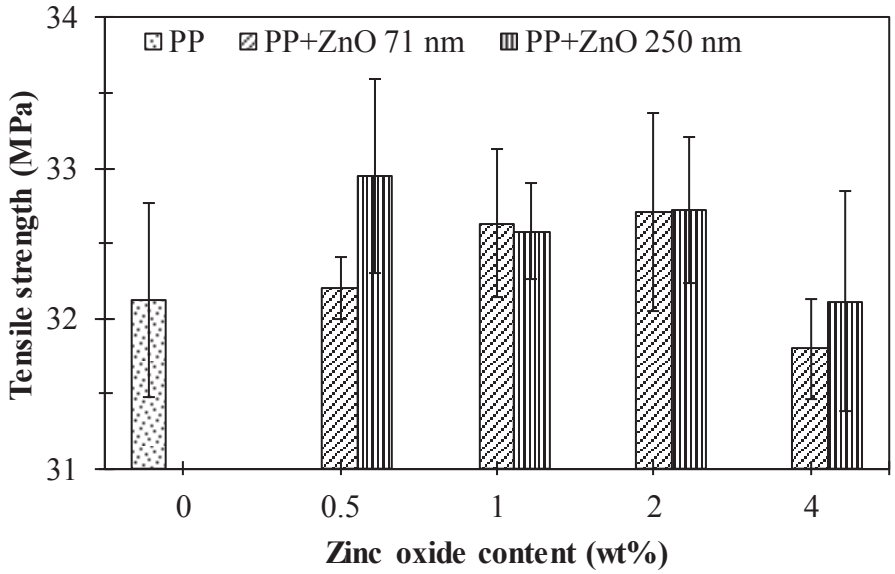

Figure 85 Tensile strength of PP/ZnO composites without PP-g-MA at various particle sizes of ZnO

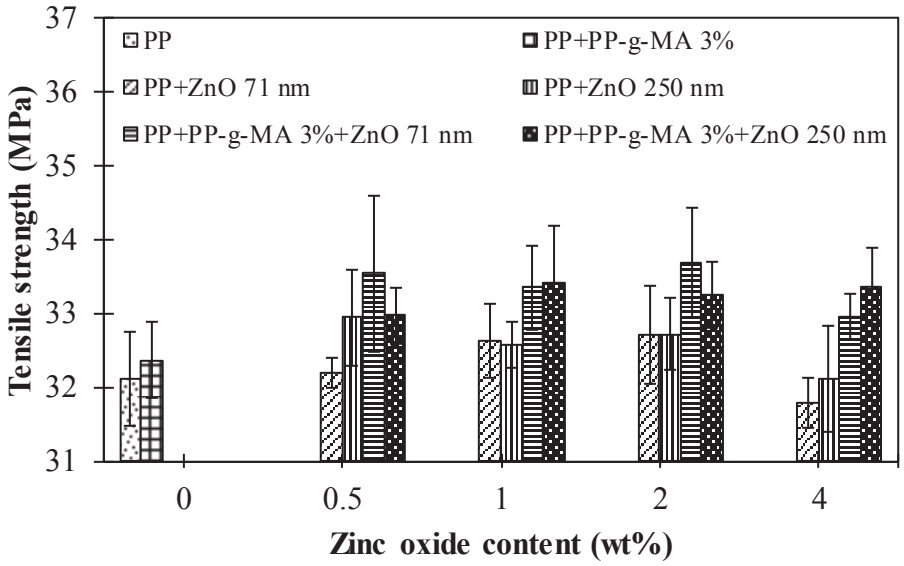

Figure 86 Tensile strength of PP/ZnO composites without and with PP-g-MA at various particle sizes of ZnO

(3) Stress at break

Figure 87-88 show the effect of particle sizes of ZnO on the stress at break of PP/ZnO composites without and with PP-g-MA compatibilizer. It can be seen that before adding PP-g-MA the stress at break of PP/ZnO 71 nm composites increased with increasing ZnO content. While stress at break of PP/ZnO 250 nm composites dropped with increasing ZnO content. This may due to PP/ZnO 71 nm composites had more percent crystallinity than PP/ZnO 250 nm composites, this led the composites more stiffness and lower toughness so the stress at break increased. The composites after adding PP-g-MA was found the stress at break of PP/ZnO 71 nm and PP/ZnO 250 nm composites with PP-g-MA had been higher than without PP-g-MA. This may due to the good dispersion of ZnO particles in the PP matrix made increased in percent crystallinity.

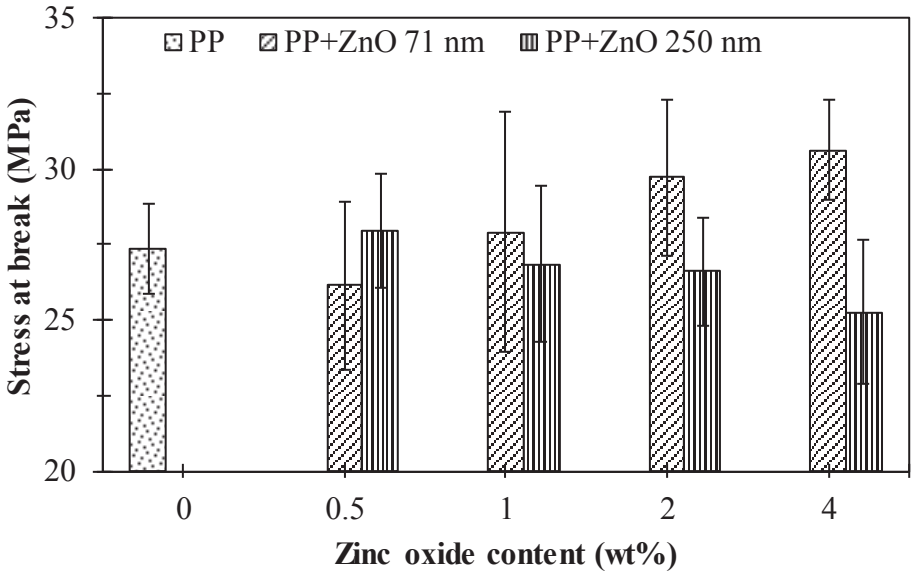

Figure 87 Stress at break of PP/ZnO composites without PP-g-MA at various particle sizes of ZnO

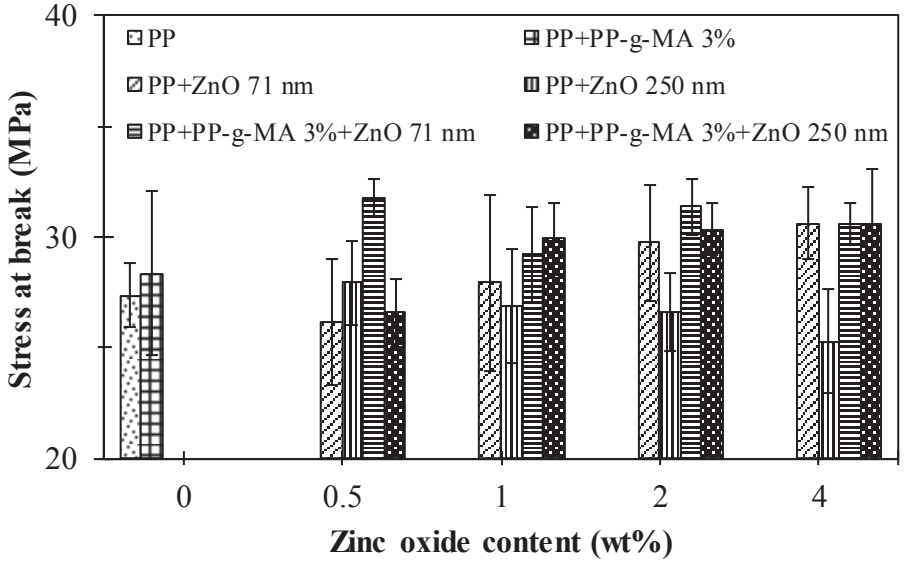

Figure 88 Stress at break of PP/ZnO composites without and with PP-g-MA at various particle sizes of ZnO

(4) Percent strain at break

Figure 89-90 show the effect of particle sizes of ZnO on the percent strain at break of PP/ZnO composites without and with PP-g-MA compatibilizer. The composites before adding PP-g-MA can be seen that the percent strain at break of PP/ZnO 71 nm composites had increased in a range of 0.5-2 wt% and lower than PP/ZnO 250 nm composites. This may due to the increased in percent crystallinity made the composites more stiffness so it decreased the percent strain at break. The composites after adding PP-g-MA was clearly found that the percent strain at break of PP/ZnO 71 nm and PP/ZnO 250 nm composites without PP-g-MA had been higher than the composites with PP-g-MA. This can be explained that the good dispersion of ZnO particles in PP matrix with adding PP-g-MA made crystalline smaller than without adding PP-g-MA.

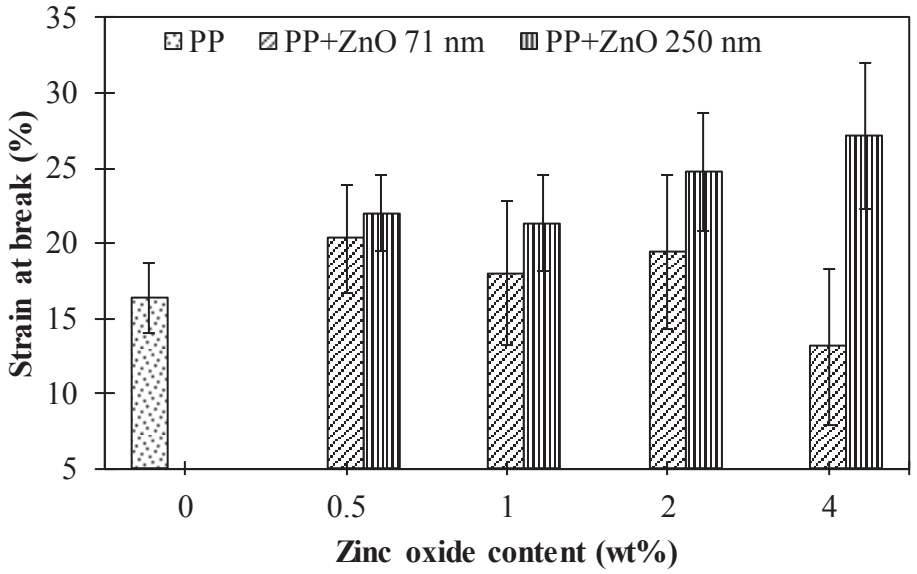

Figure 89 Percent strain at break of PP/ZnO composites without PP-g-MA at various particle sizes of ZnO

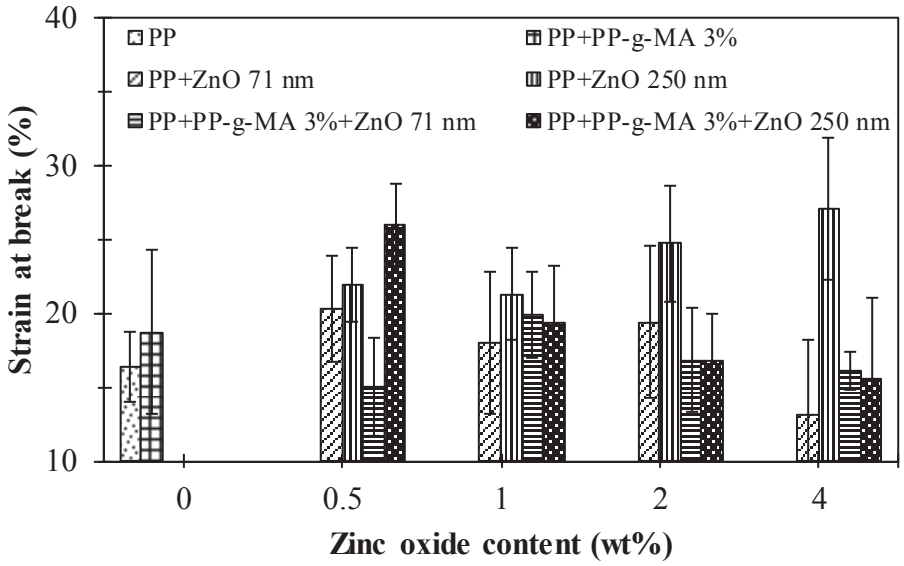

Figure 90 Percent strain at break of PP/ZnO composites without and with PP-g-MA at various particle sizes of ZnO

(5) Impact strength

Figure 91-92 show the effect of particle sizes of ZnO on the impact strength of PP/ZnO composites without and with PP-g-MA compatibilizer. The composites before adding PP-g-MA showed the impact strength of PP/ZnO 71 nm composites increased with increasing ZnO content. The impact strength of PP/ZnO 250 nm composites increased with increasing ZnO content and higher than PP/ZnO 71 nm composites. The impact strength improved due to increased energy absorption during the impact process (Yang *et al.*, 2006). The composites after adding PP-g-MA showed the impact strength of PP/ZnO 71 nm and PP/ZnO 250 nm composites were dropped compared without PP-g-MA. This may be due to the bigger crystalline of composites without PP-g-MA made it more stiffness.

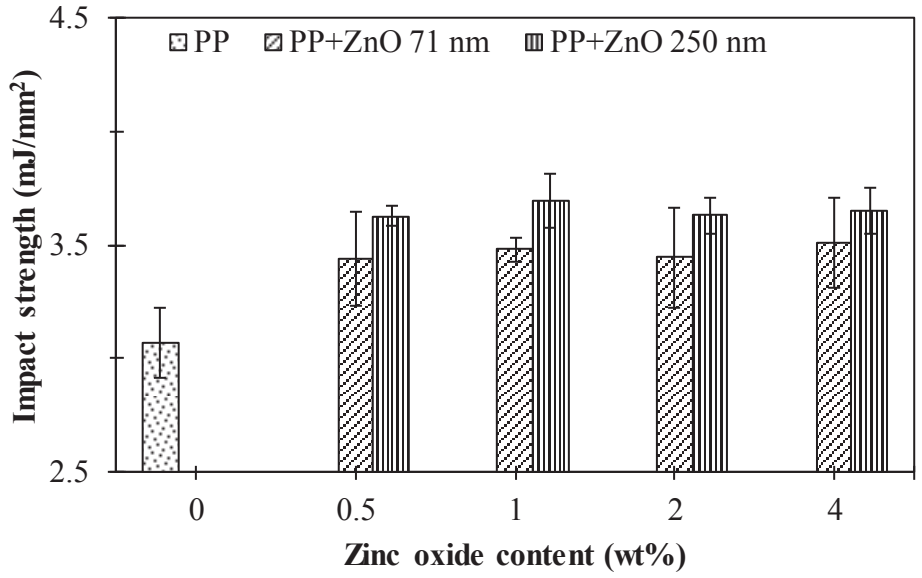

Figure 91 Impact strength of PP/ZnO composites without PP-g-MA at various particle sizes of ZnO

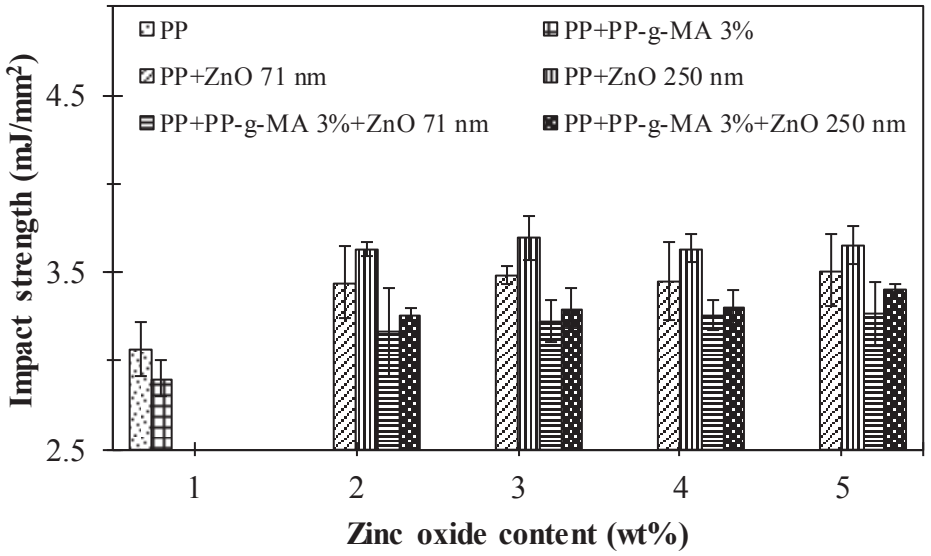

Figure 92 Impact strength of PP/ZnO composites without and with PP-g-MA at various particle sizes of ZnO

5.1.4 Dielectric Properties

Dielectric constant

Figure 93-94 show the effect of particle sizes of ZnO on the dielectric constant of PP/ZnO composites without and with PP-g-MA compatibilizer. The composites before adding PP-g-MA showed the dielectric constant of PP/ZnO 71 nm and PP/ZnO 250 nm composites slightly increased with increased ZnO content but for PP/ZnO 250 nm composites showed the dielectric constant decreased at 1 wt% of ZnO. The composites after adding PP-g-MA showed the dielectric constant of PP/ZnO 71 nm composites had been higher than PP/ZnO 71 nm composites without PP-g-MA. PP/ZnO 250 nm composites showed the dielectric constant of PP/ZnO 250 nm composites with PP-g-MA had been slightly higher than without PP-g-MA. This can be explained that the good dispersion of ZnO particles made electron transfer better than a poor dispersion.

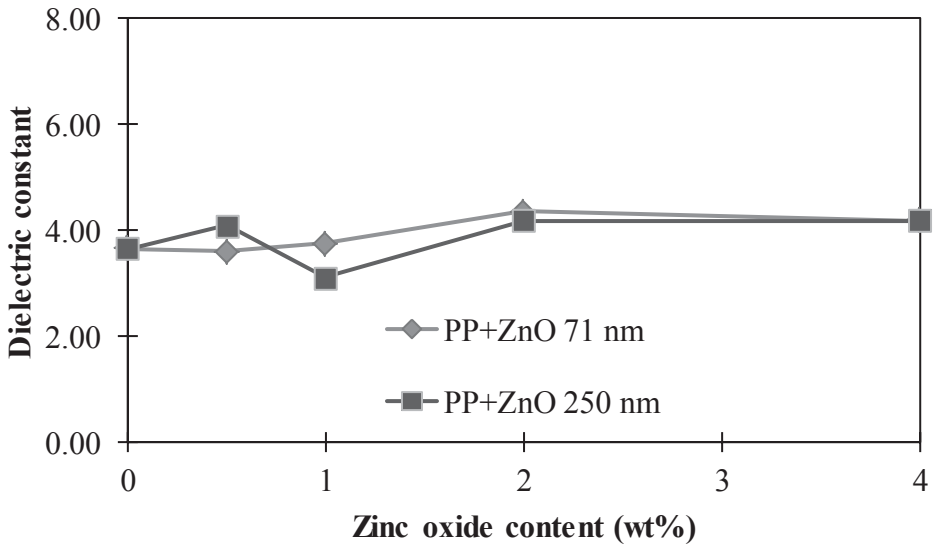

Figure 93 Dielectric constant of PP/ZnO composites without PP-g-MA at various sizes of ZnO

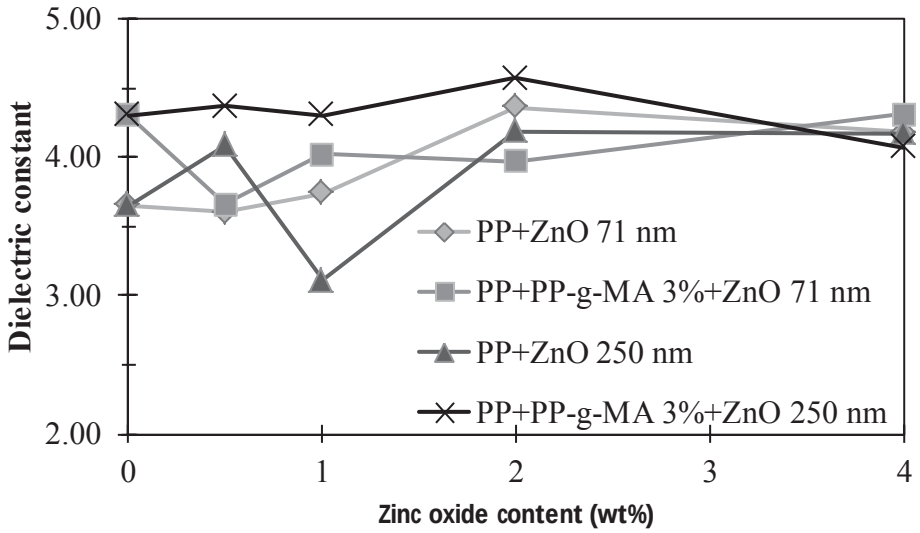

Figure 94 Dielectric constant of PP/ZnO composites without and with PP-g-MA at various particle sizes of ZnO

5.2 Effect of PP-g-MA (MZ-109D) compatibilizer on the properties of PP/ZnO composites at different shapes of ZnO

5.2.1 Dispersion and fractured surface of ZnO in PP matrix

Figures 65, 67, 95 and 96 show SEM micrographs of the impact-fractured surface of PP/ZnO composites with various shapes of ZnO without and with PP-g-MA compatibilizer. The results found that the composites before adding compatibilizer showed the dispersion of ZnO particles both sphere and rod shapes in PP matrix was poor and formed large aggregates, addition of ZnO high content had an effect of the strong agglomerates and low dispersion. After adding compatibilizer the dispersion of ZnO particles with different shapes was relatively good, only few aggregates existed of all ZnO samples. It can be seen that addition of compatibilizer improved interfacial adhesion and the dispersion of ZnO in PP matrix. The high agglomeration was found in PP filled with ZnO 71 nm both without and with PP-g-MA. The crack initiation and propagation zones that shown in Figure 69, 71, 97 and

98. It can be seen that the propagation zone has two different regions, a narrow stable crack growth region and a region of unstable crack growth. The narrow stable crack growth region lies immediately after the crack initiation site. The unstable crack growth region has cleavage type of fracture in the middle and thread like fibrils along the edges. Cleavage is associated with low-energy brittle fracture, which has bright reflecting facets. The edges of the unstable crack growth region have thread like fibrils (Saminathan *et al.*, 2008).

5.2.2 Thermal properties

(1) Melting temperature (T_m)

Figure 99-100 and Table 3 show the effect of ZnO 71 nm and rod on the T_m of PP/ZnO composites without and with PP-g-MA compatibilizer. Before adding PP-g-MA, the results found that the addition of ZnO 71 nm and rod had not significantly changed the T_m of the composites of PP/ZnO. It can be deduced that the crystallite size distribution of PP was hardly changed with the presence of ZnO (Nan-Ying, 2007). After adding PP-g-MA, the results found that the T_m had a slightly increased with PP-g-MA compatibilizer. This can be explained that the presence of PP-g-MA had a slightly increased crystallite size distribution of PP (Nan-Ying, 2007).

(a) PP

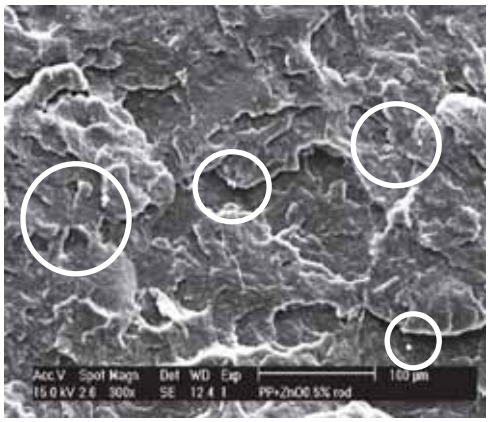

(b) ZnO (rod) 0.5 wt%

(c) ZnO (rod) 1 wt%

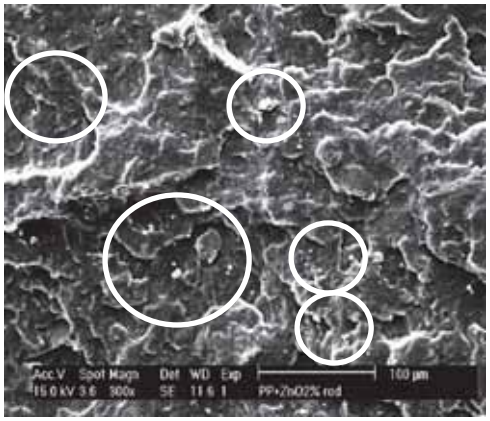

(d) ZnO (rod) 2 wt%

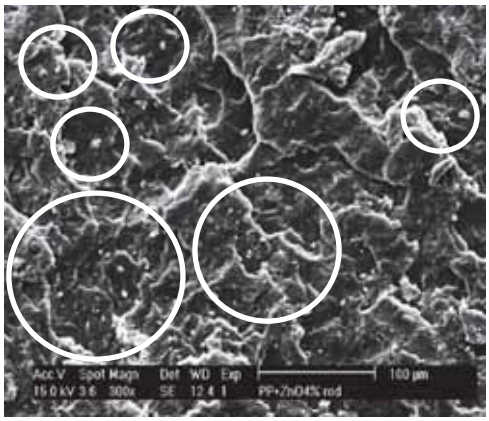

(e) ZnO (rod) 4 wt%

Figure 95 SEM micrographs of the composites of PP and ZnO rod

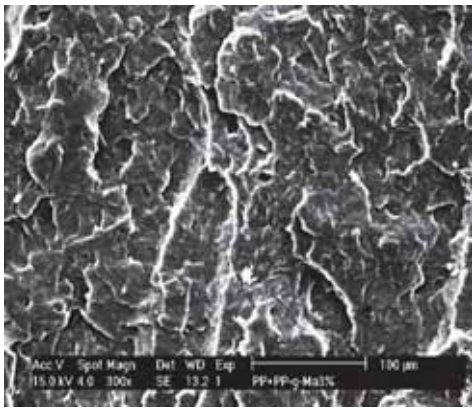

(a) PP

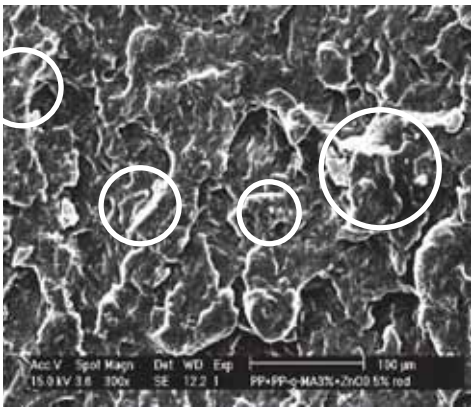

(b) ZnO (rod) 0.5 wt%

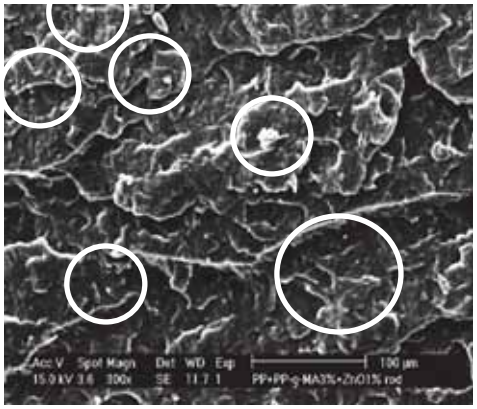

(c) ZnO (rod) 1 wt%

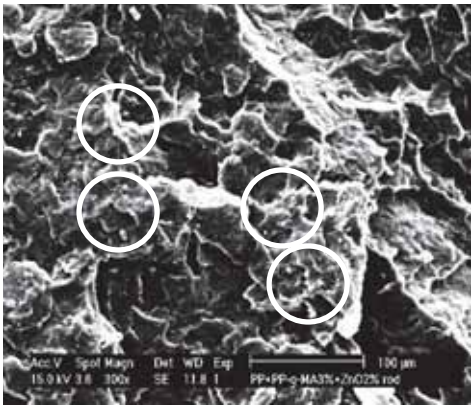

(d) ZnO 2 wt% (rod)

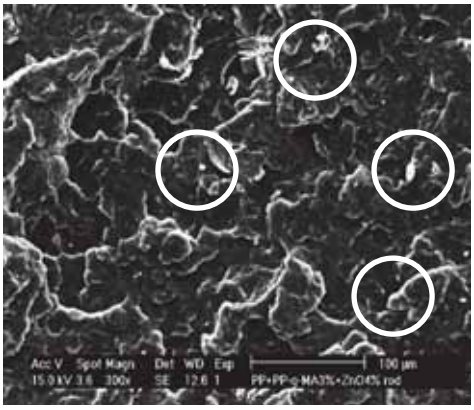

(e) ZnO (rod) 4 wt%

Figure 96 SEM micrographs of the composites of PP and ZnO rod with PP-g-MA 3 wt%

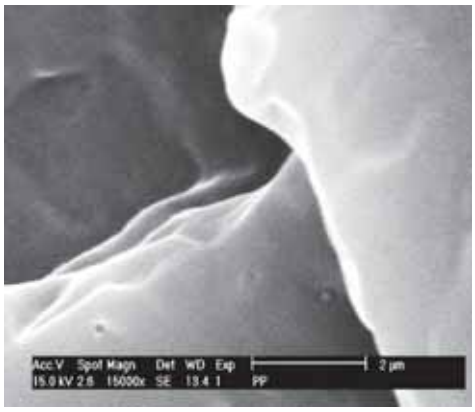

(a) PP

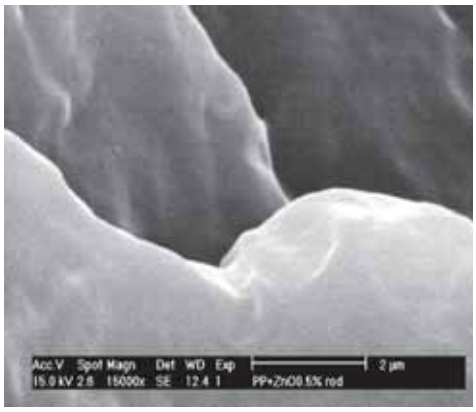

(b) ZnO (rod) 0.5 wt%

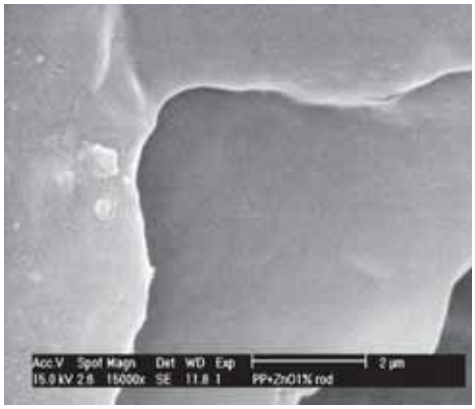

(c) ZnO (rod) 1 wt%

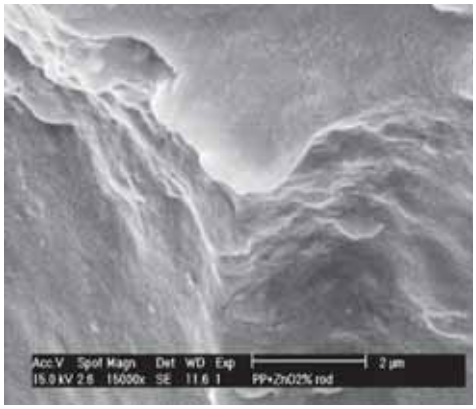

(d) ZnO (rod) 2 wt%

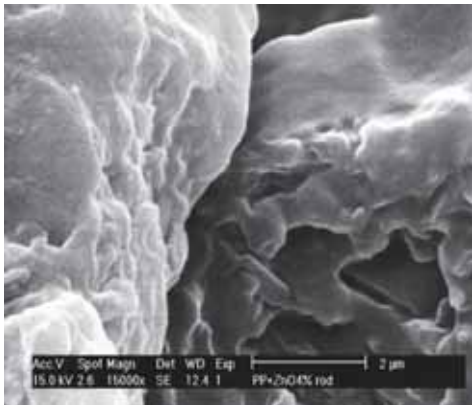

(e) ZnO (rod) 4 wt%

Figure 97 SEM micrographs of impact fractured-surface of PP/ZnO rod composites

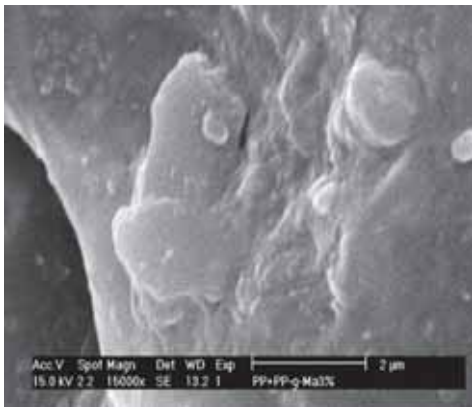

(a) PP

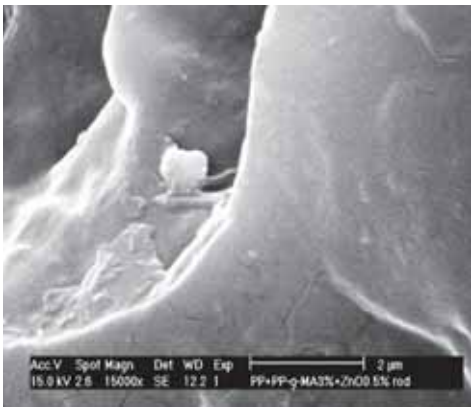

(b) ZnO (rod) 0.5 wt%

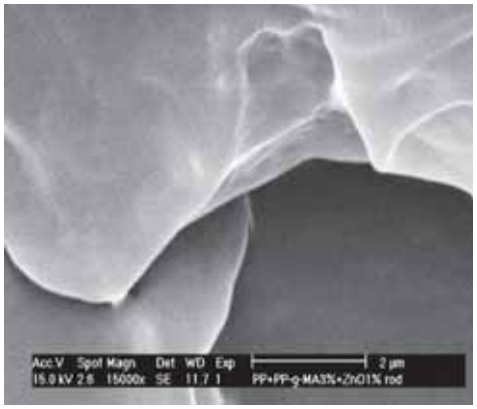

(c) ZnO (rod) 1 wt%

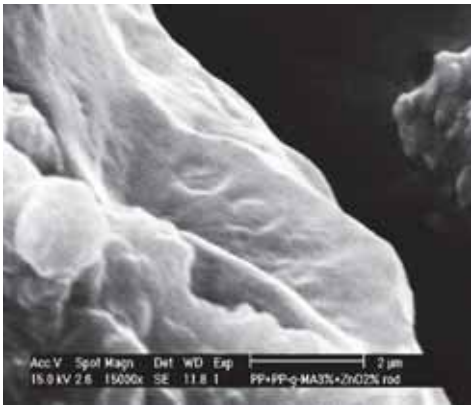

(d) ZnO (rod) 2 wt%

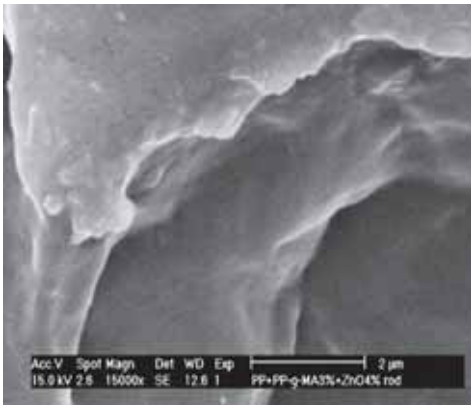

(e) ZnO (rod) 4 wt%

Figure 98 Impact fractured-surface of the composites of PP and ZnO rod with PP-g-MA 3 wt%

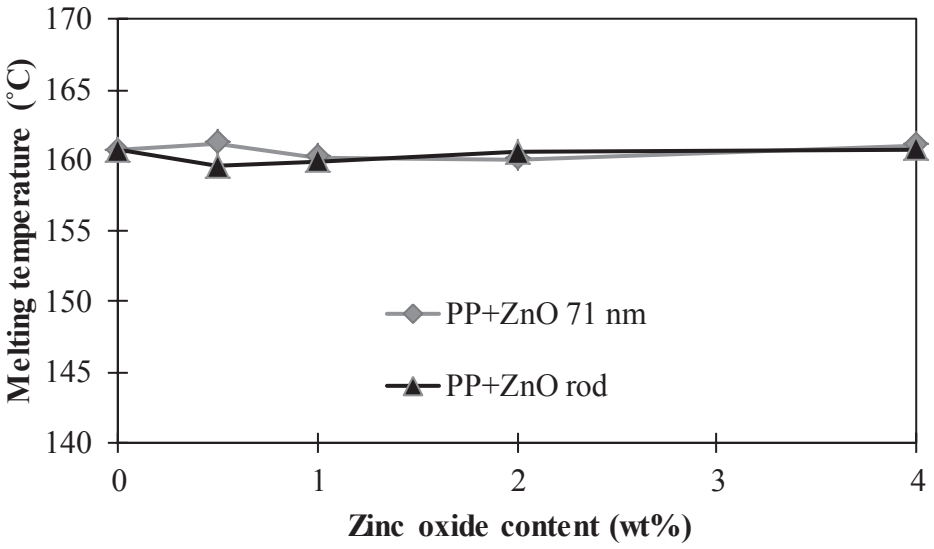

Figure 99 Melting temperatures of PP/ZnO composites without PP-g-MA at various particle shapes of ZnO

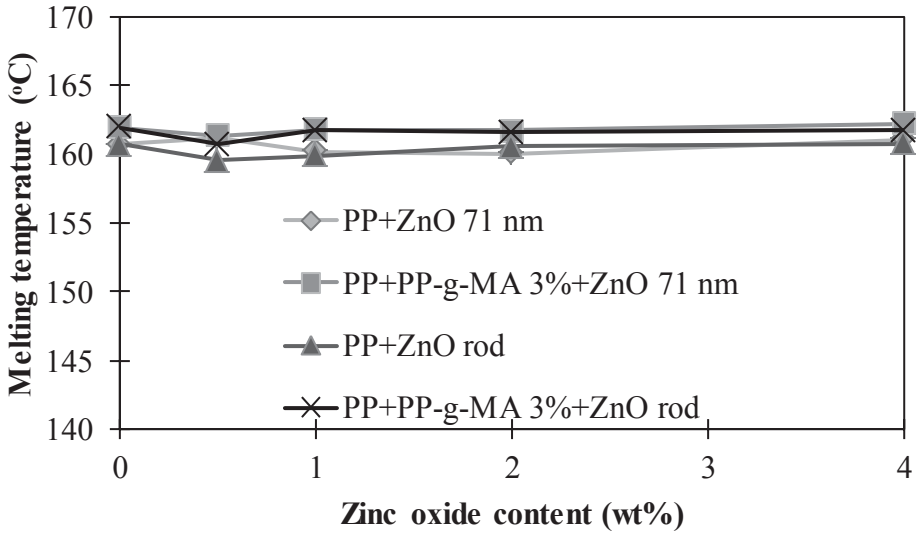

Figure 100 Melting temperature of PP/ZnO composites without and with PP-g-MA at various particle shapes of ZnO

(2) Crystallization temperature (T_c)

Figure 101-102 and Table 3 show the effect of ZnO 71 nm and rod on T_c of PP/ZnO composites without and with PP-g-MA compatibilizer. The results found that before adding PP-g-MA the addition of ZnO 71 nm and rod in PP matrix small increased in T_c with increasing ZnO content. T_c of PP/ZnO rod composites was higher than PP/ZnO 71 nm composites. The results indicated that the efficiency of ZnO as a nucleating agent for PP crystallization, but mainly at high ZnO content (Nan-Ying, 2007). The corresponding of T_c with almost constant values was in good agreement with the isothermal crystallization results. The composites after adding PP-g-MA found the T_c of PP/ZnO 71 nm and PP/ZnO rod composites had been small increased with the presence of PP-g-MA from 115 ˚C to 118 ˚C. The T_c of PP/ZnO rod composites was higher than PP/ZnO 71 nm composites. It can be explained that the incorporation of the compatibilizer improved the level of crystallinity of PP (Othman, 2006).

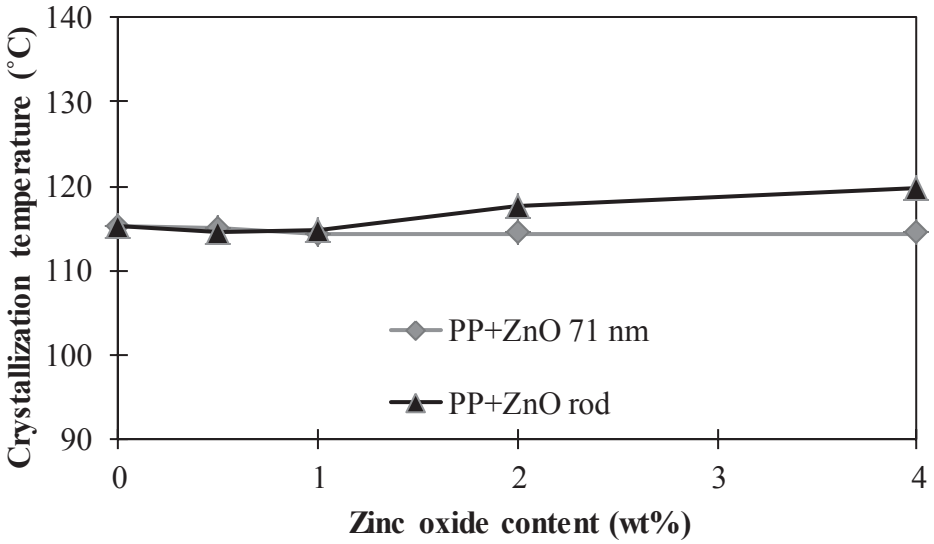

Figure 101 Crystallization temperatures of PP/ZnO composites without PP-g-MA at various particle shapes of ZnO

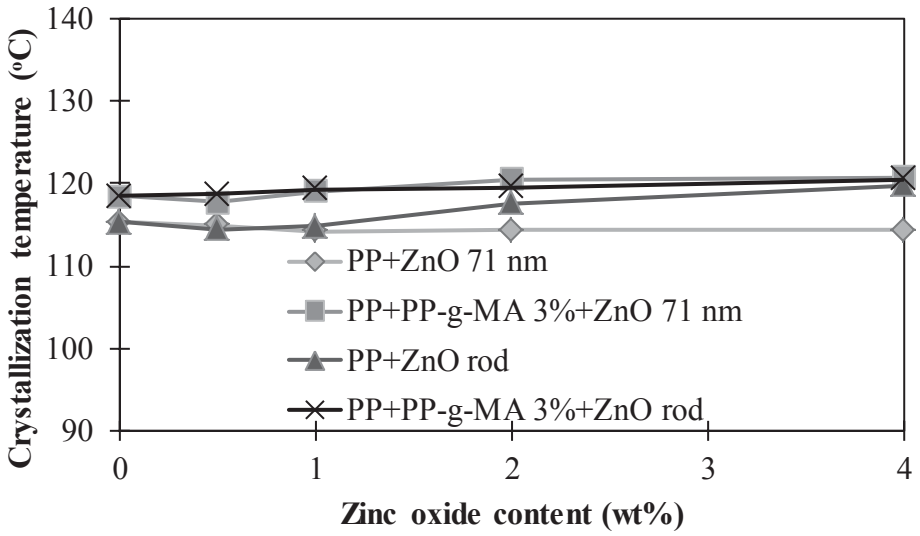

Figure 102 Crystallization temperature of PP/ZnO composites without and with PP-g-MA at various particle shapes of ZnO

Table 3 Thermal behaviors of PP/ZnO composites without and with adding PP-g-MA at various shapes of ZnO.

Sample	T_m (°C)	T_c (°C)
PP	161	115
PP+PP-g-MA 3%	162	118
PP+ZnO 71 nm	161±0.57	115±0.31
PP+ZnO rod	161±0.56	115±2.49
PP+PP-g-MA 3%+ZnO 71 nm	162±0.34	118±1.41
PP+PP-g-MA 3%+ZnO rod	162±0.47	118±0.77

(3) Percent crystallinity

Figure 103-104 show the effect of ZnO 71 nm and rod on the percent crystallinity of PP/ZnO composites without and with PP-g-MA compatibilizer. The results found that the percent crystallinity of PP/ZnO 71 nm composites without PP-g-MA had slightly increased with increasing ZnO content. PP/ZnO rod composites had higher percent crystallinity than PP/ZnO 71 nm composites. This may due to ZnO rod was better nucleating agent than ZnO 71 nm. After adding PP-g-MA, the results found that the percent crystallinity of PP/ZnO 71 nm and PP/ZnO rod composites slightly increased. The percent crystallinity of PP/ZnO rod composites after adding PP-g-MA had been higher than PP/ZnO 71 nm composites. It can be explained that PP-g-MA enhanced crystallization temperature (Nan-Ying, 2007) and dispersion of ZnO particles so the percent crystallinity was improved. The percent crystallinity of PP/ZnO 71 nm and rod composites without and with PP-g-MA was 32±2.43 %, 32±1.75 %, 28±1.11 % and 28±3.29 %, respectively.

(4) Decomposition temperature (T_d)

Figure 105-108 show the effect of ZnO 71 nm and rod on the T_d of PP/ZnO composites without and with PP-g-MA compatibilizer. The T_d was measured by TGA and was calculated at 5 (T_{d5}) and 10 (T_{d10}) %weight loss of the composites. The results found that the T_{d5} and Td_{10} of PP/ZnO composites without PP-g-MA increased with increasing filler content and were higher than the T_{d5} and Td_{10} of pure PP, which showed lower thermal stability than PP/ZnO composites. The PP/ZnO rod composites had the T_{d5} and Td_{10} higher than PP/ZnO 71 nm composites with increasing ZnO content. It can be explained that ZnO 71 nm and rod improved the thermal stability of PP because of the improvement in percent crystallinity of the PP/ZnO composites so it made more energy to break the crystalline bond. After adding PP-g-MA, the T_{d5} and Td_{10} of PP/ZnO 71 nm composites were higher than the composites without PP-g-MA at ZnO content more than 2 wt%. It can be explained that PP-g-MA made a good dispersion of ZnO particles so the percent crystallinity improved. For PP/ZnO rod composites, the results found that the T_{d5} and Td_{10} of PP/ZnO composites with PP-g-MA dropped.

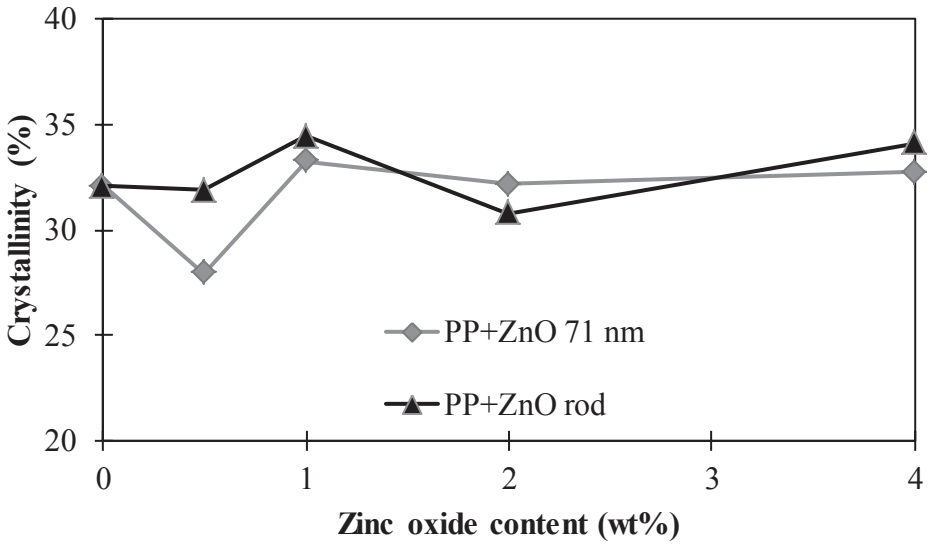

Figure 103 Percent crystallinity of PP/ZnO composites without PP-g-MA at various particle shapes of ZnO

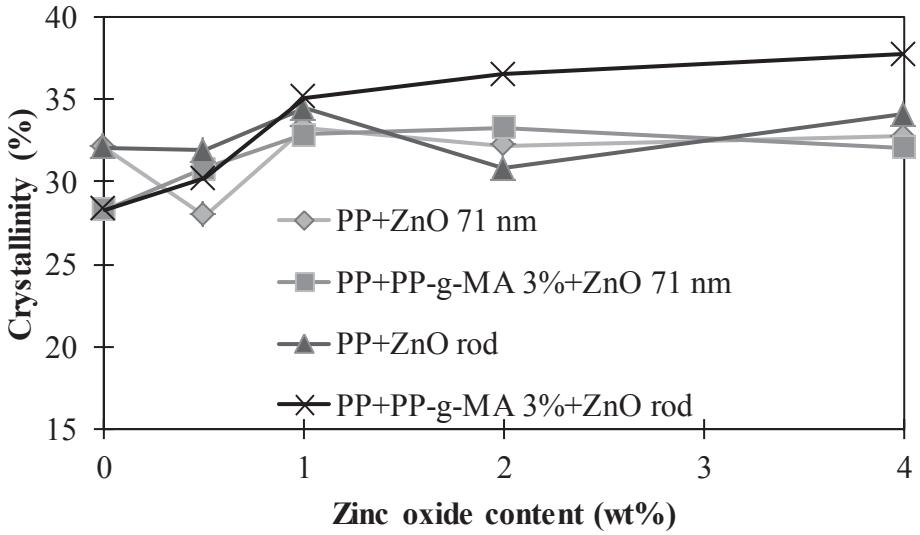

Figure 104 Percent crystallinity of PP/ZnO composites without and with PP-g-MA at various particle shapes of ZnO

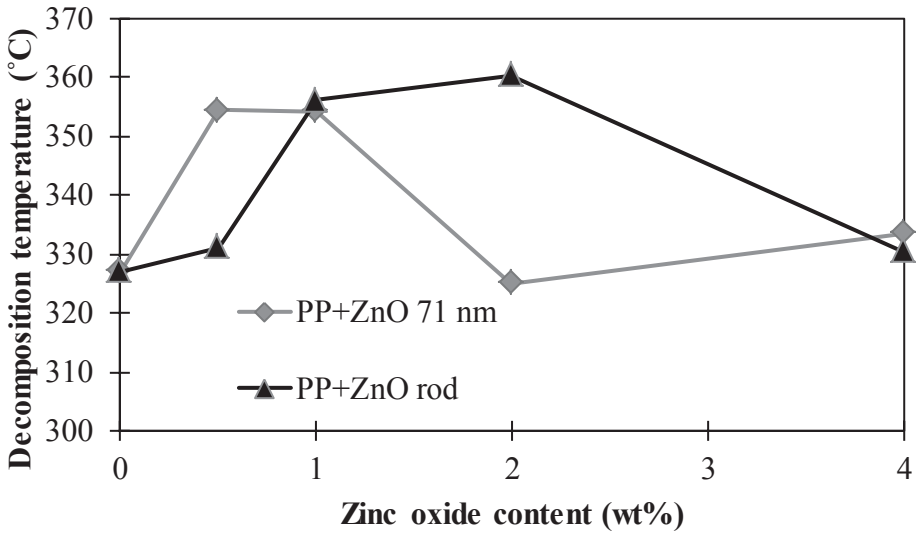

Figure 105 Decomposition temperature (T_{d5}) of PP/ZnO composites without PP-g-MA at various particle shapes of ZnO

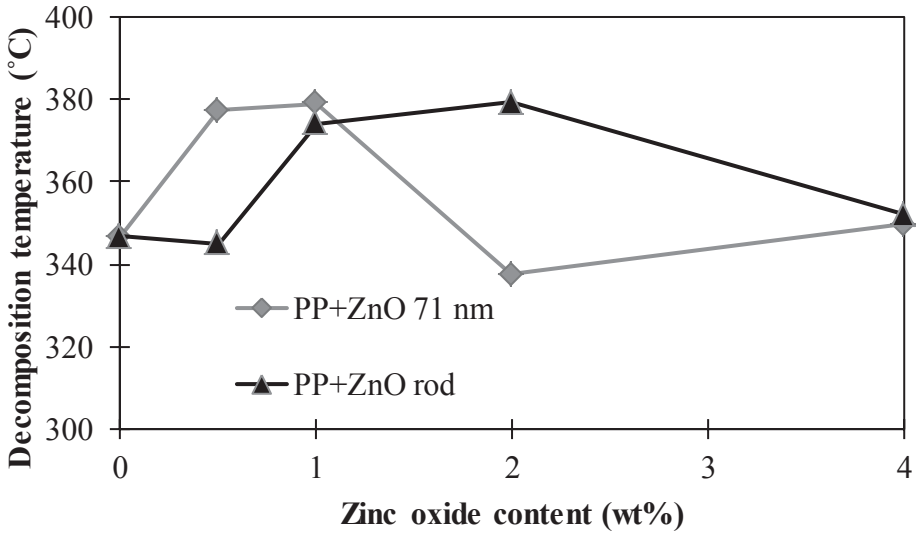

Figure 106 Decomposition temperature (T_{d10}) of PP/ZnO composites without PP-g-MA at various particle shapes of ZnO

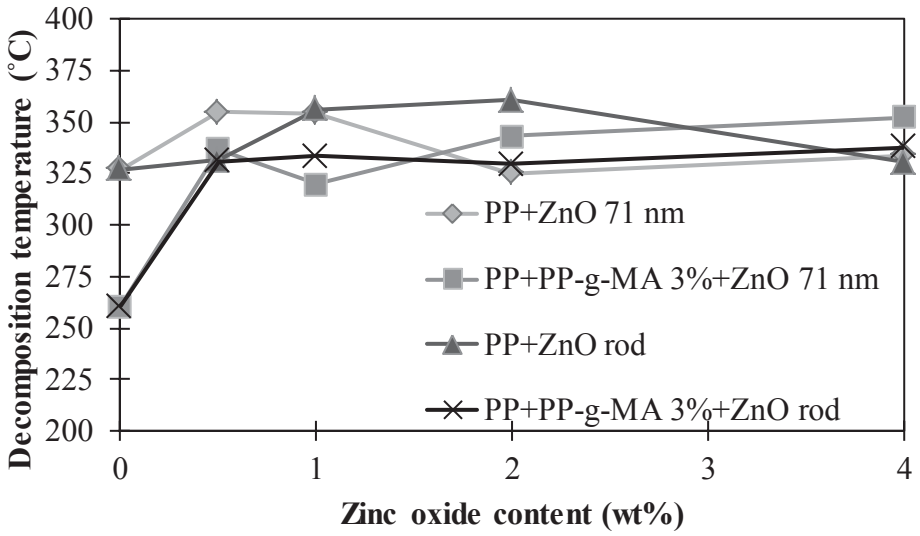

Figure 107 Decomposition temperature (T_{d5}) of PP/ZnO composites without and with PP-g-MA at various particle shapes of ZnO

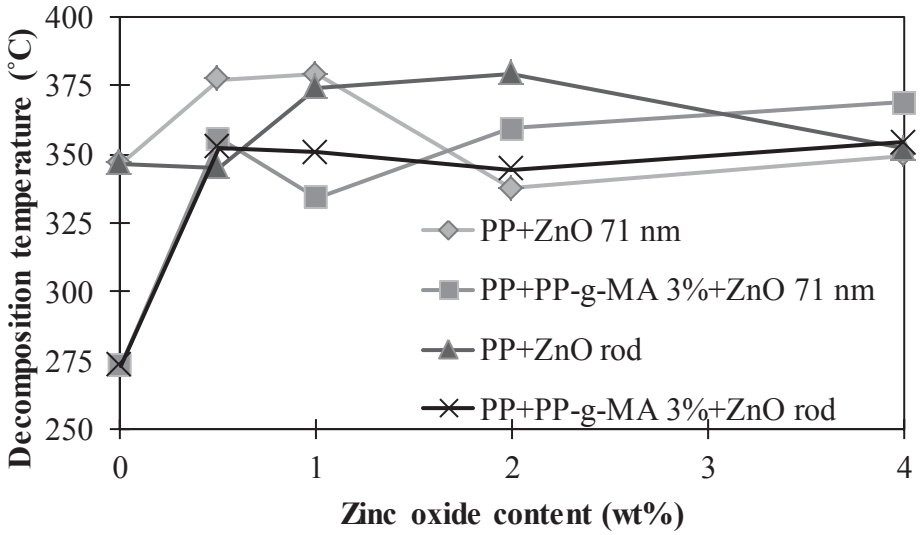

Figure 108 Decomposition temperature (T_{d10}) of PP/ZnO composites without and with PP-g-MA at various particle shapes of ZnO

5.2.3 Mechanical properties

(1) Young's modulus

Figure 109-110 show the effect of particle shapes of ZnO on Young's modulus of PP/ZnO composites without and with PP-g-MA compatibilizer. The composites before adding PP-g-MA found the Young's modulus of PP/ZnO 71 nm composites trend to be increased with increasing ZnO content. Young's modulus of PP/ZnO rod composites had significantly increased with increasing ZnO content and higher than PP/ZnO 71 nm composites. This may due to the percent crystallinity of PP/ZnO rod composites higher than PP/ZnO 71 nm composites so it led to more stiffness but lower toughness. The composites after adding PP-g-MA showed the Young's modulus of PP/ZnO 71 nm and PP/ZnO rod composites increased higher than PP/ZnO composites before adding PP-g-MA. Young's modulus of PP/ZnO rod composites without compatibilizer was higher than the composites with compatibilizer after adding ZnO more than 1 wt% of ZnO content. This can be explained that PP-g-MA enhanced interfacial adhesion (Hee-Soo, 2007) and reduced interfacial tension between the phases (O'Donnell, 1995) so the compatibility and dispersion of ZnO particles were improved so the percent crystallinity increased which made the composites more stiffness.

(2) Tensile strength

Figure 111-112 show the effect of particle shapes of ZnO on the tensile strength of PP/ZnO composites without and with PP-g-MA compatibilizer. The composites before adding PP-g-MA showed the tensile strength of PP/ZnO 71 nm composites slightly increased after adding ZnO. The tensile strength of PP/ZnO rod composites increased only 0.5 wt% of ZnO and did not change with increasing ZnO content, and had higher the tensile strength than PP/ZnO 71 nm composites. The composites after adding PP-g-MA showed the tensile strength of PP/ZnO 71 nm composites with PP-g-MA had a slightly higher than the PP/ZnO 71 nm composites without PP-g-MA. The tensile strength of PP/ZnO rod composites with PP-g-MA had been lower than without PP-g-MA and dropped after adding ZnO content more than

0.5 wt%. The tensile strength after adding PP-g-MA of PP/ZnO rod composites lower than PP/ZnO 71 nm composites. The increase in stiffness (Do Hoon *et al.*, 2007) due to the well dispersion increased the degree of crystallinity (Wacharawichanant *et al.*, 2008).

(3) Stress at break

Figure 113-114 show the effect of particle shapes of ZnO on stress at break of PP/ZnO composites without and with PP-g-MA compatibilizer. It can be seen that before adding PP-g-MA the stress at break of PP/ZnO 71 nm composites increased with increasing ZnO content. The stress at break of PP/ZnO rod composites increased with increasing ZnO content and higher than PP/ZnO 71 nm composites. This may due to PP/ZnO rod composites had more percent crystallinity than PP/ZnO rod composites, this led the composites more stiffness and lower toughness so the stress at break increased. The composites after adding PP-g-MA showed the stress at break of PP/ZnO 71 nm and PP/ZnO rod composites with PP-g-MA had been higher than without PP-g-MA. PP/ZnO rod composites increased the stress at break with increasing ZnO content and higher than PP/ZnO 71 nm composites. This may due to the good dispersion of ZnO particles in the PP matrix made increased in percent crystallinity.

(4) Percent strain at break

Figure 115-116 show the effect of particle shapes of ZnO on the percent strain at break of PP/ZnO composites without and with PP-g-MA compatibilizer. The composites before adding PP-g-MA showed the percent strain at break of PP/ZnO 71 nm composites had increased in a range of 0.5-2 wt%. PP/ZnO rod composites had a slightly increased in percent strain at break in the range of 0.5-1 wt% of ZnO content and dropped at high ZnO content. The percent strain at break of PP/ZnO rod composites had been lower than PP/ZnO 71 nm composites. This may due to the increased in percent crystallinity made the composites more stiffness so it decreased the percent strain at break. The composites after adding PP-g-MA was clearly found that the percent strain at break of PP/ZnO 71 nm and PP/ZnO rod

composites without PP-g-MA had been higher than the composites with PP-g-MA. The percent strain at break of PP/ZnO rod composites with PP-g-MA lower than PP/ZnO 71 nm composites PP-g-MA after adding ZnO more than 0.5 wt%. This can be explained that the good dispersion of ZnO particles in PP matrix with adding PP-g-MA made crystalline smaller than without adding PP-g-MA.

(5) Impact strength

Figure 117-118 show the effect of particle shapes of ZnO on the impact strength of PP/ZnO composites without and with PP-g-MA compatibilizer. The composites before adding PP-g-MA showed the impact strength of PP/ZnO 71 nm composites increased with increasing ZnO content. While the impact strength of PP/ZnO rod composites slightly increased the impact strength with increasing ZnO content and lower than ZnO 71 nm. The impact strength improved due to increased energy absorption during the impact process (Yang *et al.*, 2006). The composites after adding PP-g-MA showed the impact strength of PP/ZnO 71 nm and PP/ZnO rod composites were dropped compared without PP-g-MA. This may be due to the bigger crystalline of composites without PP-g-MA made it more stiffness.

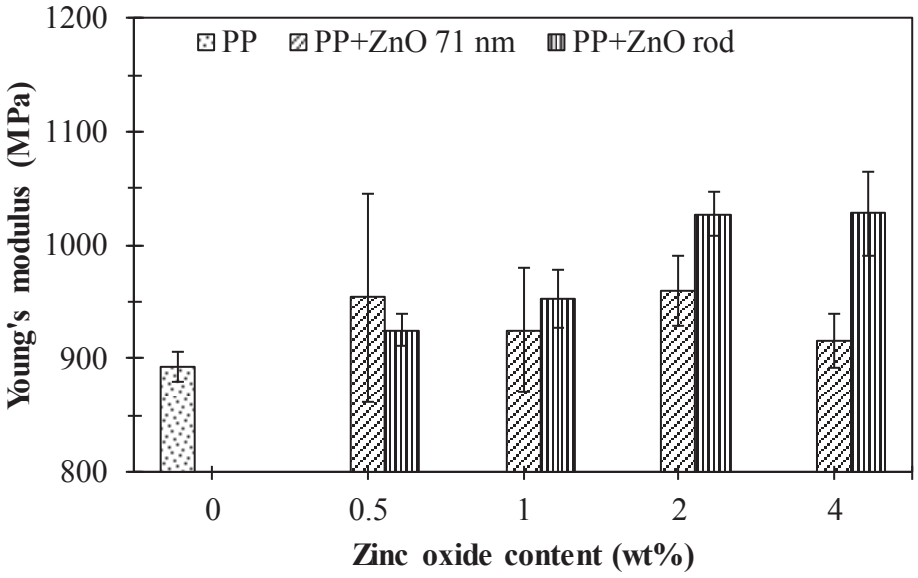

Figure 109 Young's modulus of PP/ZnO composites without PP-g-MA at various particle shapes of ZnO

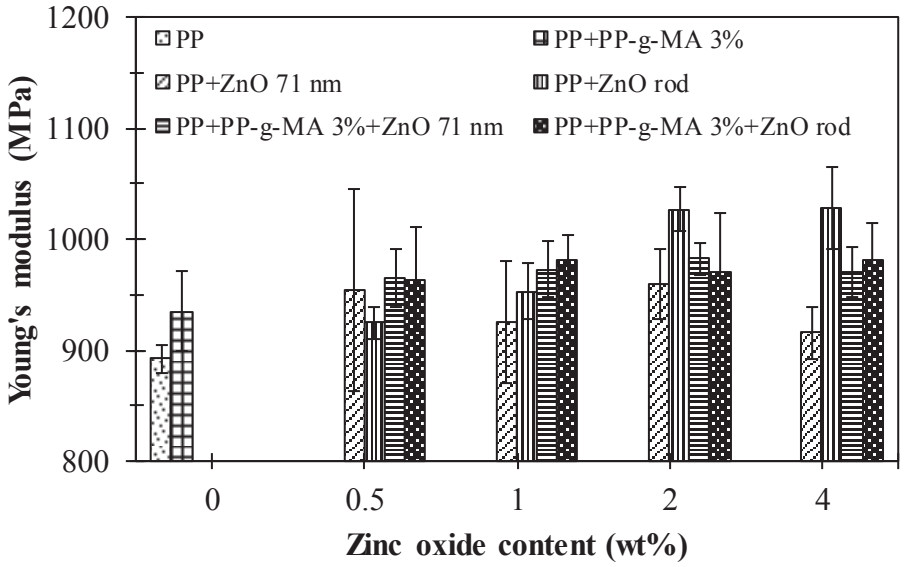

Figure 110 Young's modulus of PP/ZnO composites without and with PP-g-MA at various particle shapes of ZnO

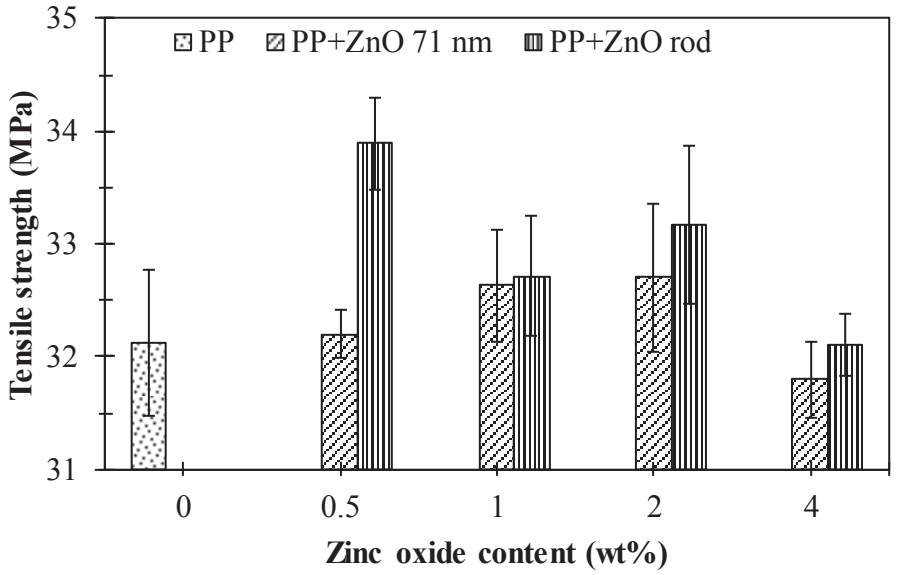

Figure 111 Tensile strength of PP/ZnO composites without PP-g-MA at various particle shapes of ZnO

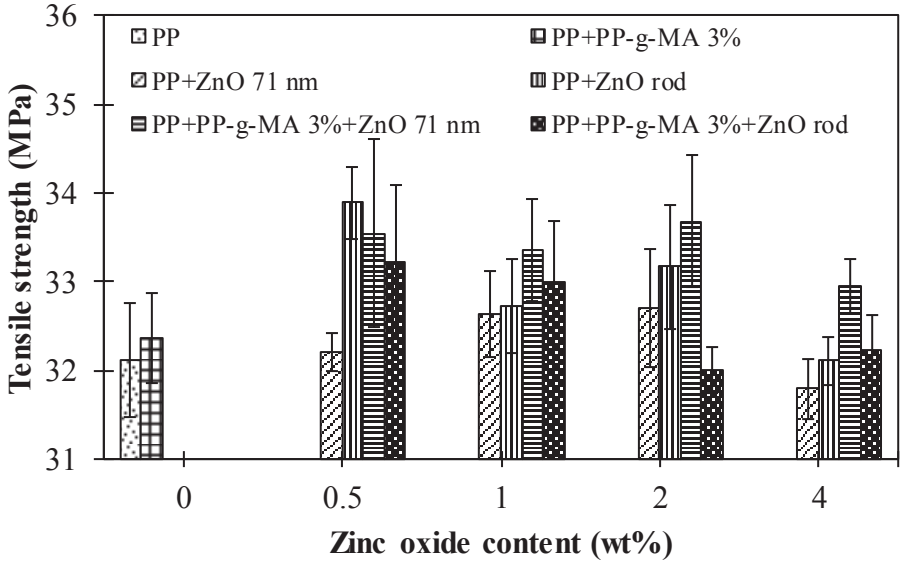

Figure 112 Tensile strength of PP/ZnO composites without and with PP-g-MA at various particle shapes of ZnO

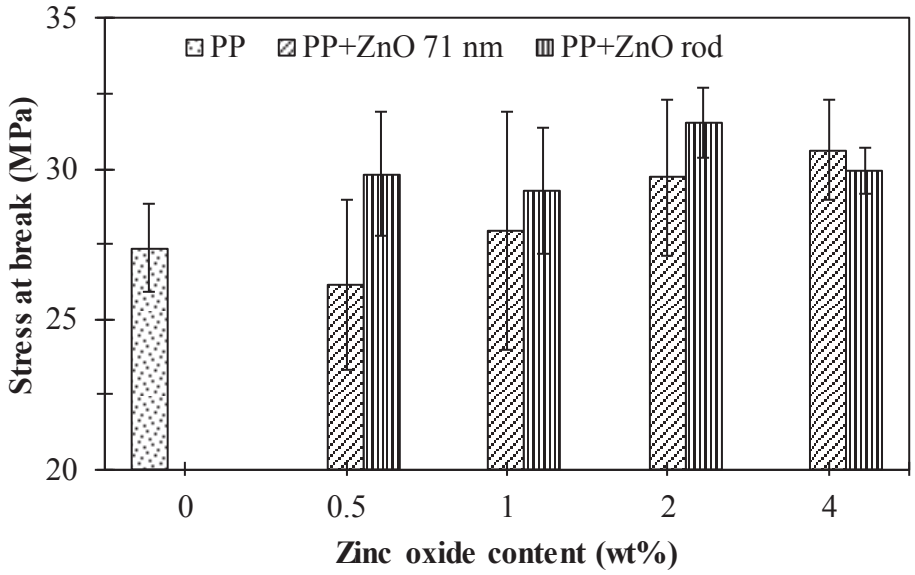

Figure 113 Stress at break of PP/ZnO composites without PP-g-MA at various particle shapes of ZnO

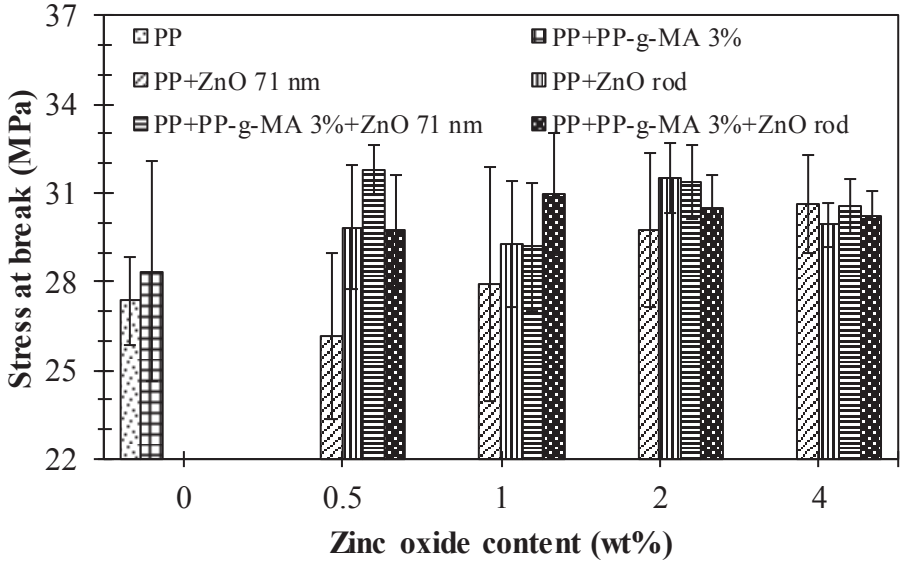

Figure 114 Stress at break of PP/ZnO composites without and with PP-g-MA at various particle shapes of ZnO

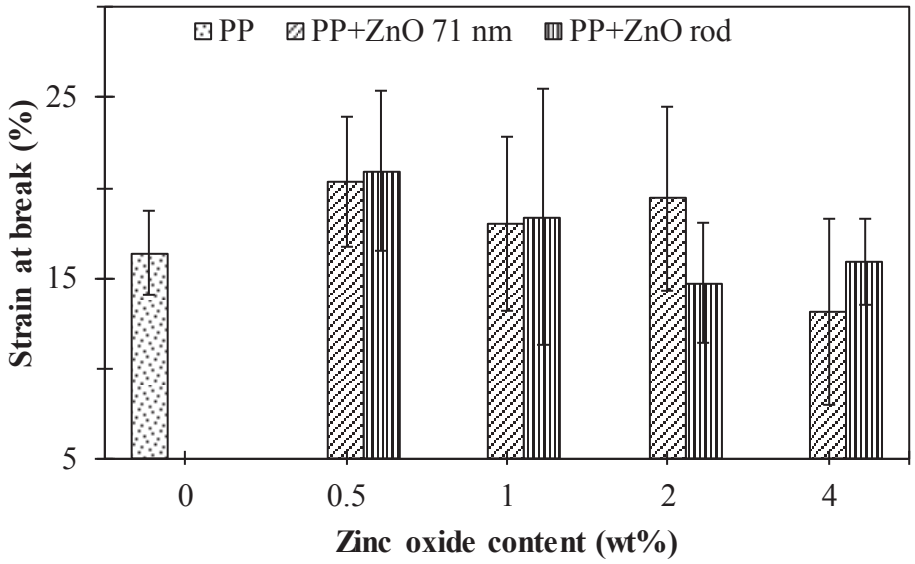

Figure 115 Percent strain at break of PP/ZnO composites without PP-g-MA at various particle shapes of ZnO

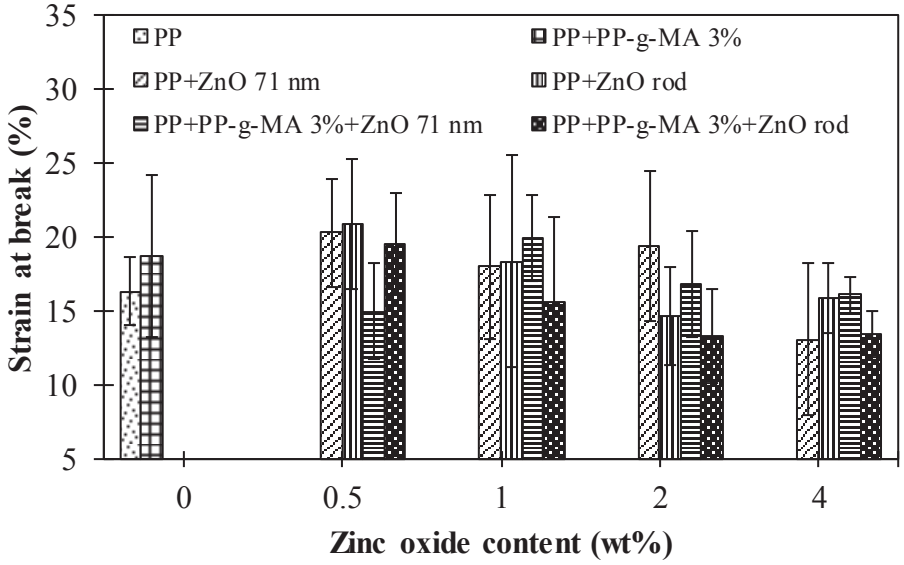

Figure 116 Percent strain at break of PP/ZnO composites without and with PP-g-MA at various particle shapes of ZnO

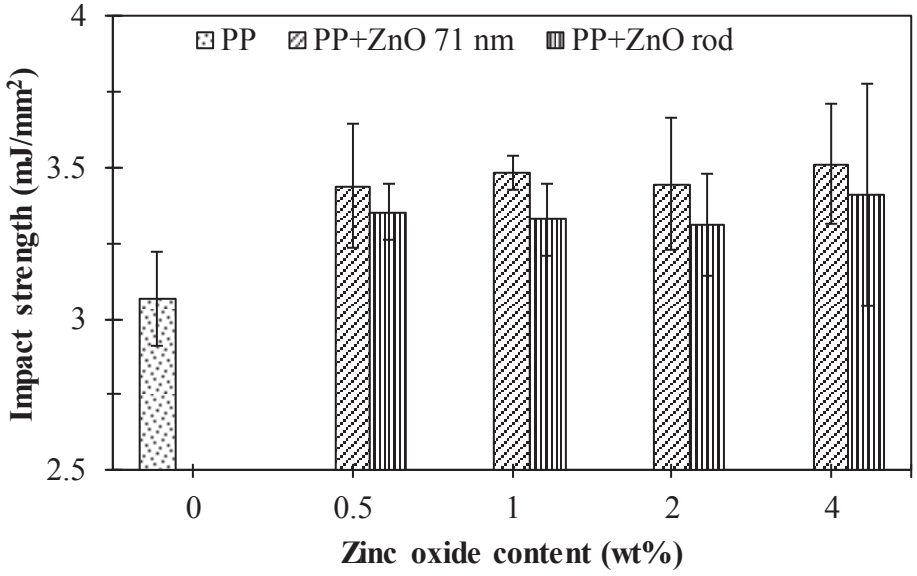

Figure 117 Impact strength of PP/ZnO composites without PP-g-MA at various particle shapes of ZnO

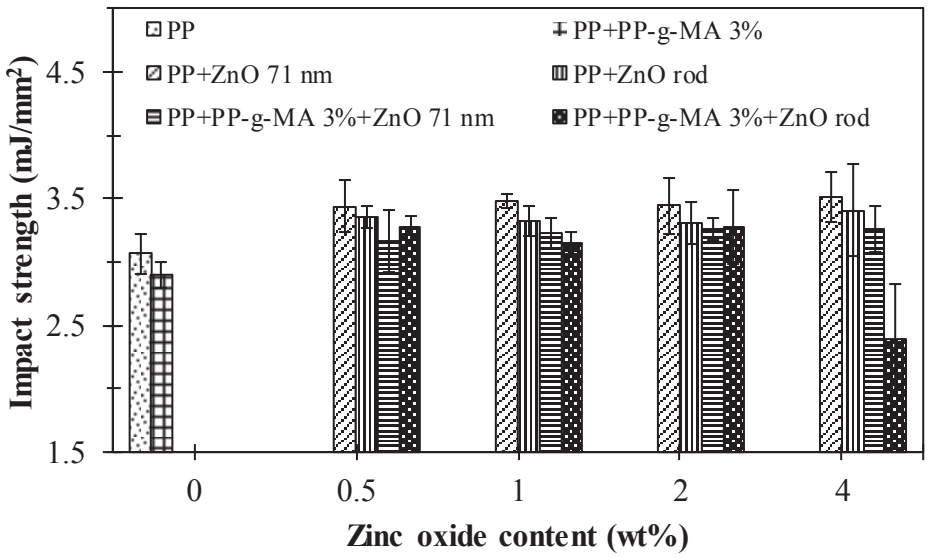

Figure 118 Impact strength of PP/ZnO composites without and with PP-g-MA at various particle shapes of ZnO

5.2.4 Dielectric Properties

Dielectric constant

Figure 119-120 show the effect of particle shapes of ZnO on the dielectric constant of PP/ZnO composites without and with PP-g-MA compatibilizer. The composites before adding PP-g-MA showed the dielectric constant of PP/ZnO 71 nm and PP/ZnO rod composites slightly increased with increased ZnO content. The composites after adding PP-g-MA showed the dielectric constant of PP/ZnO 71 nm had been higher than PP/ZnO 71 nm composites without PP-g-MA. For PP/ZnO rod composites, it was found that the dielectric constant of PP/ZnO rod with PP-g-MA had been significantly increased compared without PP-g-MA with increasing ZnO content and higher than PP/ZnO 71 nm composites with PP-g-MA. This can be explained that the good dispersion and shape of ZnO particles made electron transfer better than a poor dispersion.

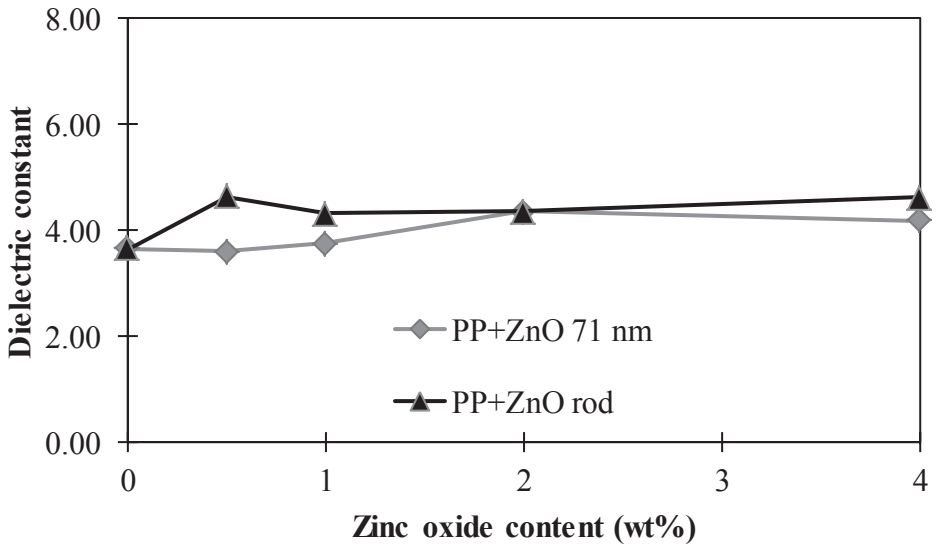

Figure 119 Dielectric constant of PP/ZnO composites without PP-g-MA at various shapes of ZnO

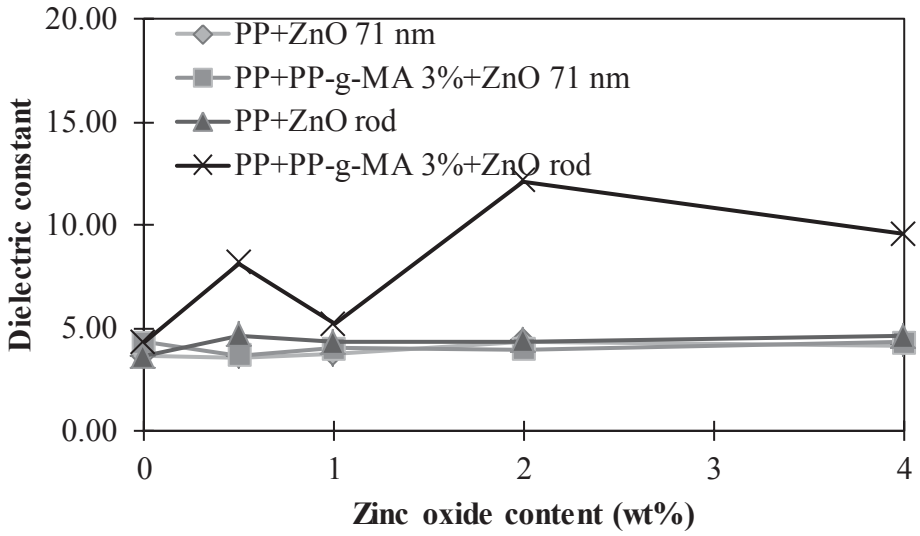

Figure 120 Dielectric constant of PP/ZnO composites without and with PP-g-MA at various particle shapes of ZnO

CHAPTER 6

CONCLUSIONS

ZnO sphere (100 nm) and rod shape can successfully synthesis by simple chemical route method in our laboratory. The dispersion of ZnO particles and mechanical properties of PP/ZnO with PP-g-MA was better than zinc stearate so PP-g-MA was more suitable for PP/ZnO composites than zinc stearate. The use of PP-g-MA at 3 wt% made a good dispersion of ZnO particles in the matrix of PP and lower agglomeration than without PP-g-MA and with PP-g-MA at 1 and 5 wt%.

The high content of MA in PP-g-MA made the Young's modulus, tensile strength and stress at break of the composites dropped but the percent strain at break and impact strength slightly higher than the composites with lower MA content. T_m of the composites without PP-g-MA and with MA content 0.55 and 1.305 wt% did not change clearly. T_c of the composites with PP-g-MA is slightly higher than without PP-g-MA but T_d of the composites without PP-g-MA is higher than with both MA content. The dielectric constant of the composites without and with PP-g-MA did not change clearly.

The effect of sizes of ZnO on the mechanical properties of the composites without PP-g-MA found that the tensile strength, percent strain at break and impact strength of the composites filled with ZnO 250 nm is higher than the composites filled with ZnO 71 nm but the PP/ZnO 71 nm composites after adding PP-g-MA showed the tensile strength, stress at break and impact strength higher than the composites filled with ZnO 250 nm. T_m of the composites without and with PP-g-MA of ZnO 71 and 250 nm did not change but T_c of the composites after adding PP-g-MA of ZnO 71 and 250 nm was slightly higher than without PP-g-MA. Percent crystallinity of the composites filled with ZnO 71 nm without PP-g-MA was higher than the composites filled with ZnO 250 nm without PP-g-MA but the composites after adding PP-g-MA

was shown in the opposite way with increasing ZnO content. T_{d5} and T_{d10} of the composites without PP-g-MA filled with ZnO 71 nm was higher than the composites without PP-g-MA filled with ZnO 250 nm. The decomposition temperature of the composites filled with 71 nm and 250 nm increased in a range of 0.5-2 wt% and dropped at 4 wt%. The composites filled with ZnO 250 nm after adding PP-g-MA showed improvement in thermal stability and higher than the composites filled with ZnO 71 nm after adding PP-g-MA. The dielectric constant of the composites filled with ZnO 71 and 250 nm without and with PP-g-MA did not change clearly.

The effect of rod and sphere shapes of ZnO on the mechanical properties of PP/ZnO composites showed the Young's modulus, tensile strength, stress at break and percent strain at break of the composites filled with ZnO rod without PP-g-MA was higher than the composites filled with ZnO 71 nm composites without PP-g-MA with increasing ZnO content. T_m of the composites filled with ZnO 71 nm and rod without and with PP-g-MA did not change with increasing ZnO content. T_c of the composites filled ZnO rod without PP-g-MA slightly increased with increasing ZnO content and higher than the composites filled with ZnO 71 nm without PP-g-MA. The composites after adding PP-g-MA did not different T_c between the composites filled with ZnO 71 nm and rod.

Percent crystallinity of the composites filled with ZnO 71 nm and ZnO rod without and with PP-g-MA slightly increased with increasing ZnO content. The percent crystallinity of PP/ZnO rod composites was slightly higher than PP/ZnO 71 nm composites. T_{d5} and T_{d10} of the PP/ZnO 71 nm composites without and with PP-g-MA increased with increasing ZnO content and dropped at 2 wt% while PP/ZnO rod composites dropped at 4 wt%. The dielectric constant of PP/ZnO rod composites with PP-g-MA increased with increasing ZnO content while the composites filled with ZnO 71 nm without and with PP-g-MA and the composites filled with ZnO rod without PP-g-MA did not change clearly.

Bibliography

Avella, M., Errico, M.E., and Gentile, G. "PMMA based nanocomposites filled with modified $CaCO_3$ nanoparticles", Macromolecular Symposia 247, (2007) : 140-146.

Ashkarrana, A.A., Iraji zada, A., Mahdavi, S.M. and Ahadian, M.M. "ZnO nanoparticles prepared by electrical arc discharge method in water", Materials Chemistry and Physics 118, (2009) : 6–8.

Bose, S., and Mahanwar, P.A. "Effect of particle size of filler on properties of nylon-6", Journal Minerals and Materials Characterization and Engineering, (2004) : 23-31.

Brian G. Polymer [Online], accessed 13 February 2011. Available from http://taggedwiki.zubiaga.org/new_content/4c0185c2fa80d32bcfd75515acd8978f.

Brent Strong, A., "Plastics : materials and processing", 3rd edition, New Jersey : Pearson Education, Inc., (2006) : 121-143, 171-176.

Cheremisinoff, N.P., "An introduction to polymer rheology and processing", Florida : CRC Press, Inc., (1993) : 179-180.

Cho, J.W., and Paul, D.R. "Nylon 6 nanocomposites by melt compounding", Polymer 42, (2001) : 1083-1094.

Chun, L.W., Ming, Q.Z., Min, Z.R., and Friedrich, K. "Tensile performance improvement of low nanoparticles filled-polypropylene composites", Composites Science and Technology 62, (2002) : 1327-1340.

Chi-Ming, C., Jingshen, W., Jian-Xiong, L., and Ying-Kit, C. "polypropylene/calcium carbonate nanocomposites", Polymer 43, (2002) : 2981-2992.

Chatterjee, A., Deopura, B.L. "High modulus and high strength PP nanocomposite filament", Composites: Part A 37, (2006) : 813-817.

ChangChun, C., Ping, L., and ChunHua, L. "Synthesis and characterization of nano-sized ZnO powders by direct precipitation method", Chemical Engineering Journal 144, (2008) : 509-513.

Chinellato, A.C., Vidotti, S.E., Hu, G.H. and Pessan, L.A. "Compatibilizing effect of acrylic acid modified polypropylene on the morphology and permeability properties of polypropylene/organoclay nanocomposites", Composites Science and Technology 70, (2010) : 458–465.

Dang Z.M., Fan, L.Z., Zhao, S.J. and Nan, C.W. "Preparation of nanosized ZnO and dielectric properties of composites filled with nanosized ZnO", Materials Science and Engineering B 99, (2003) : 386-389.

Do Hoon, K., Fasulo, P.D., Rodgers, W.R. and Paul, D.R. "Structure and properties of polypropylene-based nanocomposites: Effect of PP-g-MA to organoclay ratio", Polymer 48, (2007) : 5308-5323.

Dong, Y., Bhattacharyya, D. and Hunter, P.J. "Experimental characterisation and object-oriented finite element modelling of polypropylene/organoclay nanocomposites", Composites Science and Technology 68, (2008) : 2864–2875.

De la Orden, M.U., González Sánchez, C., González Quesada, M. and Martínez Urreaga, J. "Effect of different coupling agents on the browning of celluloseepolypropylene composites during melt processing", Polymer Degradation and Stability 95, (2010) : 201-206.

Erjun T., Guoxiang C. and Xiaolu M., "Preparation of nano-ZnO/PMMA composite particles via grafting of the copolymer onto the surface of zinc oxide nanoparticles", Powder Technology 161, (2006) : 209-214.

Fan Y., Lou J. and Shinozaki D.M., "Microstructure dependent properties of polypropylene-clay nanocomposites", Journal of Applied Polymer Science 103, (2007) : 204-210.

Franco-Marquès, E., Méndez, J.A., Pèlach, M.A., Vilaseca, F., Bayer, J. and Mutjé P. "Influence of coupling agents in the preparation of polypropylene composites reinforced with recycled fibers", Chemical Engineering Journal 166, (2011) : 1170–1178.

Golebiewski, J., and Galeski, A. "Thermal stability of nanoclay polypropylene composites by simultaneous DSC and TGA", Composites Science and Technology 67, (2007) : 3442-3447.

Gcwabaza T., Ray S.S., Focke W.W. and Maity A., "Morphology and properties of nanostructured materials based on polypropylene/poly(butylene succinate) blend and organoclay", European Polymer Journal 11, (2008) : 353-367.

Graphics Systems Corp. Solid notes [Online], accessed 13 February 2011. Available from http://gxsc.typepad.com/graphics_systems_solidnot/2009/02/why-nonlinear-analysis-using-solidworks-simulation-premium.html

Gruber, H., Knaus, S., and Liska, R. Reactive Extrusion [Online], accessed 18 January 2011. Available from http://otech7.tuwien.ac.at/reaktiv_sk_e.html

Hanna, R.D., "Polypropylene", Handbook of Plastic Materials and Technology, New York : Wiley & Sons, Inc., (1990) : 433-455.

Hongxia Z., and Robert K.Y. "A study on photo-degradation of zinc oxide (ZnO) filled polypropylene nanocomposites", Polymer 47, (2006) : 3207-3217.

Hull, J., "Compression and transfer molding", Handbook of Plastic Processes, New Jersey: John Wiley & Sons, Inc., (2006) : 455-457.

Han-Seung, Y., Hyun-Joong, Kim., Hee-Jun, P., Bum-Jae, L., and Taek-Sung, H. "Effect of compatibilizing agents on rice-husk flour reinforced polypropylene composites", Composite Structures 77, (2007) : 45-55.

Hee-Soo, K., Byoung-Ho, L., Seung-Woo, C., Sumin, K., and Hyun-Joong, K. "The effect of types of maleic anhydride-grafted polypropylene (MAPP) on the interfacial adhesion properties of bio-flour-filled polypropylene composites", Composites: Part A 38, (2007) : 1473-1482.

Hong, R.Y., Li, J.H., Chen, L.L., Liu, D.Q., Li, H.Z., Zheng, Y. and Ding, J. "Synthesis, surface modification and photocatalytic property of ZnO nanoparticles", Powder Technology 189, (2009) : 426–432.

Joong-Hee, L., Daeseung, J., Chang-Eui H., Kyong, Y.R., and Advani, S.G. "Properties of polyethylene-layered silicate nanocomposites prepared by melt intercalation with a PP-g-MA compatibilizer.", Composites Science and Technology 65, (2005) : 1996-2002.

Kissel, W.J., Han, J.H., and Meyer, J.A. "Polypropylene : structure, properties, manufacturing processes and applications", Handbook of Polypropylene and Polypropylene Composites, New York: Marcel Dekker, (2003) : 11-34.

Koenig, G., and Cramer, S. Thermal properties [Online], accessed 18 January 2011. Available from http://plc.cwru.edu/tutorial/enhanced/files/polymers/therm /therm.htm

Larson, B.F. Tensile properties [Online], accessed 18 January 2011. Available from http://www.ndt-d.org/EducationResources/CommunityCollege /Materials/Mechanical/Tensile.htm

Lily, W., Youshi, W., and Wei, L. "Preparation of ZnO nanorods and optical characterizatons", Physica E 28, (2005) : 76-82.

Ljungberg, N., Cavaillé, J.Y., and Heux, L. "Nanocomposites of isotactic polypropylene reinforced with rod-like cellulose whiskers", Polymer 47, (2006) : 6285-6292.

Lu, J.Z., Doyle, T.W., and Li, K. "Preparation and characterization of wood-(nylon 12) composites", Journal of Applied Polymer Science 103, (2007) : 270-276.

Modesti, M., Lorenzetti, A., Bon, D., and Besco, S. "Effect of processing conditions on morphology and mechanical properties of compatibilized polypropylene nanocomposites", Polymer 46, (2005) : 10237-10245.

Mittal, V. "Gas permeation and mechanical properties of polypropylene nanocomposites with thermally-stable imidazolium modified clay", European Polymer Journal 43, (2007) : 3727-3736.

Meng, W., Guizhong, Y., Min, W. and Weizhi, W. "Nonisothermal crystallization kinetics of ZnO nanorod filled polyamide 11 composites", Materials Chemistry and Physics 109, (2008) : 547–555.

Nan-Ying, N., Qin-Jian, Y., Feng, L., Qin, Z., Rongni, D., and Qiang, F. "Crystallization behavior and mechanical properties of polypropylene/ halloysite composites", Polymer 48, (2007) : 7374-7384.

O'Donnell, H.J., and Baird, Donald. "In situ reinforcement of polypropylene with liquid-crystalline polymers: effect of maleic anhydride-grafted polypropylene", Polymer 36, (1995) : 3113-3126.

Oracle Education Foundation. Uses of plastic [online], accessed 2 February 2011. Available from http://library.thinkquest.org/C003844/a_effects.htm

Othman, N., Ismail, H., Mariatti, M. "Effect of compatibilisers on mechanical and thermal properties of bentonite filled polypropylene composites", Polymer Degradation and Stability 91, (2006) : 1761-1774.

Porter, F., "Zinc oxide and chemicals", Zinc Handbook : properties, processing and use in design, New York: Marcel Dekker, (1991) : 588-589.

Rozanski A., Monasse B., Szkudlarek E., Pawlak A., Piorkowska E., Galeski A., and Haudin "Shear-induced crystallization of isotactic polypropylene based nanocomposites with montmorillonite", European Polymer Journal 10, (2008) : 88-101.

Ravindra Reddy, C., Pouyan Sardashti, A. and Simon, Leonardo C. "Preparation and characterization of polypropylene–wheat straw–clay composites", Composites Science and Technology 70, (2010) : 1674–1680.

Saminathan, K., Selvakumar, P. and Bhatnagar, N. "Fracture studies of polypropylene /nanoclay composite. Part II: Failure mechanism under fracture loads", Polymer Testing 27, (2008) : 453–458.

Sato, M., Kawata, A., Morito, S., Sato, Y., and Yamaguchi, I. "Preparation and properties of polymer/zinc oxide nanocomposites using functionalized zinc oxide quantum dots" , Eurpolymerjournal 44, (2008) : 3430-3438.

Shuang, X., Zi-Heng, L., Qun, W., Li-Jun, C., Tian-Min, H., and Guang-Tian, Z. "A novel one-step method to synthesize nano/micron-sized ZnO sphere", Journal of Alloys and Compounds 465, (2008) : 56-60.

Sichina, W.J. Characterization of Polymers Using TGA [Online], accessed 18 January 2011. Available from http://depts.washington.edu/mseuser/Equipment/Ref Notes/TGA_Notes.pdf

Singh, R.C., Singh, O., Singh, M.P., Chandi, P.S. "Synthesis of zinc oxide nanorods and nanoparticles by chemical route and their comparative study as ethanol sensors", Sensors and Actuators B: Chemical 135, (2008) : 352-357.

Special Chem. Reactive functional copolymers [Online], accessed 13 February 2011. Available from http://www.specialchem4polymers.com/tc/adhesion-promoters /index.aspx?id=3305

Suryadiansyah, H., Ismail, H., and Azhari, B. "Silica-filled polypropylene composites : the effect of ethylene diamine dilaurate and maleic anhydride grafted polypropylene on mechanical properties, water absorption, morphology, and thermal properties", Polymer Composites 29, (2008) : 1169-1176.

Sharma, B.K., Guptab, A.K., Kharea, N., Dhawanb, S.K., Gupta, H.C. "Synthesis and characterization of polyaniline–ZnO composite and its dielectric behavior", Synthetic Metals 159, (2009) : 391–395.

Tadmor, Z., and Gogos, C.G., "Twin screw and twin rotor processing equipment", Principles of Polymer Processing 2nd Edition, New Jersey : John Wiley & Sons, Inc., (2006) : 523-525.

Tonto, P., Mekasuwandumrong, O., Phatanasri, S., Pavarajarn, V., and Praserthdam, P. "Preparation of ZnO nanorod by solvothermal reaction of zinc acetate in various alcohols", Ceramics International 34, (2008) : 57-62.

University of New Mexico, Civil Engineering Department, Civil Engineering Materials Laboratory. Impact Test [Online], accessed 13 February 2011, Available from http://civilx.unm.edu/laboratories_ss/mechmat/charpy.html

Wulin, Q., Takashi, E., and Takahiro, H. "A novel technique for preparing of maleic anhydride grafted polyolefins", European Polymer Journal 41, (2005) : 1979-1984.

Wacharawichanant, S., Thongyai, S., Phutthaphan, A., Eiamsam-ang, C. "Effect of particle sizes of zinc oxide on mechanical, thermal and morphological properties of polyoxymethylene/zinc oxide nanocomposites", Polymer Testing 27, (2008) : 971–976.

Wei, S.F., Jiang, Q., and Lian, J.S. "Synthesis and characteristics of large-scale ZnO rods by wet chemical method", Transactions of Nonferrous Metals Society of China 18, (2008) : 1089-1093.

Yang K., Yang Q., Li G., Sun Y., and Feng D. "Morphology and mechanical properties of polypropylene/calcium carbonate nanocomposites", Materials Letters 60, (2006) : 805-809.

Yang D., Hu Y., Song L., Nie S., He S., and Cai Y., "Catalyzing carbonization function of α-ZrP based intumescent fire retardant polypropylene nanocomposites", Polymer Degradation and Stability 93, (2008) : 2014-2018.

Young Joon, J., Simer, Cynthia., Taein, O. "Comparision of zinc oxide nanoparticles and its nano- crystalline particles on the photocatalytic degradation of methylene blue", Materials Research Bulletin 41, (2006) : 67-77.

Zuiderduin, W.C.J., Westzaan, C., Huétink, J., and Gaymans, R.J. "Toughening of polypropylene with calcium carbonate particles", Polymer 44, (2003) : 261-275.

Zhang H., Feng J., Wang J., and Zhang M. "Preparation of ZnO nanorods through wet chemical method", Materials Letters 61, (2007) : 5202-5205.

Zhigang, J., Linhai Y., Yifan Z., and Zhude X. "Rod-like zinc oxide constructed by nanoparticles: synthesis, characterization and optical properties", Materials Chemistry and Physics, (2008) : 37-141.

APPENDIX

APPENDIX A
NOMENCLATURE

NOMENCLATURE

Abbreviations

BET	Brunauer-Emmett-Teller
$CaCO_3$	calcium carbonate
CTAB	cetyltrimethylammonium bromide
DMA	dynamic mechanical analysis
DSC	differential scanning calorimeter
EDD	ethylene diamine dilaurate
FT-IR	fourier transform infrared spectroscopy
HDPE	high density polyethylene
H_2O	dihydrogen monoxide
LDPE	lower-density polyethylene
LCP	liquid-crystalline polymer
MA	maleic anhydride
MMT	montmorillonite
MW	molecular weight
MWD	molecular weight distribution
$(NH_4)_2CO_3$	ammonium carbonate
NH_4OH	ammonium hydroxide
OMMT	organo-montmorillonite
PA	polyamides
PA11	polyamide 11
PANI	polyaniline
PBA	polybutylacrylate
PE	polyethylene
PEG	polyethylene glycol
PEI	polyethylenimine
POM	polyoxymethylene
PP	polypropylene
PP-g-MA	polypropylene grafted maleic anhydride
PMMA	polymethyl methacrylate

PS	polystyrene
PTFE	polytetrafluoroethylene
PVC	polyvinylchloride
RTD	residence time distribution
SEM	scanning electron microscope
SiO_2	silica
SSEs	single screw extruders
T_g	glass transition temperature
T_m	melting temperature
TEA	triethanolamine
TEM	transmission electron microscopy
TGA	thermo gravimetric analyzer
TSEs	twin screw extruders
UTS	ultimate tensile strength
WAXRD	wide angle x-ray diffraction
XRD	x-ray diffraction
$ZnCl_2$	zinc chloride
$Zn(NO_3)_2$	zinc nitrate
$Zn(NO_3)_2 \cdot 6H_2O$	zinc nitrate hexahydrate
ZnO	zinc oxide
ZnOH	zinc hydroxide

APPENDIX B
INTERNATIONAL PROCEEDING

International Proceeding

Thitipong Sanitchai, Sirirat Wacharawichanant and Supakanok Thongyai, "The effect of compatibilizers on morphology and mechanical properties of polypropylene/zinc oxide nanocomposites", *Pure and Applied Chemistry International Conference (PACCON 2009)*, Phitsanulok, Thailand, 14-16 Jan, 2009 (poster presentation)

Thitipong Sanitchai, Sirirat Wacharawichanant and Supakanok Thongyai, "Effect of compatibilizer on mechanical properties of polypropylene/zinc oxide nanocomposites", *Regional Symposium on Chemical Engineering (RSCE 2009)*, Manila, Philippines, 1-2 Dec, 2009 (oral presentation)

Biography

Name-Family name	Mr.Thitipong Sanitchai
Birth	4th January 1984 in Saraburi, Thailand.
Address	200 Moo.2, Tambon Muaklek, Amphur Muaklek, Saraburi 18180 Tel. 036-330144

Education

2002	High school certificate from Saraburiwitthayakhom School.
2005	received the degree of the Bachelor of Engineering, Faculty of Engineering, Silpakorn University, Nakhon Phathom, Thailand.
2010	further studied in the degree of the master of Chemical Engineering at graduate school, Faculty of Engineering and Industrial Technology, Graduate School, Silpakorn University, Thailand.